ÇUKUROVA UNIVERSITY
INSTITUTE OF NATURAL AND APPLIED SCIENCES

MSc THESIS

Betül PADAK

ADAPTIVE NEURO-FUZZY INFERENCE SYSTEMS BASED ESTIMATION OF PHOTOVOLTAIC CELL PARAMETERS USING DATA SET OBTAINED OUTDOOR MEASUREMENTS OF PHOTOVOLTAIC MODULE

DEPARTMENT OF ELECTRICAL AND ELECTRONICS ENGINEERING

ADANA, 2021

ABSTRACT

MSc THESIS

ADAPTIVE NEURO-FUZZY INFERENCE SYSTEMS BASED ESTIMATION OF PHOTOVOLTAIC CELL PARAMETERS USING DATA SET OBTAINED OUTDOOR MEASUREMENTS OF PHOTOVOLTAIC MODULE

Betül PADAK

ÇUKUROVA UNIVERSITY
INSTITUTE OF NATURAL AND APPLIED SCIENCES
DEPARTMENT OF ELECTRICAL AND ELECTRONICS ENGINEERING

Supervisor : Assoc. Prof. Dr. Murat AKSOY
Year: 2021, Pages: 99
Jury : Assoc. Prof. Dr. Murat AKSOY
: Asisst. Prof. Dr. Oğuzhan TİMUR
: Asisst. Prof. Dr. Zehan KESİLMİŞ

Solar energy, which will play an important role in energy supply in the near future, is the primary energy source among renewable energy sources. Recently, solar energy systems have become one of the most interesting topics due to their many advantages. By using experimental data, to extract the parameters of photovoltaic (PV) panels which is a solar energy system plays an important role in the design, evaluation and efficiency of PV panels. In this context, studies on obtaining different operating conditions and performance characteristics of PV panels have increased remarkably in recent years.

In this study, unknown parameters of single diode model equivalent circuit, also known as five parameter models of photovoltaic cell; photo current (I_{ph}), diode saturation current (I_0), diode ideality factor (n), serial resistance (R_s) and parallel resistance (R_p) were tried to be estimated with ANFIS using experimental data. Manufacturer datasheet information and ANFIS output results are compared in the MATLAB/Simulink environment; $I-V$ and $P-V$ characteristics have been obtained. Simulation results showed that the use of ANFIS in the extraction of unknown parameters of the PV module is a useful tool.

Key words: PV Model, Parameters of PV Cell, ANFIS

ÖZ

YÜKSEK LİSANS TEZİ

FOTOVOLTAİK MODÜLLERİNİN DIŞ ÖLÇÜMLERİNDEN ELDE EDİLEN VERİ SETLERİNİ KULLANARAK FOTOVOLTAİK HÜCRE PARAMETRELERİNİN ANFİS TABANLI TAHMİNİ

Betül PADAK

ÇUKUROVA ÜNİVERSİTESİ
FEN BİLİMLERİ ENSTİTÜSÜ
ELEKTRİK ELEKTRONİK MÜHENDİSLİĞİ ANABİLİM DALI

Danışman : Doç. Dr. Murat AKSOY
Yıl: 2021, Sayfa: 99
Juri : Doç. Dr. Murat AKSOY
: Dr. Öğr. Üyesi Oğuzhan TİMUR
: Dr. Öğr. Üyesi Zehan KESİLMİŞ

Yakın gelecekte enerji arzında önemli bir rol oynayacak olan yenilenebilir enerji kaynaklarından güneş enerjisi, yenilenebilir enerji kaynakları arasında birincil enerji kaynağıdır. Son zamanlarda, birçok avantajından dolayı güneş enerjisi sistemleri en ilgi çekici konulardan biri haline gelmiştir. Deneysel verileri kullanarak bir güneş enerjisi sistemi olan fotovoltaik (PV) panellerin parametrelerini anlamak, PV panellerin tasarımı, değerlendirilmesi ve verimliliğinde önemli bir rol oynar. Bu bağlamda PV panellerinin farklı çalışma koşulları ve performans karakteristiklerinin elde edilmesi ile ilgili çalışmalar son yıllarda dikkat çekici bir biçimde artış göstermiştir.

Bu çalışmada, fotovoltaik hücrenin beş parametre modeli olarak da bilinen tek diyot modelinin bilinmeyen parametreleri olan; foto akım (I_{ph}), diyot doyma akımı (I_0), diyot idealite faktörü (n), seri direnç (R_s) ve paralel direnç (R_p) deneysel veriler kullanılarak ANFIS ile tahmin edilmeye çalışılmıştır. Üretici veri sayfası bilgileri ve ANFIS çıktı sonuçları MATLAB/Simulink ortamında karşılaştırılarak $I-V$ ve $P-V$ karakteristikleri elde edilmiştir. Simülasyon sonuçları PV modül bilinmeyen parametrelerin çıkarılmasında ANFIS kullanılmasının faydalı bir araç olduğunu göstermiştir.

Anahtar Kelimeler: PV Modeli, PV Hücresinin Parametreleri, ANFIS.

EXTENDED SUMMARY

Solar energy is considered as the direct or the indirect origin of the almost all-other energy sources in the world. Humans, like all other living things, make use of the sun for the need for warmth and food. However, The way people use the solar energy can alter.

For instance, fossil fuels originated from plant extracts from the ancient geological times, have been used for transportation and electricity generation for ever known. Likewise, biomass, a type of energy produced by living organisms, converts solar energy into a fuel, and this fuel can then be used for heat or electricity. Wind energy, which has been used to provide mechanical energy or transport for hundreds of years, uses solar heated air and air currents created by the rotation of the earth. Today, wind turbines transform wind power into electricity as well as traditional uses. Even hydroelectricity is caused by the sun. Hydroelectricity is dependent on the water evaporating by the sun and then returning to Earth as rain to supply water in the dams.

Besides these sources that we indirectly obtain energy from sunlight, photovoltaics are the process of converting sunlight into electricity by using solar cells directly. Today, it is a clean, renewable and sustainable alternative energy source that is growing rapidly and increasingly important for conventional fossil fuel power generation. As well as most of the photovoltaic devices are used for purely practical and economic reasons today, one of its most important benefits is undoubtedly that it is the most environmentally friendly source that generates electricity. While other fossil fuel production units pollute the environment and contribute to global warming, PV's do not release pollutants during operation (Shivalkar et al. 2015; Wang et al., 2014). In addition, PVs are easy to operate, less mechanical wear and long-life systems (Sundareswaran, 2015). For example, it may

be more economical to install photovoltaic systems in rural areas where there is no electricity grid or where it is very costly and difficult to install the grid.

The main component of PV systems is the PV cell. The basic structure of a photovoltaic cell is created by combining a P-type and an N-type semiconductor. This structure is called a p-n connection (Villalva and Gazoli, 2009). The sun is absorbed in the semiconductor junction and forms a new electron hole pair. Under the influence of the electric field of the p-n junction, the voids flow from the n region to the p region, and the electrons from the p region to the n region. Thus, the current is formed. Therefore, in an equivalent circuit model, a diode is typically used to model a photovoltaic cell.

Among the various diode equivalent circuit models, the single diode equivalent circuit model is most commonly used based on the balance between precision and simplicity. In this model there are five parameters which must be determined. These are photo current (I_{ph}), saturation current (I_0), diode ideality factor (n), series resistance (R_s) and shunt resistance (R_p). Although the single diode equivalent circuit model is a simple model, it is difficult to determine the parameters due to the nonlinear and closed forms of the equivalent circuit model.

Methods for calculating PV module parameters include mainly analytical methods and flexible computing (soft computing) approaches. Analytical methods use mathematical equations to determine PV module parameters based on the physical properties of equivalent circuits. Soft computing methods are the sum of several methods that take advantage of the tolerance of uncertainty and instabilities to achieve easy workability, robustness, and low solution costs. The basic components are fuzzy logic, neural programming and probability theorems. The underlying idea of soft computing is to construct the cognitive approach model of human intelligence. The role model of soft computing is human intelligence (Zadeh, 1994).

Recently, the adaptive network-based inference system (ANFIS), one of the flexible computing methods, has been used for various applications in many disciplines. This method, which combines both neural networks and fuzzy logic together, consists of combining the learning ability of neural networks with the advantages of fuzzy logic such as decision-making and data grading. ANFIS is able to determine all rules based on measured or desired values depending on the structure of the problem being addressed.

In this thesis, the mathematical equivalent circuits of photovoltaic solar panels, which is one of the single diode circuit model parameters that are not included in the manufacturer's catalog data; photo-current (I_{ph}), diode saturation current (I_0), idealite diode factor (n), parallel resistance (R_p) and series resistance (R_s) values are calculated using ANFIS.

GENİŞLETİLMİŞ ÖZET

Güneş enerjisi, doğrudan veya dolaylı olarak dünyadaki neredeyse tüm enerjinin kaynağıdır. İnsanlar, diğer tüm canlılar gibi, sıcaklık ve yemek ihtiyacı için güneşten faydalanırlar. Bununla birlikte, insanlar güneş enerjisini birçok farklı şekilde de kullanmaktadırlar. Örneğin, eski jeolojik çağlardan kalma bitki özü olan fosil yakıtlar, ulaşım ve elektrik üretimi için kullanılır ve aslında fosil yakıtlar milyonlarca yıl öncesine ait güneş enerjisi depolamıştır. Benzer şekilde, yaşayan organizmalar tarafından üretilen bir enerji çeşidi olan biokütle, güneş enerjisini bir yakıta dönüştürür ve bu yakıt daha sonra ısı veya elektrik için kullanılabilir. Yüzlerce yıldır mekanik enerji sağlamak veya taşınım yapmak için kullanılan rüzgâr enerjisi, güneş tarafından ısıtılan hava ve dünyanın dönüşü ile oluşturulan hava akımlarını kullanır. Bugün rüzgâr türbinleri, rüzgâr gücünü geleneksel kullanımlarının yanı sıra elektriğe de dönüştürür. Hidroelektrik bile güneşten kaynaklanmaktadır. Hidroelektrik, suyun güneş tarafından buharlaşmasına ve barajlarda su sağlamak için daha sonra Dünya'ya yağmur olarak geri dönmesine bağlıdır.

Güneş ışığından dolaylı olarak enerji elde ettiğimiz bu kaynakların yanında, fotovoltaikler, güneş ışığını doğrudan güneş pilleri kullanarak elektriğe dönüştürme işlemidir. Bugün, geleneksel fosil yakıtlı elektrik üretimi için hızla büyüyen ve giderek daha önemli olan temiz, yenilenebilir ve sürekliliği olan bir alternatif enerji kaynağıdır. Günümüzde fotovoltaik cihazların büyük kısmı, tamamen pratik ve ekonomik nedenlerden dolayı kullanılmakla birlikte, fotovoltaiklerin en önemli yararlarından biri de kuşkusuz onun elektrik üreten en çevreci kaynak olmasıdır. Diğer fosil yakıtlı üretim birimleri çevreyi kirletip küresel ısınmaya katkı sağlarken, PV'ler işletme sırasında kirletici madde salmazlar (Shivalkar ve ark. 2015; Wang ve ark., 2014). Bunun yanında PV'ler işletilmesi kolay, mekanik yıpranması az ve uzun ömürlü sistemlerdir (Sundareswaran, 2015). Örneğin, elektrik şebeke hattının

olmadığı veya şebeke hattının kurulmasının çok masraflı ve zor olduğu kırsal kesimlerde fotovoltaik sistemlerin kurulması daha ekonomik olabilmektedir.

PV sistemlerinin temel bileşeni PV hücresidir. Bir fotovoltaik hücrenin temel yapısı, bir p tipi ve bir n tipi yarı iletkenin bir araya getirilmesi ile oluşturulur. Oluşturulan bu yapıya bir p-n bağlantısı adı verilir (Villalva ve Gazoli, 2009). Güneş, yarı iletken bağlantıda absorbe edilir ve yeni bir boşluk-elektron çifti oluşturur. p-n bağlantısının elektrik alanının etkisi altında, boşluklar n bölgesinden p bölgesine ve elektronlar da p bölgesinden n bölgesine akar. Böylece akım oluşur. Bu nedenle, eşdeğer bir devre modelinde, bir fotovoltaik hücreyi modellemek için tipik olarak bir diyot kullanılır.

Çeşitli fotovoltaik eşdeğer devre modelleri arasında kesinlik ve basitlik arasındaki dengeye dayanarak, tek diyot eşdeğer devre modeli en yaygın şekilde kullanılır. Bu modelde belirlenmesi gereken beş parametre vardır. Bunlar, fotoakım (I_{ph}), doygunluk akımı (I_0), diyot idealite faktörü (n), seri direnç (R_S) ve şönt direncidir (R_p). Tek diyot eşdeğer devre modeli basit bir model olsa da eşdeğer devre modelinin doğrusal olmayan ve kapalı biçimleri nedeniyle parametrelerin belirlenmesi zorlaşır.

PV modül parametrelerini hesaplama yöntemleri, temel olarak analitik yöntemleri ve esnek hesaplama yaklaşımlarını içerir. Analitik yöntemler eşdeğer devrelerin fiziksel özelliklerine göre PV modül parametrelerini belirlemek için matematiksel denklemleri kullanır. Esnek hesaplama yöntemleri, kolay işlenebilirlik, sağlamlık ve düşük çözüm maliyetleri elde etmek için belirsizlik ve kararsızlıkların toleransından faydalanan çeşitli yöntemlerin toplamıdır. Temel bileşenleri; bulanık mantık, sinirsel programlama ve olasılık teoremleridir. Esnek hesaplamanın temelinde yatan fikir, insan zekasının bilişsel yaklaşım modelini oluşturmaktır. Esnek hesaplamanın rol modeli ise insan zekasıdır (Zadeh, 1994).

Son zamanlarda, esnek hesaplama yöntemlerinden olan uyarlamalı ağ tabanlı çıkarım sistemi (ANFIS), birçok bilim dalında çeşitli uygulamalar için

kullanılmıştır. Hem sinir ağlarını hem de bulanık mantığı bir arada bulunduran bu yöntem, sinir ağlarının öğrenme kabiliyeti ile bulanık mantığın karar verme ve veri derecelendirme gibi üstünlüklerinin birleştirilmesinden meydana gelmektedir. ANFIS, ele alınan problemin yapısına bağlı olarak ölçülen veya istenen değerler üzerinden tüm kuralları belirleyebilmektedir.

Bu çalışmada, fotovoltaik hücrenin beş parametre modeli olarakda bilinen tek diyot modelinin bilinmeyen parametreleri olan; foto akım (I_{ph}), diyot doyma akımı (I_0), diyot idealite faktörü (n), seri direnç (R_S) ve paralel direnç (R_p) deneysel veriler kullanılarak ANFIS ile tahmin edilmeye çalışılmıştır. Üretici veri sayfası bilgileri ve ANFIS çıktı sonuçları MATLAB/Simulink ortamında karşılaştırılarak $I-V$ ve $P-V$ karakteristikleri elde edilmiştir. Alınan sonuçların ANFIS ile yakınlığı karşılaştırılmıştır.

ACKNOWLEDGEMENTS

I would like to my heartfelt thanks my supervisor Assoc. Dr. Murat AKSOY and Bülent BÜYÜKGÜZEL for their knowledge and experience, who were not spared their support during the preparation of this thesis.

I owe my deepest thanks to family and my elder sister Melek who supported me in opening the door to new horizons.

I would like to express my deepest gratitude to my elder sister Assoc. Dr. Müzeyyen ERTÜRK and her husband Assoc. Dr. Ali Serol Ertürk since they supported me in every sense during the thesis process.

CONTENTS **PAGE**

ABSTRACT I
ÖZ II
GENİŞLETİLMİŞ ÖZET III
EXTENDED SUMMARY III
CONTENTS XII
LIST OF TABLES XIV
LIST OF FIGURES XVI
LIST OF ABBREVATIONS XXII
1. INTRODUCTION 1
1.1. The Photovoltaic Effect and PV cell 2
1.2. Content of the thesis 5
2. LITERATURE REVIEW 7
3. MATERIAL AND METHOD 13
3.1. MATERIAL 13
3.1.1. Photovoltaic 13
3.1.2. Fundamentals of Semiconductor Physics 14
3.1.2.1. The Band Gap Energy 15
3.1.2.2. Solar Spectrum 19
3.1.2.3. The p–n Junction of Semiconductors 20
3.1.3. Energy Conversion in Photovoltaic Cell 24
3.1.4. Electric circuit models of PV cells 26
3.1.4.1. The Simplest Equivalent Circuit for a Photovoltaic Cell 26
3.1.4.2. A More Accurate Equivalent Circuit for a PV Cell 30
3.1.5. The $I-V$ curve of PV and basic parameters 32
3.1.5.1. Effect of solar radiation value and temperature on photovoltaic cell's $I-V$ characteristic curve 34

3.1.5.1.(1). Effect of Solar Radiation Intensity 34
3.1.5.1.(2). Effect of Temperature 36
3.1.6. Factors Affecting Characteristics of the PV Cell 37
3.2. Method 39
3.2.1. Artificial neural networks 39
3.2.1.1. Neuron Modeling 40
3.2.1.2. Architecture 42
3.2.2. Adaptive Neuro Fuzzy Inference System 44
3.2.2.1. Fuzzy Inference System (FIS) 44
3.2.2.2. Adaptive Network 45
3.2.2.3. ANFIS Architecture 46
3.2.2.4. ANFIS's Learning Algorithm 49
3.2.3. STUDIES ON THE THESIS 50
3.2.3.1. Recommended ANFIS and PV Model 52
4. RESULT AND DISCUSSION 57
5. CONCLUSION 77
REFERENCES 93
CIRRICULUM VITAE 99

LIST OF TABLES **PAGE**

Table 4.1. Training and Test data sets best R^2 values 69
Table 4.2. Real and Estimated datas for training data set 69
Table 4.3. Real and Estimated datas for training data set 72
Table 4.4. Real and Estimated datas for training data set 74
Table 5.1 Best R^2 for PV cell five unknown parameters 77

LIST OF FIGURES **PAGE**

Figure 1.1. Ilustration o the structure of a typical solar 3
Figure 1.2. Equivalent circuit of the PV cell 4
Figure 1.3. I-V curve of the PV cell 5
Figure 3.1. Electron order of silicon semiconductor 14
Figure 3.2. Covalent bond arrangement of silicon atoms. 15
Figure 3.3. Representation of energy bands for (a) metals and (b) semiconductors. 16
Figure 3.4. (a) Formation of electron-hole pair by the action of a photon with sufficient energy content. (b) an electron can recombine with the hole. 17
Figure 3.5. (a) An electron moving to a gap in the energy band of the nearby atom and (b) displacement of the hole. 18
Figure 3.6. Photon energy-wavelength graph for silicon semiconductor 19
Figure 3.7. Solar spectrum of silicon semiconductor for AM = 1.5. 20
Figure 3.8. The donor atom in silicon crystal. 21
Figure 3.9. Identification of the donor atom 22
Figure 3.10. The Acceptor atom in silicon crystal 22
Figure 3.11. Identification of the acceptor atom 23
Figure 3.12. The n and p regions combined along a joint 24
Figure 3.13. The electrical field formed by immobile, charged atoms 24
Figure 3.14. Pushing electrons and holes towards the poles by the electric field. .. 25
Figure 3.15. Direction of electrons and electric current in photovoltaic cell. 25
Figure 3.16. A Simple equivalent circuit for a photovoltaic cell. 27
Figure 3.17. Short circuit current of photovoltaic cell 27
Figure 3.18. Open circuit voltage of photovoltaic cell 28
Figure 3.19. Diode characteristic curve 29

Figure 3.20. Photovoltaic current-voltage relationship when dark (no sunlight) and light (an illuminated cell)..... 29
Figure 3.21. Simple PV equivalent circuit with parallel resistor added..... 30
Figure 3.22. A PV equivalent circuit with series resistance 31
Figure 3.23. A more complex equivalent circuit for a PV cell involves both parallel and serial resistors. 32
Figure 3.24. P-V curve of a PV module..... 33
Figure 3.25. I-V curve of a PV module 34
Figure 3.26. The Effect of Radiation Intensity Value on the Current- Voltage and Power-Voltage Values of the Photovoltaic Cell..... 35
Figure 3.27. The Effect of Temperature Value on the Current- Voltage and Power-Voltage Values of the Photovoltaic Cell 37
Figure 3.28. Effect of parallel resistance on curve *I -V* 38
Figure 3.29. Effect of series resistance on the *I -V* curve 39
Figure 3.30. Schematic representation of a biological neuron..... 40
Figure 3.31. A sample ANN mathematical modeling of a neuron..... 41
Figure 3.32. Activation function for (a) the fixed restrictor, (b) purelin, (c) log-sigmoid, and (d) bipolar sigmoid..... 42
Figure 3.33. The architecture and the Taxonomy of feedforward and feedback neural networks..... 43
Figure 3.34. A schematic representation of a FIS..... 45
Figure 3.35. Adaptive network 46
Figure 3.36. (a) Sugeno fuzzy interference system “If-Then” and fuzzy logic mechanism and (b) ANFIS architecture 47
Figure 3.37. ANFIS architecture for the recommended photovoltaic model..... 53
Figure 4.1. ANFIS models proposed for estimating equivalent electrical circuit parameters..... 57
Figure 4.2. FLC Sugeno model interface..... 58

Figure 4.3. ANFIS graphical user interface 59
Figure 4.4. ANFIS model structure..... 61
Figure 4.5. Membership functions for Solar irradiance data..... 62
Figure 4.6. Membership functions for cell temperature data 63
Figure 4.7. Output membership functions of the model created by Grid partitioning method..... 64
Figure 4.8. Rule editor designed for ANFIS 65
Figure 4.9. Rule editor designed for ANFIS 66
Figure 4.10. Loading the training data set 67
Figure 4.11. Training error of the ANFIS mode 67
Figure 4.12. For the training data set Comparison of actual data and ANFIS extracted data for equivalent parameters of PV modules namely I_{ph}.. 68
Figure 4.13. For the testing data set Comparison of actual data and ANFIS extracted data for equivalent parameters of PV modules namely I_{ph}.. 68
Figure 4.14. Real data of I-V curve 70
Figure 4.15. Estimated data of I-V curve..... 70
Figure 4.16. Real data of P-V Curve..... 71
Figure 4.17. Estimated data of P-V curve..... 71
Figure 4.18. Real data of I-V curve 72
Figure 4.19. Estimated data of I-V curve..... 73
Figure 4.20. Real data of P-V curve..... 73
Figure 4.21. Estimated data of P-V curve..... 74
Figure 4.22. Real data of I-V curve 75
Figure 4.23. Estimated data of I-V curve..... 75
Figure 4.24. Real data of P-V curve..... 76
Figure 4.25. Estimated data of P-V curve..... 76
Figure 5.1. Real and Estimated values graph for I_{ph} 78
Figure 5.2. Real and Estimated values graph for I_0..... 78

Figure 5.3. Real and Estimated values graph for R_p 79
Figure 5.4. Real and Estimated values graph for n 79
Figure 5.5. Real and Estimated values graph for R_s 80
Figure 5.6. Change of photo current due to solar irradiation for real data 81
Figure 5.7. Change of photo current due to solar irradiation for ANFIS data 81
Figure 5.8. Change of photo current due to cell temperature for real data 82
Figure 5.9. Change of photo current due to cell temperature for ANFIS data 82
Figure 5.10. Change of diode saturation current due to solar irradiation for real data 83
Figure 5.11. Change of diode saturation current due to solar irradiation for ANFIS data 83
Figure 5.12. Change of diode saturation current due to cell temperature for real data 84
Figure 5.13. Change of diode saturation current due to cell temperature for ANFIS data 84
Figure 5.14. Change of parallel resistance due to solar irradiation for real data 85
Figure 5.15. Change of parallel resistance due to solar irradiation for ANFIS data 85
Figure 5.16. Change of parallel resistance due to cell temperature for real data 86
Figure 5.17. Change of parallel resistance due to cell temperature for ANFIs data 86
Figure 5.18. Change of diode ideality factor due to solar irradiation for real data . 87
Figure 5.19. Change of diode ideality factor due to solar irradiation for ANFIS data 87
Figure 5.20. Change of diode ideality factor due to cell temperature for real data. 88
Figure 5.21. Change of diode ideality factor due to cell temperature for ANFIS data 88
Figure 5.22. Change of series resistance due to solar irradiation for real data 89
Figure 5.23. Change of series resistance due to solar irradiation for ANFIS data .. 89
Figure 5.24. Change of series resistance due to cell temperature for real data 90

Figure 5.25. Change of series resistance due to cell temperature for ANFIS data . 90

LIST OF ABBREVATIONS

h : Planck constant [$6.63 \times 10^{-34}\ J\ s$]

v : Frequency of the photon [Hz]

c : Speed of light [$2.998 \times 10^{8}\ m/s$]

λ : Wavelength of the photon [m]

E_g : Forbidden band energy [eV]

AM : Air mass [$1/cos\theta$]

G : Solar irradiation [W/m2]

I : Current [A]

I_d : Diode current [A]

V_d : Diode voltage [V]

I_m : Maximum current [A]

I_0 : Diode saturation current [A]

I_p : Shunt current [A]

I_{ph} : Photo current [A]

I_{sc} : Short circuit current [A]

k : Boltzmann constant [1.381×10^{-23} J/K]

n : Ideality factor [modül sabiti]

P : Power [W]

P_m : Maximum power [W]

PV : Photovoltaic

q : Electron charge [1.602×10^{-19} C]

R_S : Series resistance [Ω]

R_p : Parallel resistance [Ω]

T : Temperature [K]

T_C : Cell temperature [^{o}C]

V : Voltage [V]

V_m : Maximum voltage [V]

V_{OC} : Open circuit voltage [V]

1. INTRODUCTION

Depending on the growing world population and evolving technology, the inability of existing limited resources to meet the growing energy needs of societies further highlights importance of the concept of energy. The fact that fossil fuels have a limited lifespan and the negative environmental effects of these fuels have pushed modern societies into the search for clean, environmentally friendly and renewable energy sources from the second half of the 20th century. It has been aimed to reduce the dependence on fossil fuels in meeting the world's energy demand by accelerating scientific studies on alternative energy sources, especially solar, wind, geothermal and hydrogen energy.

In addition to being an unlimited and clean energy source, solar energy has become a scientific study area where research activities have intensified, especially since its practical applications do not require complex technology. Even though solar energy technologies display differences in terms of technological level, methodology, material and so that they are differentiated into groups as thermal solar technologies and photovoltaic technology. Low temperature systems and condensing systems are examples of thermal solar technologies.

Low temperature systems, each of which serves a characteristic purpose and is divided into various groups in terms of their structural and functional functions, have a wide range of usage among thermal solar technologies with their ease of production and operation. Planar and vacuum solar collectors, solar furnaces, solar chimneys, solar pools, product drying and water treatment systems can be shown as examples of applications of low temperature systems. Condensing systems separated from low temperature systems with complex structures and high energy potentials are another important thermal solar technology developed to meet the energy needs in the regional sense. Parabolic groove collectors, parabolic dish systems and central receiver systems are the most common concentrator system applications.

Photovoltaic technology, a characteristic feature of semiconductor materials and based on a basic physical process expressed as a photovoltaic effect, is a high-tech solar energy application that examines the conversion of sunlight directly into electrical energy. As a result of the increasing need for clean and environmentally friendly energy sources due to the harmful effects of fossil fuel consumption on public health and the environment, research activities related to photovoltaic technology gained intensity especially towards the end of the 20th century. In 2002, photovoltaics became the fastest growing and developing energy technology (Kropp, 2009).

Scientific studies on photovoltaic systems can be considered in two groups, including applications and parametric studies for improving the current production technology. In different operating conditions, scientific activities related to parametric studies covering research subjects such as obtaining performance characteristics of photovoltaic cells, detection of the most cohesive photovoltaic cell and examining the effects of basic cell parameters on power transformation have been particularly focused on recent periods (Bouzidi et al., 2007; Chegaar et al.,2006).

Photovoltaic systems can work connected or independent from the network. Especially in areas far from the settlements where network connectivity is expensive, it is more economically convenient to use. The main uses of photovoltaic systems are satellites, meteorological stations, lighting applications, traffic warning signs, gas stations, irrigation systems, cooling and drying applications.

1.1. The Photovoltaic Effect and PV cell

The most known direct way of converting solar energy into electricity is photovoltaic (PV). It is based on the observation of Henri Becquerel in 1839, called as photovoltaic effect. In general, the photovoltaic effect is defined as the generation of electrical voltage between the two electrodes connected to a liquid and solid

system upon exposure to light in the system. In practice, all of the photovoltaic systems include a p-n junction in a semiconductor, where photovoltage is generated, as shown in Figure 1.1.

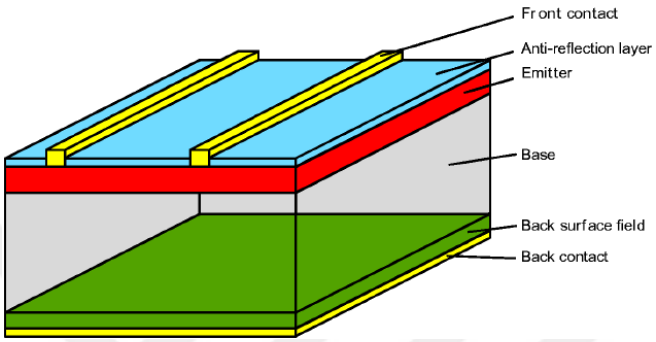


Figure 1.1. Ilustration o the structure of a typical solar (Goetzberger & Hoffmann, 2005).

Indeed, the process of PV functions through the photovoltaic effect on semiconductor materials. The process works in such a way that when the cell is exposed to light, some of the incident light is absorbed by the semiconductor material and loosens the electrons, allowing the electric charge to flow freely through the material. The existing built-in electrical field in PV cells forces electrons emitted by light absorption to flow in a certain direction. This area is exposed by doping in silicon with elements such as phosphorus or boron to form p-type or n-type zones. Operating the current on an external circuit is possible by placing metal contacts at the top and bottom of the photovoltaic cell. The current is generated quietly without moving parts and does not require maintenance except cleaning the top of the module in order to maintain the light pass through the system. The equivalent circuit of the PV cell is shown in Figure 1.2. Along with a diode that represents the movement of the p-n junction, the current produced from light consists of a current generator that represents the I_L.

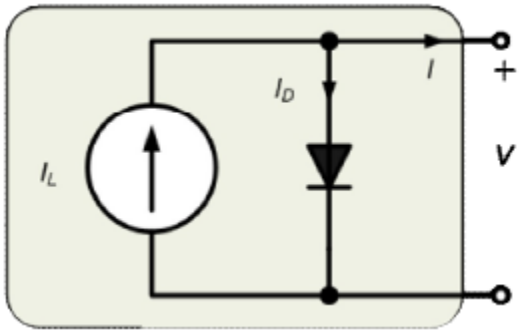


Figure 1.2. Equivalent circuit of the PV cell (Buyukguzel,2011).

The current transferred outside the PV cell is obtained using this equivalent circuit as follows.

$$I = I_L - I_0[\exp\left(\frac{qV}{kT}\right) - 1] \quad (1.1)$$

The typical I-V characterity of the PV cell is shown in Figure 1.3. The output power of the PV cell is equal to the product of its current and voltage. No power is produced on short circuit (maximum current, zero voltage) or open circuit (maximum voltage, zero current) or short circuit (maximum current, zero voltage).

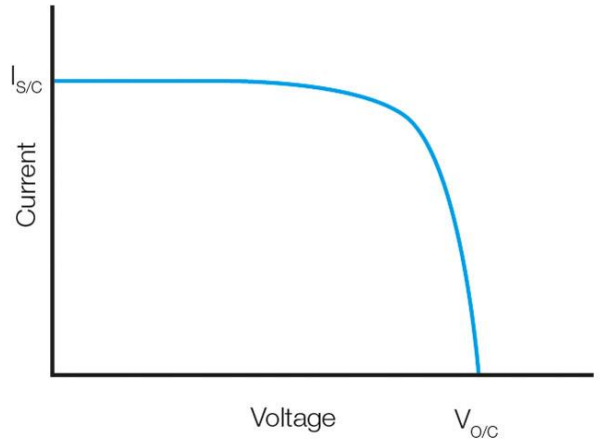


Figure 1.3. *I-V* curve of the PV cell (Buyukguzel,2011).

Depending on the increase in the solar radiation, an increase in the output current occurs and finally the horizontal part of the curve goes on upwards. On the other hand, a shift to left happens with an increase in the cell temperature whereas opposite is observed when the temperature decreased. Therefore, photovoltaic cell characteristics vary depending on cell temperature and solar radiation.

1.2. Content of the thesis

In this thesis, the mathematical equivalent circuits of photovoltaic solar panels, which is one of the single diode circuit model parameters that are not included in the manufacturer's catalog data; photo-current (I_{ph}), diode saturation current (I_0), idealite diode factor (n), parallel resistance (R_p) and series resistance (R_s) values are calculated using ANFIS.

2. LITERATURE REVIEW

Photovoltaic is defined as the material that can convert the energy contained in light photons into electrical voltage and current. An electron in a photovoltaic material can get rid of the atom holding it up, causing a photon of sufficient short wavelength and sufficiently high energy. These electrons can be shifted towards a metal contact as an electric current if a close electric field is provided. It is very interesting that photovoltaics can absorb 6000 times more solar energy than the total energy demand of the earth's surface (Masters, 2004).

Scientific studies on photovoltaic technology began in 1839 by French physicist Edmund Becquerel discovering the potential difference between the poles of a illuminated metal electrode immersed in a weak electrolyte solution (Becquerel, 1839). In 1876, as a result of the first applications of the photovoltaic effect in solid put forward by Adams and Day in 1876, selenium photovoltaic cells with a power conversion yield of 1 − 2% were produced (Adams and Day, 1876).

As a result of his success in the quantum field, Albert Einstein won the 1921 Nobel Prize in Physics for his theoretical work on the principle of photovoltaic action in 1904. In 1940, silicon crystals were widely used in PV cell production, thanks to a method developed by Polish scientist Czochralski.

Studies on the use of PV cells as a practical energy source have been focused on since 1950. The Vanguard I satellite was supported with PV cells in 1958. PV cells have played an important role for many years, especially in meeting the energy needs of satellites, as cost is a less important parameter in space vehicles than weight and safety. As a result of high-efficiency and low-cost PV cell production in the 1980s, PV system applications were accelerated in many areas such as lighting systems, emergency communication stations, agricultural irrigation systems, in addition to space technology studies.

Many methods have been studied in the literature for the prediction of the parameters of the single diode model of the PV cell which is the main component of PV systems.

In the literature, conventional parameter estimation methods are divided into two categories (Kashif et.al, 2011):

i. Analytical techniques
ii. Numerical extraction techniques (soft computing)

Methods for calculating PV module parameters include mainly analytical methods and flexible computing (soft computing) approaches. Analytical strategies use mathematical equations to elucidate PV module parameters based on the physical properties of equivalent circuits. Soft computing methods are the sum of several methods that take advantage of the tolerance of uncertainty and instabilities to achieve easy workability, robustness, and low solution costs. The basic components are fuzzy logic, neural programming and probability theorems. The underlying idea of soft computing is to construct the cognitive approach model of human intelligence. The role model of soft computing is human intelligence (Zadeh, 1994).

Expanding the methods of Lee et al. (1992), Chegaar et al. (2006) provided a simple and successful method including using an auxiliary function and a computer fitting routine to evaluate ideality factor, series resistance, shunt conductivity, and saturation current in illuminated solar cells.

Karatepe et al. (2005), reported a neural network-based strategy with the aim of improving accuracy of a photovoltaic module. Based on their results, they revealed that solar radiation and temperature are the main equivalent parameters of a PV module. Using a series of current-voltage curves, the dependence of circuit parameters on environmental factors is investigated. In addition, they determined that the relationship between solar radiation and temperature are not linear so that

they cannot be expressed with any analytical equations. Therefore, they used the neural network to overcome this problem in their studies. In this way, using some measured current-voltage curves, the neural network was trained once and the equivalent circuit parameters were simply estimated by simply reading solar radiation and temperature samples very quickly, without the need to solve complex nonlinear mathematical equations required in conventional methods.

Bouzidi et al. (2007) introduced a new method based on the consideration of serial and shunt resistance or measurements of current-voltage characteristics in determining the parameters of an illuminated single diode solar cell.

Kim et al. (2010) proposed a method by making assumptions different from actual working conditions to obtain accurate parameter values and avoid operational complexity. By means of this method, the determination of the characteristic curve of an ideal non-resistant solar cell is performed by using the I-V characteristic curves measured and reported by the solar cell manufacturers and thus calculates the difference between the obtained and the actual measured curves.

Farivar et al. (2010) offered an approach that uses manufacturer datasheet information to find single diode model parameters unlike other methods.

Kulaksız (2011), used ANFIS in a single diode model of PV cells to get serial resistance, ideality factor and parallel resistance. In his study, the input parameters of ANFIS are the material type of the PV module, the open circuit voltage, the short circuit current, and the unit area under the I-V curve.

Wei et al. (2011) used a chaotic particle swarm optimization algorithm (CPSO) to extract solar cell model parameters. In the study, the local convergence of global search performance and particle swarm optimization (PSO) was constructed by making it a chaos study.

AlHajri et al. (2012) demonstrated a strategy as an application of sample search technique to extract the parameters of different solar cell models. The

proposed technique was facilitated to solve an abstract function that manages the I-V relationship of a solar cell when there is no direct analytical solution.

Caracciolo et al. (2012) presented a simple and accurate method to explore the single diode model parameters of an illuminated and dark solar cell and its extension to the PV solar module. The suggested method is based on obtaining experimental data on the I-V characteristics of the illuminated or dark solar cell / PV solar module under constant climatic conditions.

Özçalık et al. (2013) examined the creation of a diode mathematical model of PV solar cells in MATLAB and how the variables that affect the energy production affect the characteristics.

Bendib et al. (2013) proposed a method based on fuzzy control techniques. This technique is applied to find various parameters in a single diode solar cell model.

Wolf et al. (2013) demonstrated a method that uses both analytical and statistical methods to determine the parameters of PV cells/modules using curve fitting.

Patel et al. (2014) proposed a simple, effective and reasonable method to predict all five parameters of a solar cell from a single illuminated I-V characteristic using a teaching-based optimization teaching algorithm (TLBO). It was found that the values of the parameters obtained by TLBO algorithm are in aligned with the values of the reported parameters.

Salem et al. (2014) presented an artificial intelligence (AI) technique to predict equivalent circuit parameters of PV modules. Series resistance, diode ideality factor, and parallel resistance are the parameters discussed in their work are. From the analytical solution of the PV mathematical model, they obtained the training data for both paradigms from the analytical solution of the PV mathematical model.

Ghani et al. (2014) introduced a new approach to calculating all five parameter values. The proposed method is on the basis of solving the single-diode

current-voltage equation defined by using the Lambert-W function in five experimental points along the current-voltage curve.

Bai et al. (2014) introduced a new composite method to predict the five parameters with manufacturer template data. Under STC conditions, two differential values at the short and open circuit points of the I-V curve were used to obtain five parameters.

Humada et al. (2015) presented comprehensive extraction of DC parameters of solar cells using mathematical techniques based on single and double diode models.

Mares et al. (2015) proposed a new procedure to extract the parameters of the single diode model under standard test conditions using only the basic data listed by all manufacturers on the datasheet.

ALQahtani et al. (2015) presented a new approach to correctly extract Iph, Isat, A, Rs and Rp which are five unknown parameters of the photovoltaic (PV) module single diode model. The method of extracting parameters includes a new dP / dI = 0 equation at the maximum power point, instead of dI / dV = -1 / Rp which is the equation typically used in the literature. The new equation prevents dependence on the Rp value. Besides, it does not require any complicated calculation and a boring combination of other equations to subtract five parameters for a PV module.

Hansen (2015) presented an algorithm to determine the parameters for the photovoltaic module performance model encoded in the software package PVsyst ™ version 6. The method operates on the measured current-voltage (I-V) under a range of irradiation and temperature conditions. He explained the method and showed his steps using the data for the 36-cell crystalline silicon module. He qualitatively compared his method with another technique to estimate the parameters for the PVsyst ™ version 6 model.

Toprak et al. (2016) calculated the unknown parameters of the single diode Rs model with the Simplified Explicit Method and Slope Method, using the catalog

information of the solar panel manufacturer firm sold for commercial purposes to determine the panel parameters. They created the I-V and P-V characteristics under different solar radiation intensity conditions in MATLAB environment and compared their closeness with experimental data.

Hussein (2017) provided a precise, closed-form expression for numerically solvable Rs while calculating the diode ideality factor in small increments to calculate the basic parameters required for the electrical characterization of PV modules, thus formulating four equations to calculate unknown parameters.

Stornelli et al. (2019) proposed a simplified five parameter estimation method for a single diode PV panel model. This method, based on an iterative algorithm, is based on estimating five parameters, starting with the data provided by the manufacturer of the single diode model. In the first step, it is tried to find the optimum value of the diode ideality factor and in the second step, the R_p value is calculated to increase the accuracy.

3. MATERIAL AND METHOD

In this section, information will be given about the photovoltaic cell first, then the ANFIS method to be used to predict the parameters of the photovoltaic cell will be introduced.

3.1. Material

3.1.1. Photovoltaic

Photovoltaic cell or solar cell are semiconductor materials that convert sunlight coming into their surface directly into electrical energy. Sunlight consists of energetic particles called photons. The energy of a photon is calculated by the following aquation which is known the Planck law (Chegaar et al., 2004).

$$E = hv = h\frac{c}{\lambda}\ (J) \tag{3.1}$$

In (3.1), h, v, c and λ represent the Planck constant ($6.63 \times 10^{-34}\ J\ s$), the frequency of the photon (Hz), the speed of light ($2.998 \times 10^{8}\ m/s$), the wavelength (m) of the photon, respectively. Since the energy in the atomic order is often expressed as eV ($1\ eV = 1.6 \times 10^{-19}\ J$), Planck equality can be arranged as follows by taking as μm the unit of wavelength:

$$E = \frac{1.24}{\lambda}\ (eV) \tag{3.2}$$

In order for the power conversion to take place in a photovoltaic cell, a photon of the semiconductor material equal to or higher than the forbidden band energy (E_g) must be absorbed by said cell. An electron in the semiconductor material encounters a photon with sufficient energy content and moves from the valence band

to the conduction band, and the resulting electron-hole pair (EHP) forms the basis of the energy conversion process in photovoltaic systems (Messenger et al., 2004).

3.1.2. Fundamentals of Semiconductor Physics

Semiconductors are materials in the 4A group of the periodic table and used in photovoltaic cell production. It is the semiconductor silicon with the most common use in photovoltaic technology. Silicium has 14 protons in its nucleus and thus 14 orbital electrons. As seen in Figure 3.1., silicon has 4 valence electrons in its outermost orbit, and it is +4 valued.

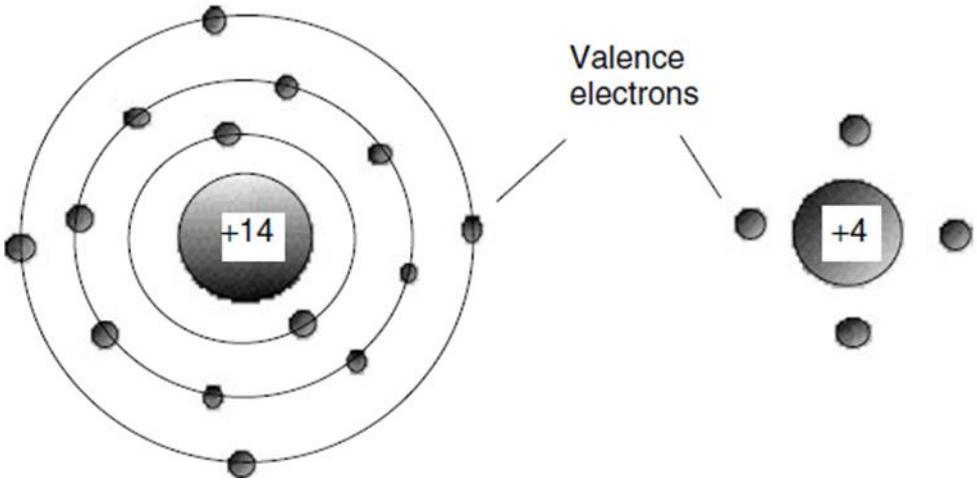


Figure 3.1. Electron order of silicon semiconductor (Masters,2004).

As shown in Figure 3.2., each atom in pure silicon crystal, completes the number of valence electrons to eight, by forming a covalent bond in tetrahedral form with four adjacent atoms.

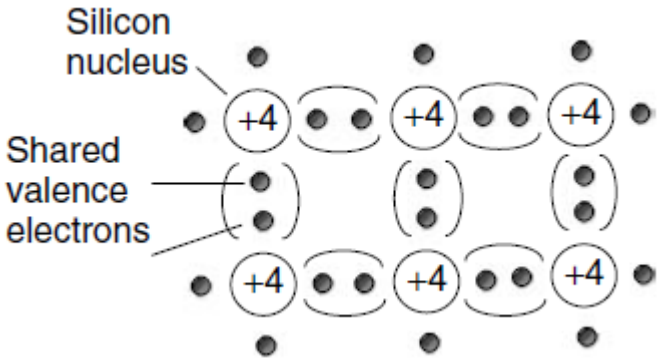


Figure 3.2. Covalent bond arrangement of silicon atoms (Masters,2004).

3.1.2.1. The Band Gap Energy

Silicon shows a super insulating property since it does not contain free electrons at absolute zero temperature. Some electrons in the valence band move to the conduction band by increasing the bond energies with increasing temperature.

Quantum theory reveals the differences between metals and semiconductors using the band energy diagrams shown in Figure 3.3. Accordingly, each electron is located in the band suitable for its energy level. The band with the highest energy level is the transmission band, and the electron density in this band determines the level of conductivity of the material. In metals, the transmission band is partially full, while in semiconductors it is completely empty at absolute zero temperature.

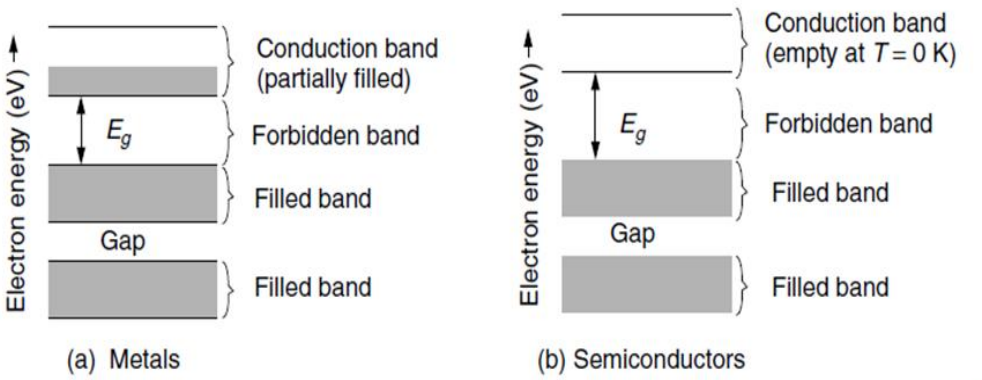


Figure 3.3. Representation of energy bands for (a) metals and (b) semiconductors (Masters, 2004).

According to the Quantum theory, the gaps between the energy levels where electrons can be found are called the forbidden band. The energy required for an electron to pass through its energy level to the conduction band is called the forbidden band energy and is denoted by E_g. The forbidden band energy unit is usually expressed as eV.

Forbidden band energy for silicon semiconductor is $E_g = 1.12\ eV$. This value is equal to the energy that an electron needs in order to be released by defeating the electrostatic force between the nucleus and it. If a photon with an energy content greater than 1.12 eV is absorbed by a PV cell, an electron passes into the transmission band by leaving a positively charged space behind it. The excited electrons and spaces lose their energy within a very short time ($10^{-12}\ s$). The electrons are on the underside of the transmission band, while the gaps are clustered on the upper part of the valence band. As a result, each electron loses a radiation energy equal to the forbidden band energy and rejoins with the gaps in the valence band. Figure 3.4. shows the formation and recombination of an electron-hole pair.

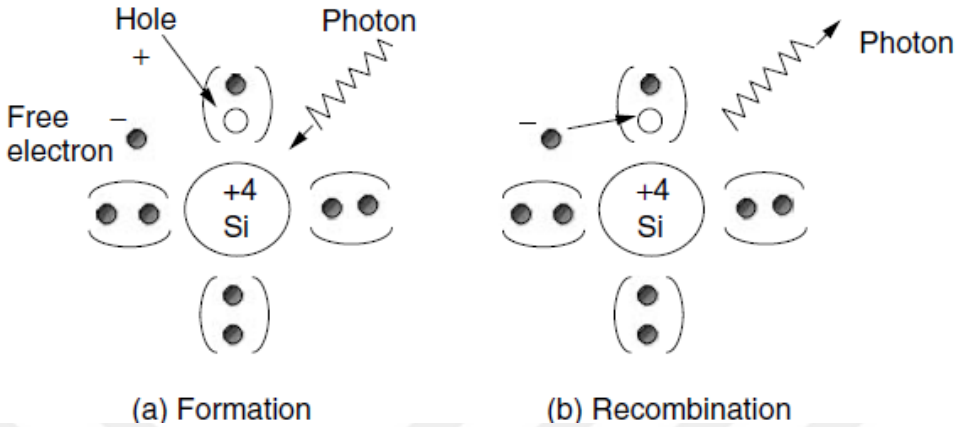


Figure 3.4. (a) Formation of electron-hole pair by the action of a photon with sufficient energy content. (b) an electron can recombine with the hole (Masters, 2004).

Like the negatively charged electrons, positively charged holes in the silicon crystal also have the ability to move freely. A valence electron belonging to a filled energy band of an atom can easily move into a space in the energy band of a nearby atom, as seen in Figure 3.5. This event can be identified by the fact that a student who lectures in the classroom leaves the her/his desk to drink water. In the example, the student represents a free electron, and the desk he/she abandoned represents the hole. When another student in the classroom gets up from his seat and sits in the queue vacated by his friend, he also provides a new vacancy. As a result of this situation gaining continuity within the classroom, the constant displacement of the empty desk can be considered as the movement of a gap in the semiconductor crystal.

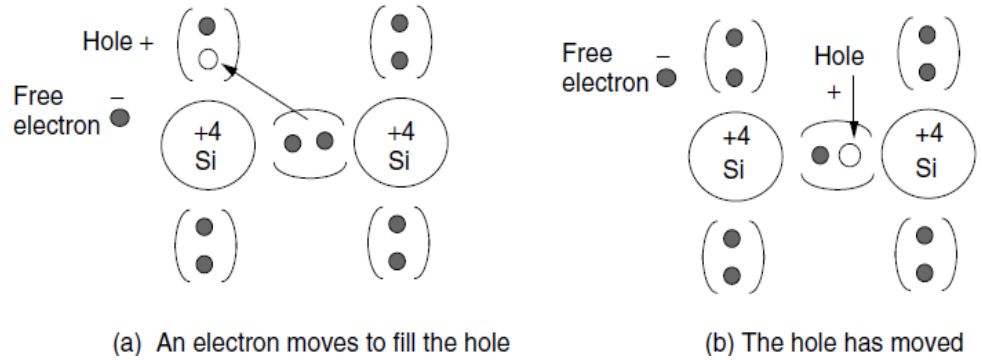


Figure 3.5. (a) An electron moving to a gap in the energy band of the nearby atom and (b) displacement of the hole (Masters, 2004).

Determining the minimum frequency and maximum wavelength values that a photon must have in order to form an electron-hole pair in the silicon semiconductor is important in terms of determining the available and lost energy quantities in the silicon photon energy-wavelength graph shown in Figure 3.6.

According to equation (3.1) photons with wavelengths longer than 1.11 μm for silicon semiconductor will not be able to form a pair of electron-hole and their energies will be spent as heat in the cell. Because a photon can stimulate only one electron, if it is cooled by a photon silicon semiconductor with a high energy content due to the short wave length, the extra energy above 1.12 eV is consumed as heat in the cell (Luque et al., 2003; Würfel, 2005).

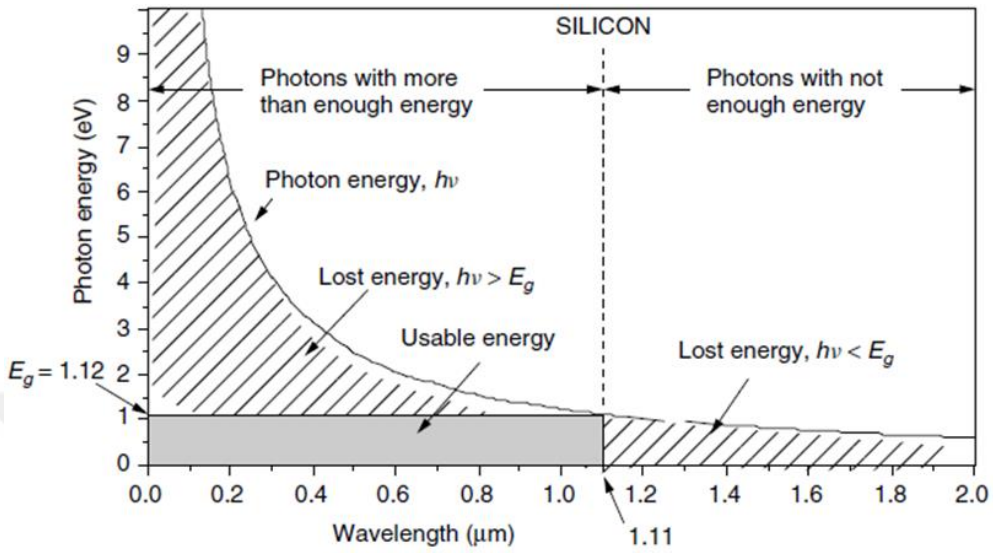


Figure 3.6. Photon energy-wavelength graph for silicon semiconductor (Masters,2004).

3.1.2.2. Solar Spectrum

The sun can be considered a source of radiation with similar spectral properties to a black object at a surface temperature of 5800 K. The solar constant is described as a radiation flux measured on the surface, a unit perpendicular to the sun's rays outside the atmosphere, and its value is 1377 W/m^2 . Some of the sun's rays are absorbed by various components during their movements in the atmosphere. The amount of solar energy reaching the earth significantly depends on the location of the sun's rays relative to a point on the earth. This position is expressed by the factor $air\ mass$ (AM) (Muneer et al., 2004; Şen et al., 2008; Markvart et al., 2003).

$$AM = 1/cos\theta \tag{3.3}$$

The conditions AM = 1 and AM = 1.5, which correspond to 0 ° and 48 ° values of the zenite angle (θ), are widely used in studies related to photovoltaic

technology. For AM = 1.5, Figure 3.7. shows the solar spectrum. 2% of the spectrum consists of ultraviolet, 54% is visible and 44% is made of infrared rays. Since 20.2% of the solar energy coming to the unit surface consists of photons with a wavelength longer than 1.11 μm, it cannot be used in energy conversion. Similarly, 30.2% of the total radiation energy is consumed as heat in the cell as it has a greater energy content than the forbidden band energy.

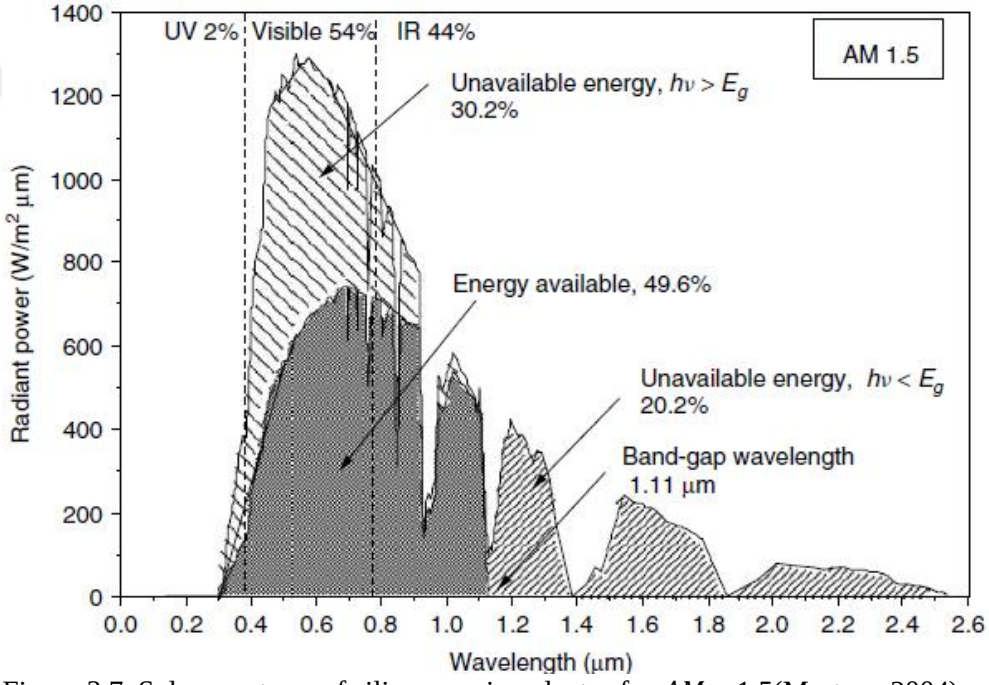


Figure 3.7. Solar spectrum of silicon semiconductor for AM = 1.5(Masters, 2004).

3.1.2.3. The p–n Junction of Semiconductors

As long as a photovoltaic cell is provoked by photons with a higher energy content than the forbidden band energy, the formation of electron-space pairs in the semiconductor material continues. The main problem here is that the charge carriers disappear before completing the energy conversion as a result of the recombination of electrons and holes. To prevent recombination, a force is needed to keep the

electrons in the transmission tape away from the holes. This force is provided by an electrical field created in the semiconductor material. This electrical field prevents recombination by pushing electrons and voids in opposite directions. In order to create an electric field in the semiconductor material, two different regions are created in the crystal. One of the regions is created by adding an element in the 3A group of the periodic table to the pure silicon crystal at very low concentrations. The other region is formed by adding an element in the 5A group of the periodic table to the pure silicon crystal.

As an example, if phosphorus in the 5A group of the periodic table is added to the silicon crystal, four valence electrons of phosphorus covalently bond with four valence electrons of silicon, and the fifth valence electron of phosphorus is released within the crystal as shown in Figure 3.8. Such atoms are given a donor atom step because it supplies the crystal with extra electrons.

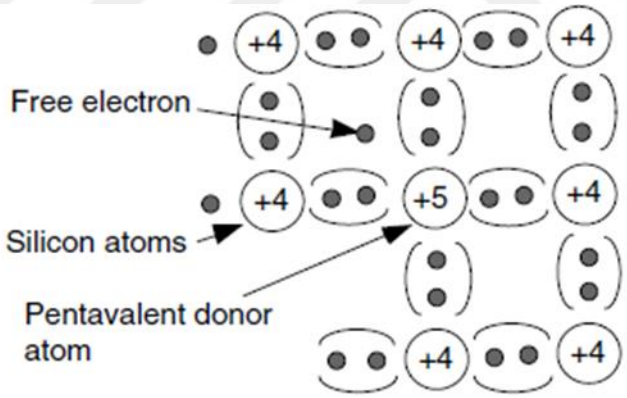


Figure 3.8. The donor atom in silicon crystal (Masters, 2004).

As seen in Figure 3.9., the donor atom can be represented by a stationary, positively charged ion and an electron capable of free movement within the crystal.

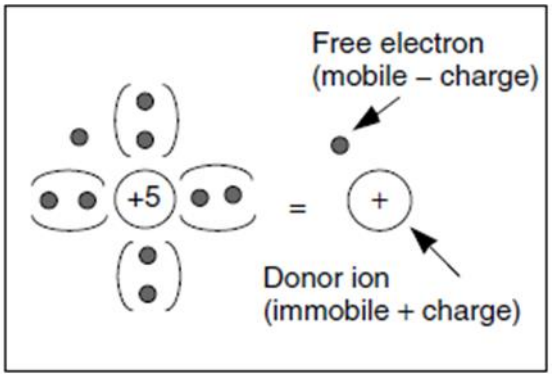


Figure 3.9. Identification of the donor atom (Master, 2004).

If boron in the 3A group of the periodic table is added into the silicon crystal, three valence electrons of boron and four valence electrons of silicon makes covalent bonds among themselves, and so electron deficiency occurs in the crystal. An electron belonging to the neighboring silicon atom can easily fill the existing hole as seen in Figure 3.10. These atoms are called acceptors atoms because they cause the need for electrons in the crystal.

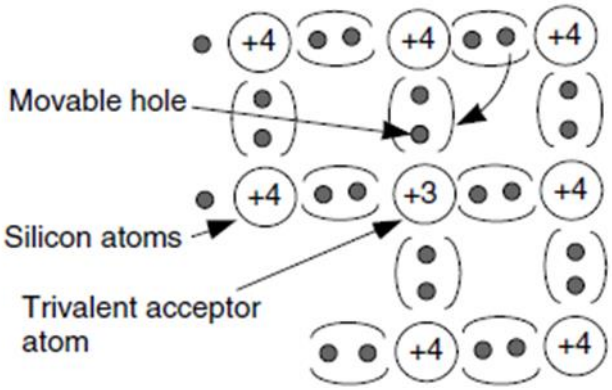


Figure 3.10. The Acceptor atom in silicon crystal (Masters, 2004).

As indicated in Figure 3.11., the acceptor atom can be expressed by a fixed, negatively charged ion, and a hole with free mobility within the crystal.

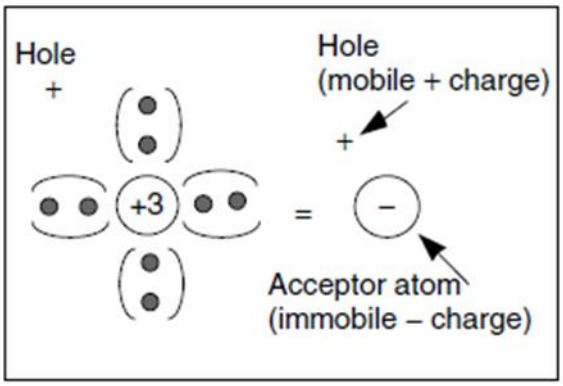


Figure 3.11. Identification of the acceptor atom (Masters, 2004).

Since there is an excess of electrons in the area where the donor atoms are located in the silicon crystal, this section is called *n-type material*. On the other hand, the section containing the acceptor atoms is called *p-type material* since there is an excess of hole in this area in the crystal.

As seen in Figure 3.12., when n-type material and p-type material are combined along a joint boundary, moving electrons in the n region and moving holes in the p region begin to move towards each other. As stated in Figure 3.13, when an electron crosses the joint boundary, it fills a hole and occurs a constant, positively charged ion in the n region while it forms a stable, negatively charged ion in the p region. These inert and charged atoms create an electric field by preventing the movement of electrons and holes from the joint boundary. The width of the free zone is approximately 1 μm. This region pushes the holes towards the p region and the electrons towards the n region.

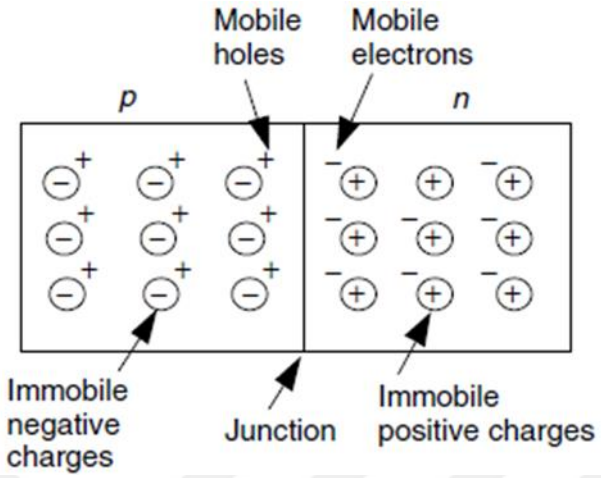


Figure 3.12. The n and p regions combined along a joint (Masters, 2004).

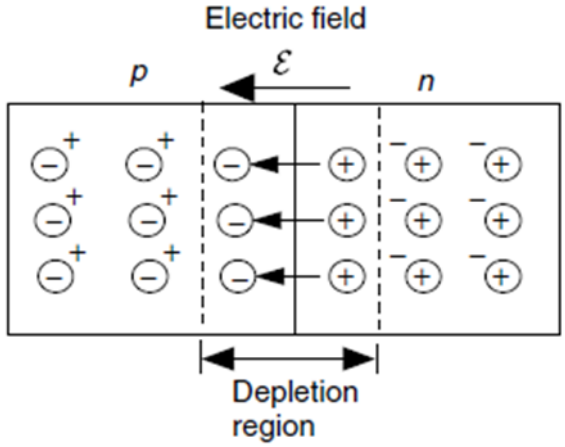


Figure 3.13. The electrical field formed by immobile, charged atoms (Masters, 2004).

3.1.3. Energy Conversion in Photovoltaic Cell

When a photovoltaic cell is exposed to sunlight, electron-hole pairs are formed in the crystal thanks to photons with sufficient energy content. When these mobile charge carriers approach the joint region, the electrons are pushed towards

the n region and the holes towards the p region owing to the electrical field within the charge-free zone as seen in Figure 3.14.

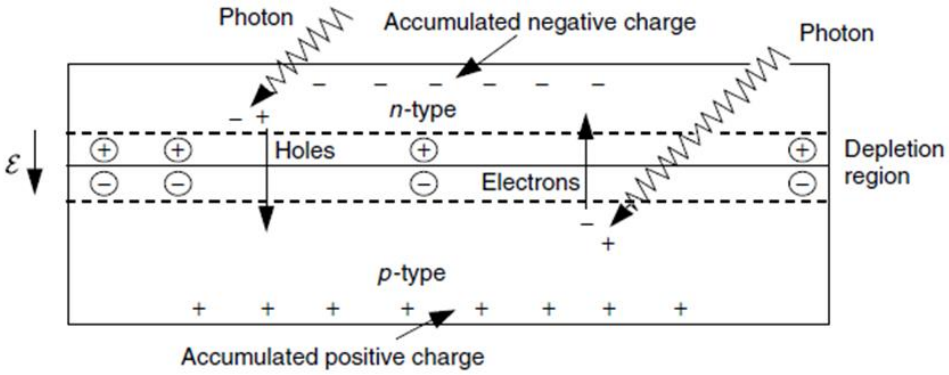


Figure 3.14. Pushing electrons and holes towards the poles by the electric field (Masters, 2004).

Adding opposite charges at two poles of the crystal creates a potential difference. If a conductive wire and two poles are combined as in Figure 3.15., electrons in the n region move towards the holes in the p region. Here, electrons reunited with holes complete the circuit. The direction of the current occurs in the opposite direction to the electron movement. In other words, it is from region p to region n.

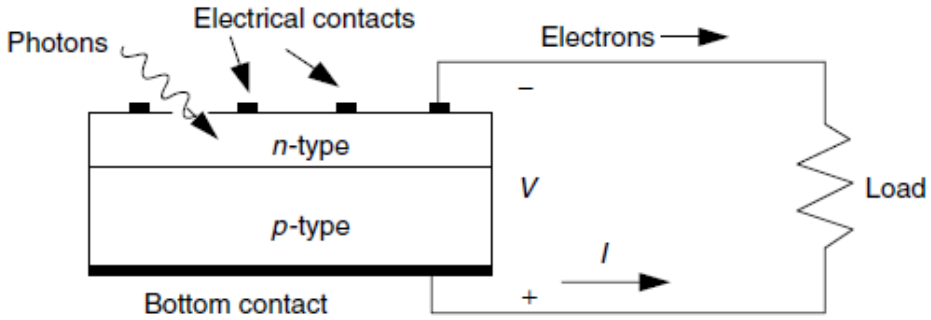


Figure 3.15. Direction of electrons and electric current in photovoltaic cell (Masters, 2004).

3.1.4. Electric circuit models of PV cells

During exposure to sunlight, what happens to p-n joint, let's consider. Space electron pairs can occur when photons are absorbed. If these moving charge carriers reach the periphery of the junction, the electric field in the depletion zone will push the gaps to the p side and the electrons to the n side as shown in Figure 3.14. While the p-side accumulates voids, the n-side accumulates electrons. This case, creates a voltage that can be used to transmit current to a charge (Masters, 2004)..

If the electrical contacts are attached to the top and bottom of the cell, the electrons will flow to the connecting wire by the n-side, along the charge and back to the p-side as shown in Figure 3.15 (Masters, 2004).

Since the wire cannot gap, it is only electrons that move around the circuit. When electrons reach the p -side, they reunite with the gaps that complete the circuit. Traditionally, the positive current flows in the opposite direction of the electron flow, hence current arrow in the manner shows the current from the p-side towards the load again to the n-side (Masters, 2004).

3.1.4.1. The Simplest Equivalent Circuit for a Photovoltaic Cell

Figure 3.16 depicts the elements of a simple equivalent circuit model for a photovoltaic cell. As it can be seen, real diode, parallel to an ideal current source are the main elements. In the presence of an ideal current source, a current proportional to the solar flux is obtained (Masters, 2004).

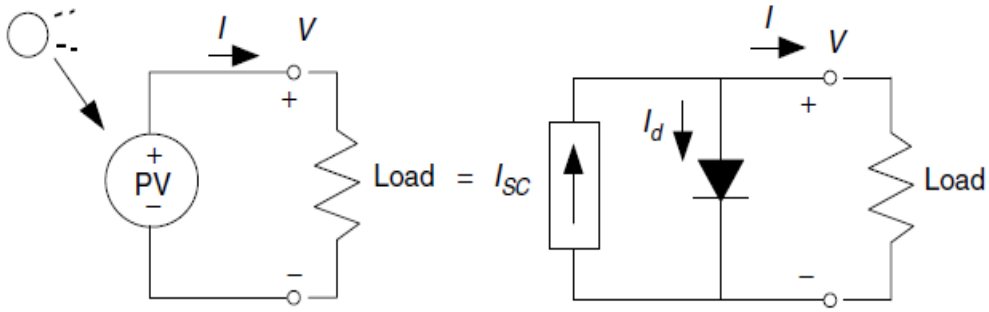


Figure 3.16. A Simple equivalent circuit for a photovoltaic cell. (Masters, 2004).

There are two particularly interesting conditions for the actual PV and equivalent circuitry. As shown in Figures 3.17. and 3.18., the first is the current flowing (short circuit current, I_{SC}) when the terminals are shorted together, and the second is the voltage at the end when the terminals are left open (open circuit voltage, V_{OC}). When the ends of the equivalent circuit for the PV cell are short-circuited together, no current flows on the diode (real) diode, as $V_d = 0$, so all current from the ideal source passes through the short-circuit cables. Since this short circuit current should be equal to I_{SC}, the size of the ideal current source itself should be equal to I_{SC} (Masters, 2004).

The two most important performance parameters in a photovoltaic cell are short circuit current and open circuit voltage. The short circuit current of the photovoltaic cell is the current measured when the poles of the circuit are shorted, as seen in Figure 3.17 (Masters, 2004).

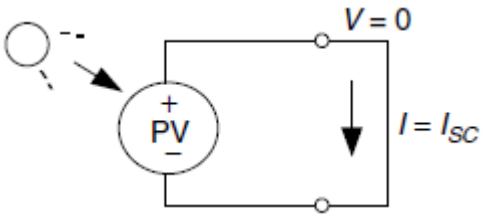


Figure 3.17. Short circuit current of photovoltaic cell (Masters, 2004).

The open circuit voltage is the voltage read from the poles of the photovoltaic cell, when the current passing through the circuit is equal to zero, as expressed in Figure 3.18.

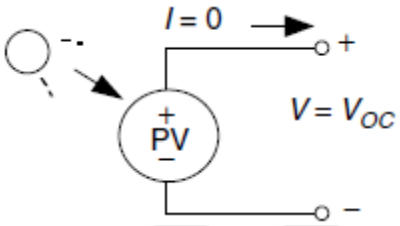


Figure 3.18. Open circuit voltage of photovoltaic cell (Masters, 2004).

Now we can write a voltage and current equation for the equivalent circuit of the PV cell shown in Figure 3.16.

$$I_d = I_0(e^{\frac{qV_d}{kT}} - 1) \tag{3.10}$$

$$I = I_{SC} - I_d \tag{3.11}$$

and then when we put (3.10) in place of (3.11), we get

$$I = I_{SC} - I_0(e^{\frac{qV_d}{kT}} - 1) \tag{3.12}$$

It is interesting to note that the second term in (3.12) is simply the negative-sign diode equation. This means that a graph of (3.12) is the inverse I_{SC} added only to the diode curve in Figure 3.19.

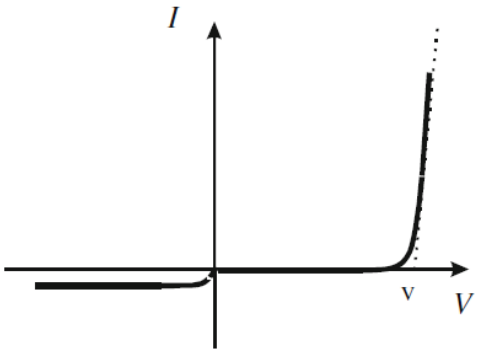


Figure 3.19. Diode characteristic curve (Di Piazza and Vitale, 2013).

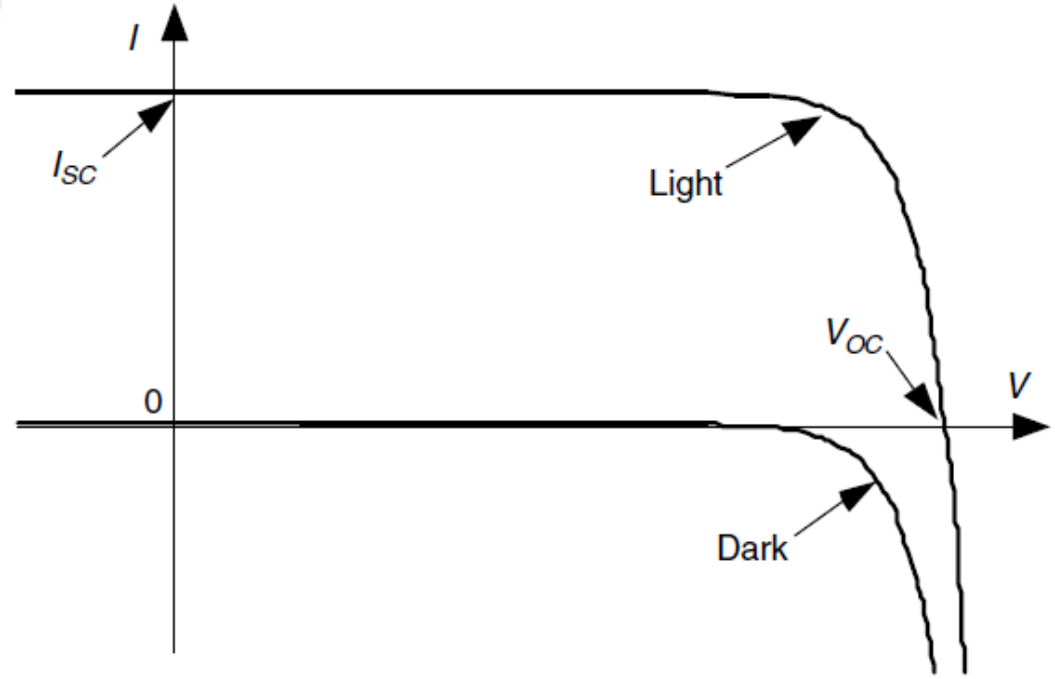


Figure 3.20. Photovoltaic current-voltage relationship when dark (no sunlight) and light (an illuminated cell) (Masters, 2004).

The dark curve is just the inverted diode curve. The luminous curve is the dark curve plus I_{SC}.

When the ends from the PV cell are left open, $I = 0$ and we can solve (3.12) for the open circuit voltage V_{OC} (Masters, 2004);

$$V_{OC} = \frac{kT}{q}\ln(\frac{I_{SC}}{I_0} + 1) \quad (3.13)$$

3.1.4.2. A More Accurate Equivalent Circuit for a PV Cell

There can be times when a more complex PV equivalent circuit than present in Figure 3.21 can be required. For instance, consider the effect of shading on a wired cell array in series. If any string is in the dark (shaded), it will not generate current. In our simplified equivalent circuit for the shaded cell, the current passing through the current source of this cell is zero, and the diode is back biased so that no current can pass (except for a small amount of reverse saturation current). This means that the simple equivalent circuit will not power a load if any of its cells are shaded. Whereas it is true that PV modules are very sensitive to shading, the situation is not so bad. Thus, we need a more complicated model if we can deal with facts like the shading problem.

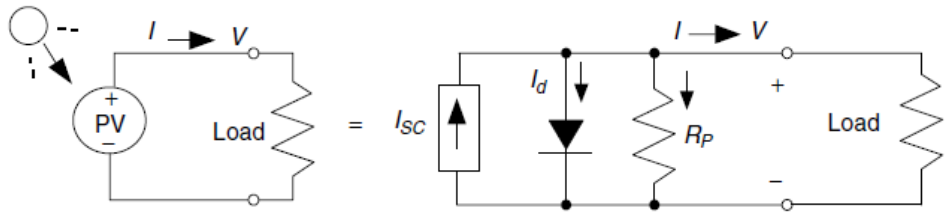


Figure 3.21. Simple PV equivalent circuit with parallel resistor added. (Masters, 2004).

Figure 3.21 shows a PV equivalent circuit containing some parallel leakage resistance R_P . In this case, I_{SC} which is the ideal current source, gives current to the diode, parallel resistor and load:

$$I = (I_{SC} - I_d) - V / R_P \quad (3.14)$$

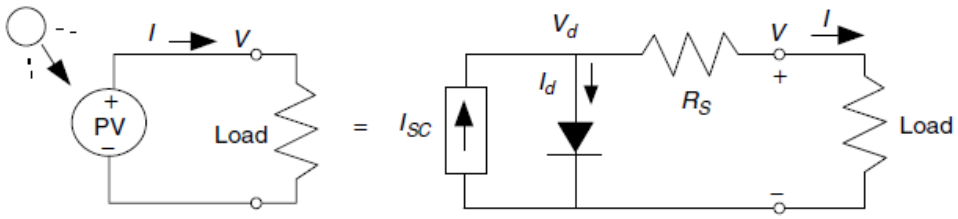


Figure 3.22. A PV equivalent circuit with series resistance (Masters, 2004).

A better equivalent circuit will include parallel resistance as well as series resistance. Before developing this model, consider Figure 3.22, where the original PV equivalent circuit was only replaced to include some series resistors R_S. Some of these may be contact-related contact resistance between the cell and the cable ends, and some may be because of the resistance of the semiconductor itself.

$$I = I_{SC} - I_d = I_{SC} - I_0(e^{\frac{qVd}{nkT}} - 1) \tag{3.15}$$

$$V_d = V + I * R_S \tag{3.16}$$

$$I = I_{SC} - I_0\{\exp\left[\frac{q(V+I*R_S)}{nkT}\right] - 1 \tag{3.17}$$

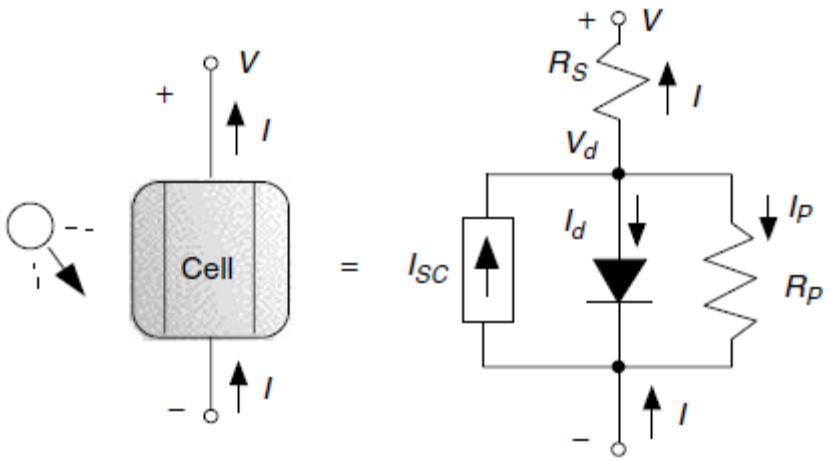


Figure 3.23. A more complex equivalent circuit for a PV cell involves both parallel and serial resistors. (Masters, 2004).

Finally, let's generalize the PV equivalent circuit by including both series and parallel resistors as shown in Figure 3.23. We can write the following equation for current and voltage:

$$I = I_{SC} - I_0 \left\{ \exp\left[\frac{q(V+I*R_S)}{nkT}\right] - 1 \right\} - \left(\frac{V+I*R_S}{R_P}\right) \quad (3.18)$$

3.1.5. The $I - V$ curve of PV and basic parameters

In the case of connection a single PV module to a load that can be a dc motor running a pump or be a battery, at first, the module sitting in the sun will generate an open circuit voltage V_{oc}, but the current will not flow as shown in Figure 3.18. If the module's terminals are short-circuited together, the short circuit current I_{SC} will flow, but the output voltage will be zero. This is shown in Figure 3.17. In both cases, since power is the product of current and voltage, it is not powered by the module and is not powered by the load. When the load is actually connected, some combination of current and voltage will appear and power will be given. To find out how much power, we need to consider the $I - V$ characteristic curve of the module as well as the $I - V$ characteristic curve of the load.

Figures 3.24. and 3.25. show a general $P - V$ and $I - V$ curve for a PV module obtained using MATLAB, that defines many key parameters, including open circuit voltage V_{OC} and short circuit current I_{SC}. In addition, power provided by the module is the product of voltage and current is also shown. At both ends of the $I - V$ curve, the output power is zero because the current or voltage is zero at these points.

The maximum power point (MPP) is the point close to the knee of the $I - V$ curve, where the current and voltage product reaches its maximum. The voltage and current in MPP are sometimes determined as V_M and I_M for the general situation and

determined V_R and I_R (for nominal voltage and nominal current) under special conditions that corresponding to idealized testing conditions.

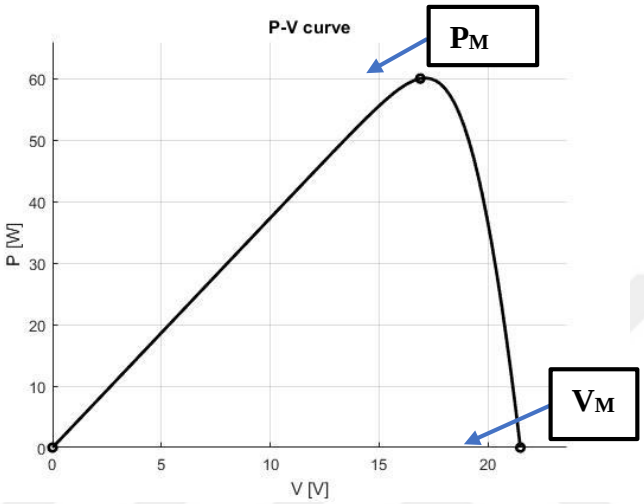


Figure 3.24. P-V curve of a PV module

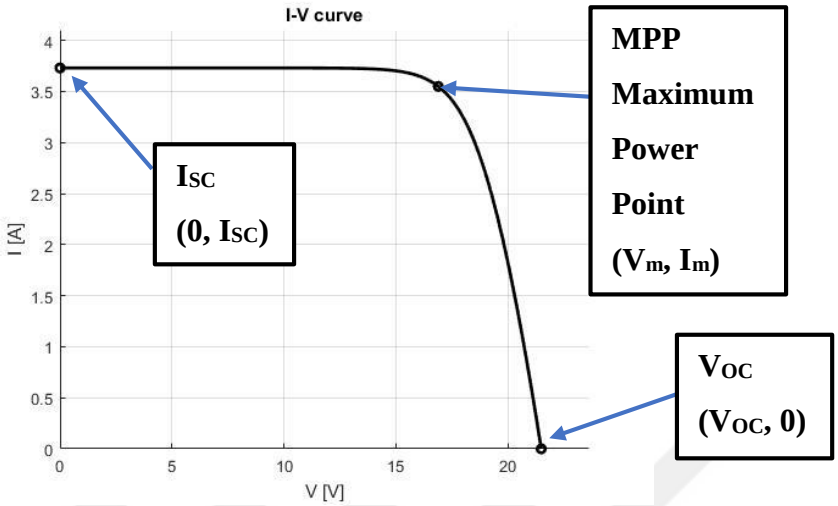


Figure 3.25. $I-V$ curve of a PV module

3.1.5.1. Effect of solar radiation value and temperature on photovoltaic cell's $I-V$ characteristic curve

Model simulations for photovoltaic cells; In addition to its characteristic features during operating conditions, the continuously changing radiation intensity and temperature parameters during the day significantly change the current value obtained through the photovoltaic panel.

3.1.5.1.(1). Effect of Solar Radiation Intensity

As a result of the increase in the value of the radiation coming from the sun; Since the increase in the number of photons falling on the photovoltaic panel will increase the probability of removing electrons from the n-type semiconductor material on the panel, the amount of current produced by the panel also increases. At the same time, the open circuit voltage increases slightly with the effect of radiation intensity. The increase in the radiation intensity due to the increase of both values increases the power value obtained from the photovoltaic panel.

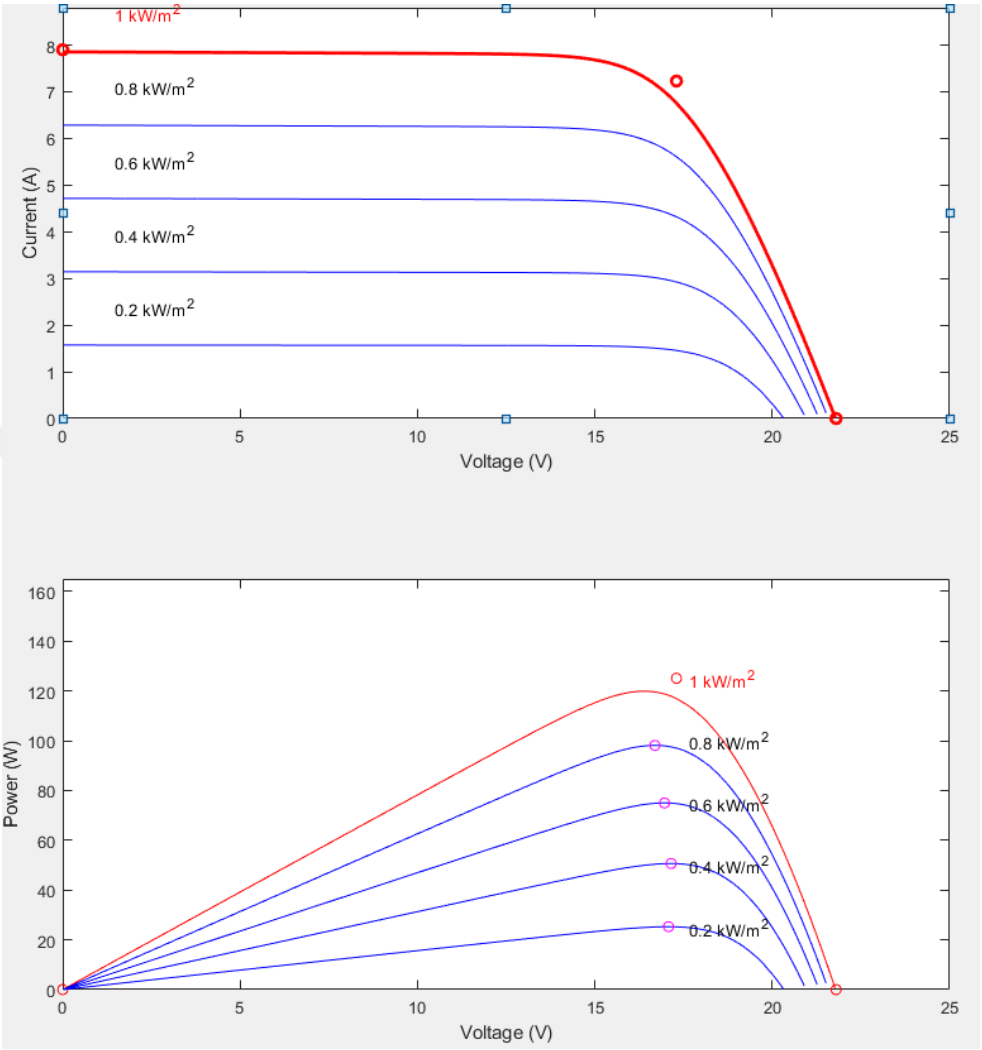


Figure 3.26. The Effect of Radiation Intensity Value on the Current- Voltage and Power-Voltage Values of the Photovoltaic Cell

The graph shown in Figure 3.26 shows the change in the current and voltage values of the photovoltaic cell as a result of the change in radiation intensity. The photon current (I_{ph}) obtained from the photovoltaic cell as a result of the change of irradiation intensity changes significantly. In order to calculate the photon current

(I_{ph}) value obtained from the photovoltaic cell at certain irradiance, the following equation (3.19) is used.

$$I_{ph} = \frac{G}{G_{ref}}[I_{ph,ref} + \mu_{Isc}(T_C - T_{C,ref})] \quad (3.19)$$

Here;

$I_{ph,ref}$ is photon current reference value *(A),*

G is radiation intensity (W/m^2)

G_{ref} is radiation intensity reference value (W/m^2)

μ_{Isc} is temperature coefficient of short current (A/K)

T_C is photovoltaic cell temperature *(K)*

$T_{C,ref}$ is photovoltaic cell reference temperature (K)

Standard test conditions (STC) $T_{C,ref} = 25\ ℃$, $G_{ref} = 1000\ (W/m^2)$

3.1.5.1.(2). Effect of Temperature

When light energy from the sun falls on photovoltaic cells, it significantly changes the temperature of the photovoltaic cell. With the changing temperature value, the current and voltage values of the photovoltaic cell vary significantly, which changes the amount of power obtained from the photovoltaic cell. Increasing the temperature value increases the current value produced by the photovoltaic cell, while causing the voltage value to decrease significantly. This change as a result of the temperature effect causes the maximum power point value to decrease to lower levels. As a result of this situation, the efficiency to be obtained from the photovoltaic cell decreases. The change of the current and voltage values occurring in the photovoltaic cell with the temperature change is shown in Figure 3.27.

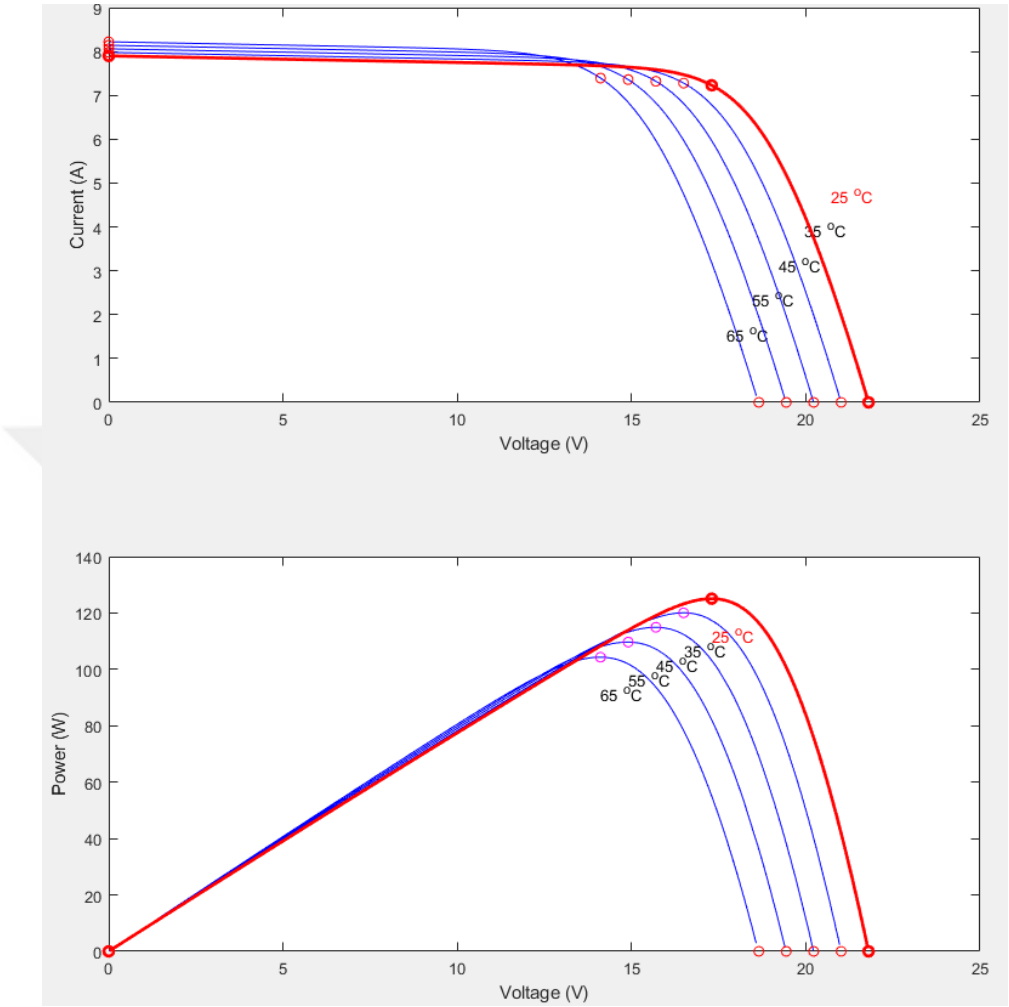


Figure 3.27. The Effect of Temperature Value on the Current- Voltage and Power-Voltage Values of the Photovoltaic Cell

3.1.6. Factors Affecting Characteristics of the PV Cell

Described in Section 3.1.4, the solar cell model regards the ideal behavior of a solar cell under ideal current and diode conditions. In some cases, such kind of a level-forward models are inadequate to present the characteristics of the solar cells. Several effects might affect, which are not taken into account, the reaction of the solar cells.

Parallel resistance is a cell parameter of a photovoltaic cell that affects the characteristic of area between the short circuit current and the maximum power point on the *I* - *V* curve. Decrease of parallel resistance of the photovoltaic cell, the area under the *I* - *V* curve as seen in Figure 3.28., so it reduces the output power from the photovoltaic module.

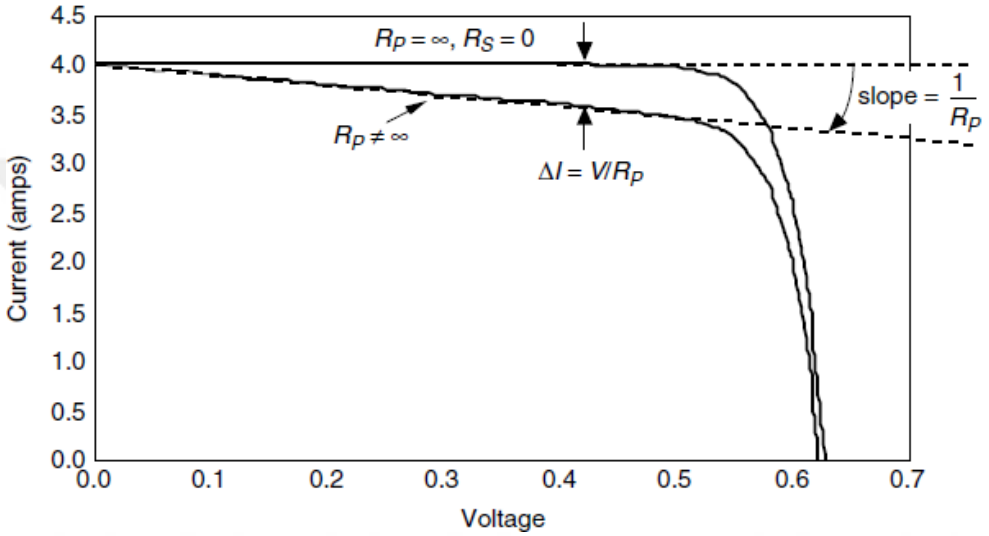


Figure 3.28. Effect of parallel resistance on curve *I* -*V* (Masters, 2004).

Series resistance is a cell parameter of the photovoltaic cell that affects the characteristic of area between the open circuit voltage and the maximum power point on the *I* -*V* curve. As a result of the increase of the series resistance of the photovoltaic cell, as seen in Figure 3.29., the value of the area under the *I* - *V* curve decreases and accordingly the output power obtained from the photovoltaic module decreases.

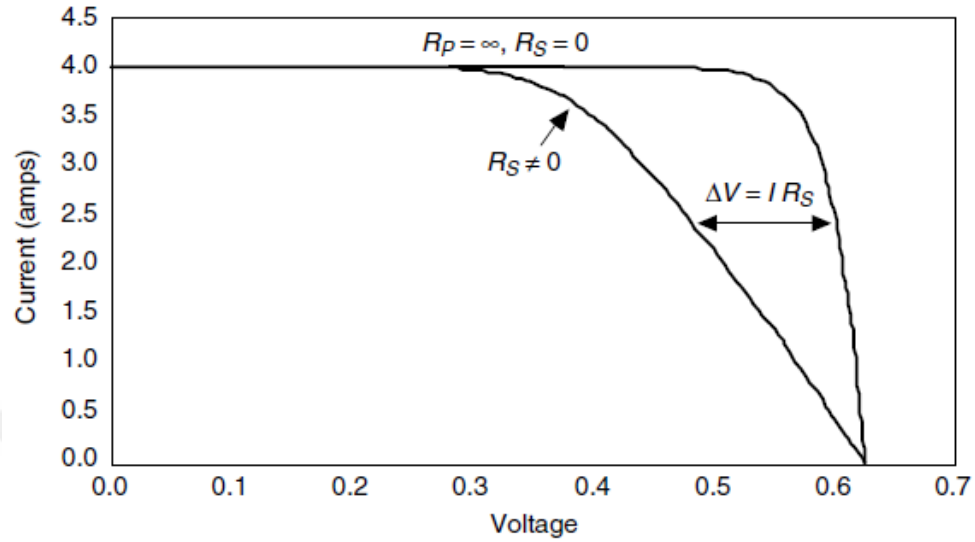


Figure 3.29. Effect of series resistance on the *I -V* curve (Masters, 2004).

3.2. Method

This section describes in detail the theoretical background of Artificial Neural Network (ANN) and Adaptive Neuro-Fuzzy Inference System (ANFIS).

3.2.1. Artificial neural networks

In general, an artificial neural network (ANN) is a system developed with the aim of information processing that allowing the functioning in a similar way to acting procedure of the biological nervous systems. The working procedure of the ANN is developed as similar to human brain, which has the ability of processing huge and complex nonlinear data and information and has also the characteristic of working parallel, distributed and local processing and adaptation. The design of ANN resembles brain systematic in terms of building, learning for architectural and business techniques. Due to the accuracy of ANN and its ability to develop complex nonlinear models, it has been widely accepted by scientists for various purposes (Suparta et al.,2016)

This section will describe ANN's capabilities, such as neuron modeling, architecture, and the learning process.

3.2.1.1. Neuron Modeling

The interconnected neurons in the brain that can be seen from the Figure 3.30 for illustration that act as a tool to process information depending on the human senses. As it can be clearly seen from Figure 3.30, a biological neuron comprises of a cell body covered by a cell membrane (Haykin,2009). Moreover, in each of the cells, branched referred as dendrites which has the function of transporting information to the cells of the body through the axons.

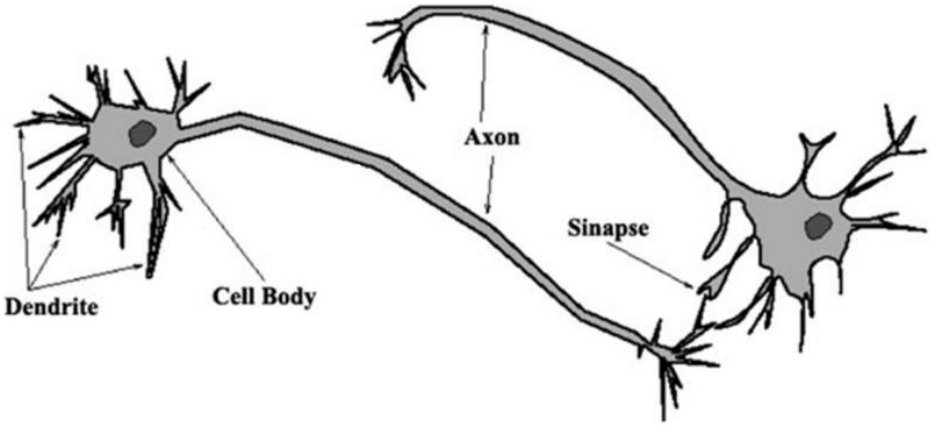


Figure 3.30. Schematic representation of a biological neuron (Haykin,2009)

axon is a long single fiber that convey the signal from the body of the cell to the next neuron. The small area between the neuron and the neighbor neuron, which also referred as the meeting point among dendrites and axons, is called as synapse. This area conducts the function of transporting the information. The information reaching this area coded as electrical signals. Then, the electric signal are counted. The number of electrical signals reacting to new electrical signal input that will be used by the adjacent neuron are calculated. Regardless of the limit or

threshold values, if the electrical signals cannot be distinguished from the predetermined threshold, the synapses will be delayed. The backwardness of synapses causes inhibition of the relationship between the two neurons. In parallel with the biological neuron model, McCulloch and Pitt (1943) reported a model neuron having the property of transmitting and receiving processing-like information processes occurring in biological neurons. The basics of the current ANN model are based on this neuron modelling. Determining the function and function of the network are determined by a neuron. A representative mathematical model of neurons applied in ANN model can be seen in Fig. 3.31.

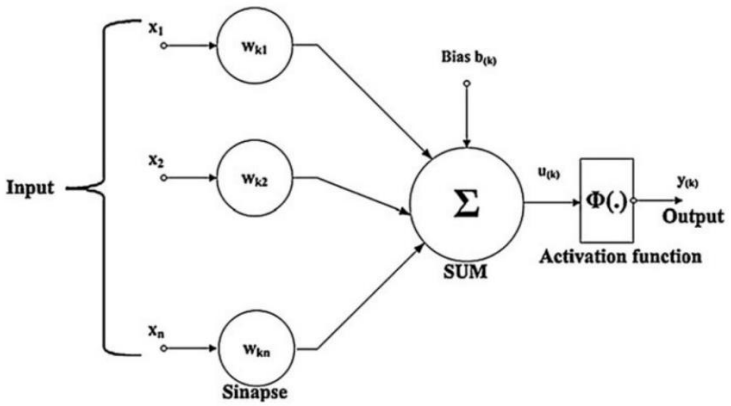


Figure 3.31. A sample ANN mathematical modeling of a neuron (Suparta et al.,2016).

The neuron modeling based on Figure 3.31. can be illustrated by the following math equation:

$$u_{(k)} = \sum_{j=1}^{n} w_{kj}\, x_j \; and \; y_{(k)} = \varphi\left(u_{(k)}\right) + b_{(k)} \tag{3.21}$$

where $u_{(k)}$ is the output of the adder function of the neuron model, w_{kj} is the weighted in the path of synapse j to k neuron, and x_j is data or input signal on path

synapse j. The output of the neuron is represented by $y_{(k)}$, where it is dependent on the activation function $\varphi(.)$ and, the bias $b_{(k)}$. Numerous activation function can be used in the modelling of neurons, some of which are linear function, fixed limiting function, bipolar sigmoid function and sigmoid function as they are shown in Figure 3.32. (Duch and Jankowski 1999; Dorofki et al. 2012).

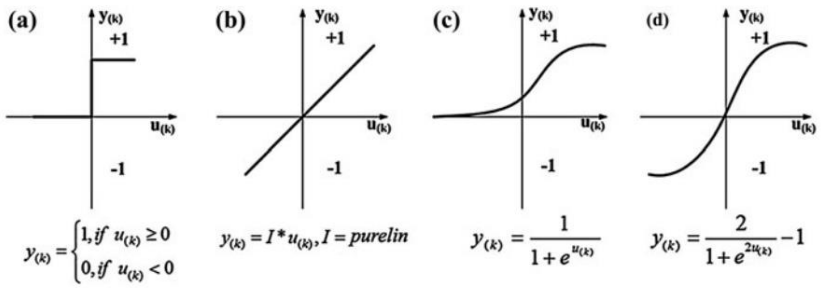


Figure 3.32. Activation function for (a) the fixed restrictor, (b) purelin, (c) log-sigmoid, and (d) bipolar sigmoid (Suparta et al.,2016).

3.2.1.2. Architecture

Net architecture is called as a pattern formed by the connections between neurons and other neurons. In normal, the architecture of the ANN consists of three layers, which are input, hidden and output layer. The input layer has the role of input or data receiver from an external stimulant. Then, the information is conveyed to the next layer so that there can be more than one neuron in this layer. Depending on the number of inputs to be used, the number of neurons can be altered in this layer. The next hidden can possess more data; indeed, electrical signal, than the previous layer. The result of the data processed in this layer using existing functions such as arithmetic and mathematics, then, directed to output layer. The output layer is the point where a decision about the validity of the data analyzed depending on the current limits of the activation function. The output of this layer can be used as output for the current situation.

The used connection model in the ANN architecture is deterministic on the categorization as feedforward neural network and the feedback neural network (Jain et al. 1996; Tang et al. 2007; Haykin 2009). In Figure 3.33 the taxonomy of the both ANN architectures can be seen. In feed forward neural network, there exist no feedback link in the architecture so that incoming signal is allowed to move only one direction. That is, the output of each layer cannot affect the that of others. Also, it can be developed by means of single or multiple layers. Generally, the multilayer component consists of three layers such that input, output and hidden layers. ANN types which use feed forward neural networks are single layer sensor, multi-layer sensor and radial basic function (Suparta et al.,2016).

Feedback neural network or repeater is another architecture and has a design similar to feed forward neural networks. The main difference from feed forward neural networks is the functionality of being present additional feedbacks slow or feedback on the previous layer. That is, the data or electrical signal is allowed to propagate forward and feedback and so that can be an input to the neurons before and can take role in dynamic applications (Suparta et al.,2016).

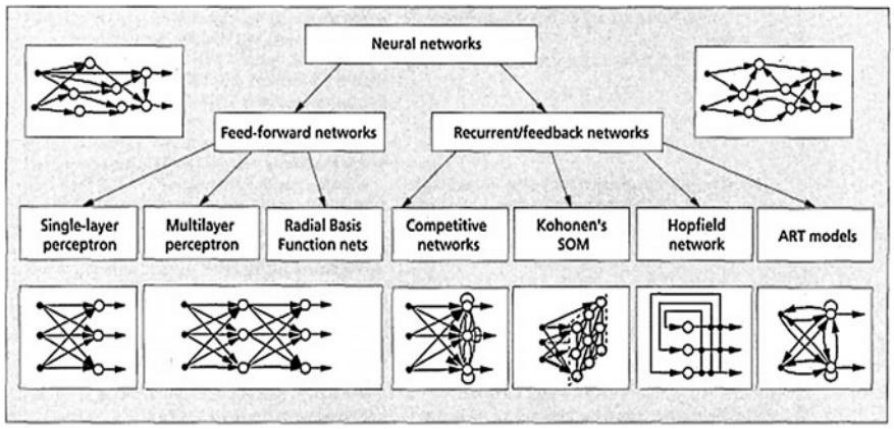


Figure 3.33. The architecture and the Taxonomy of feedforward and feedback neural networks (Jain et al., 1996).

3.2.2. Adaptive Neuro Fuzzy Inference System

Network-based fuzzy inference system (ANFIS) is a combination of two soft computing methods, ANN and fuzzy logic (Jang 1993). The qualitative aspects of human knowledge can be changed through the fuzzy logic and can gain a sensitive quantitative analysis process. However, there is no defined method of transformation and human thought into a rule-based fuzzy inference system (FIS). Also, it takes quite a long time to set up the membership functions (MFs) (Jang 1993). Unlike ANN, it has a higher ability to adapt to its environment in the learning process. Therefore, ANN can be used to automatically set MFs and reduce the error rate in setting rules in fuzzy logic.

3.2.2.1. Fuzzy Inference System (FIS)

There exist three major components, which are called as the basic rules where it consists of the selection of fuzzy logic rules “If-Then;” as a function of the fuzzy set membership; and reasoning fuzzy inference techniques from basic rules to get the output, in a Fuzzy Inference System (FIS). The detailed structure of the FIS can be seen in Figure 3.34. The FIS functions when the input consisting the actual value is converted to fuzzy values using the fuzzification protocol through the membership function, where the fuzzy value has a range between 0 to 1. The main rules and databases are called the knowledge base, where both are key parameters in decision-making. Under normal conditions, the database includes definitions such as information in the fuzzy sets parameter with a function that has been defined for each existing linguistic variable. Improving a database typically involves in turn the followings: defining a universe, determining the number of linguistic values to be used for each linguistic variable, and creating a membership function. Taken into consideration the rules, it includes fuzzy logic operators and a conditional statement "If-Then". In this point, basic rules can be formed from a human or automatic generation with search rules that use input-output data numerically. Takagi- Sugeno,

Mamdani and Tsukamoto are among the some of the several types of FIS (Cheng et al. 2005). In particular, it has been observed that FIS is predominantly applied in the Takagi-Sugeno model as an application of ANFIS method.

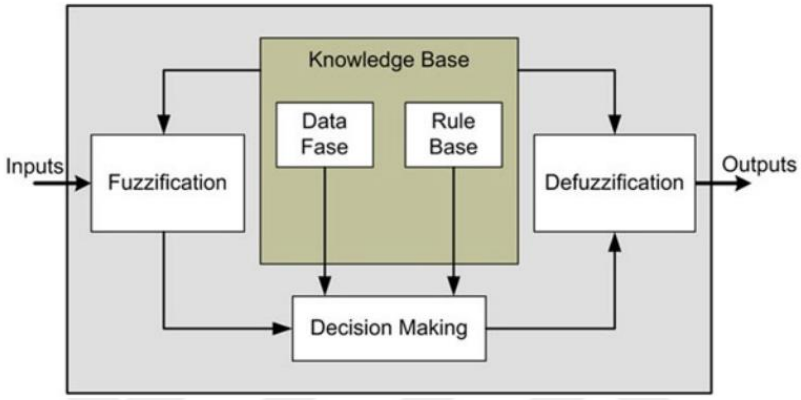


Figure 3.34. A schematic representation of a FIS (Suparta et al.,2016).

3.2.2.2. Adaptive Network

Adaptive network is an example of a feed forward neural network with multiple layers. In the learning process, these networks often use the supervised learning algorithm. In addition, the adaptive network has architectural features consisting of several adaptive nodes that are directly connected together without any weight value between them. Different function and task are coded for each node in this network. Incoming signal and parameters present in the node can have great influence on the output. The occurrence of error in the adaptive network can be minimized by the used learning rule (Jang, 1993).

The basics of the all of the learning algorithms including gradient descent and back propagation used in the learning process of the basic adaptive network were proposed by Werbos in 1970 (Jang 1993). Up to now, even if the back propagation and gradient descent techniques are still employed; nevertheless, the deficiencies in the back propagation algorithm causing the reduction in the capacity and the

accuracy of the adaptive networks during the decision-making process. The slow convergence rate and the tendency to always stick to the local minimum are important problems in the back propagation algorithm. For this reason, Jang (1993) proposed an alternative learning algorithm, namely the hybrid learning algorithm, which has a better capacity to accelerate convergence and prevent trapped formation in the local minima.

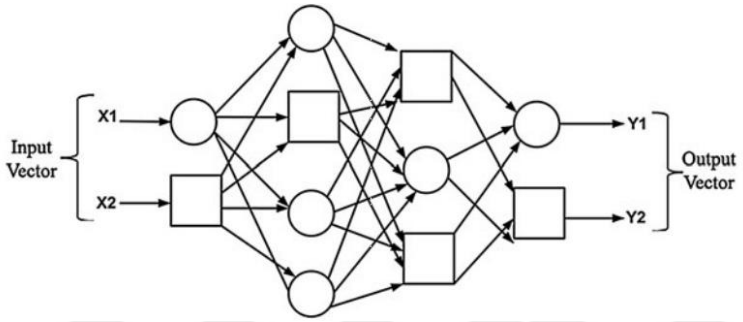


Figure 3.35. Adaptive network (Suparta et al.,2016).

3.2.2.3. ANFIS Architecture

ANFIS architecture is an adaptive network that uses supervised learning on the learning algorithm, with a function similar to the Takagi-Sugeno fuzzy inference system model. Figures 3.36 a) and b) show the fuzzy fuzzy reasoning mechanism for the Takagi-Sugeno model and ANFIS architecture. In terms of simplicity, let's suppose that there exist two inputs x and y and one output f. Two rules are used in the method of "If-Then" for Takagi–Sugeno model, as follows:

$$Rule\ 1 = If\ x\ is\ A_1\ and\ y\ is\ B_1\ \ Then\ f_1 = p_1x + q_1x + r_1 \tag{3.22}$$

$$Rule\ 2 = If\ x\ is\ A_2\ and\ y\ is\ B_2\ \ Then\ f_2 = \ p_2y + q_2y + r_2 \tag{3.23}$$

where A_1, A_2 and B_1, B_1 are the membership functions of each input x and y, while p_1, q_1, r_1 and p_2, q_2, r_2 are the linear parameters of the Takagi-Sugeno fuzzy inference model.

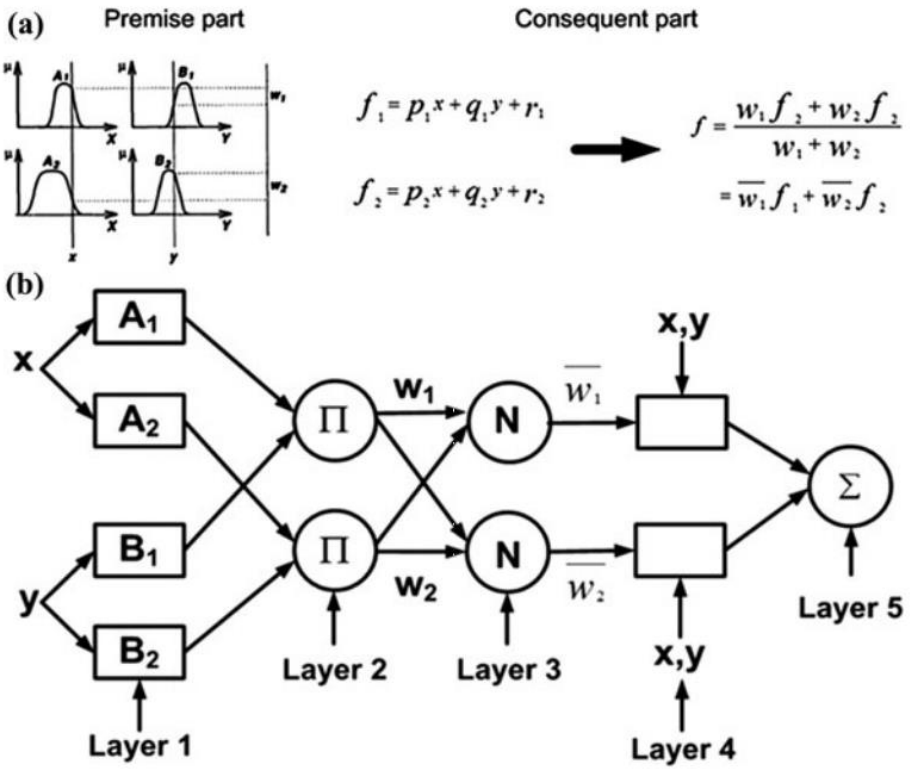


Figure 3.36. (a) Sugeno fuzzy interference system "If-Then" and fuzzy logic mechanism and (b) ANFIS architecture (Suparta and Alhasa 2013)

Looking at Figure 3.36, there exist five layers in the ANFIS architecture. The first and fourth layers contain an adaptive node, while the other layers contain a fixed node. A short description of each layer is as follows (Suparta et al.,2016):

Layer 1: A function parameter is obeyed by each node in this layer. Each node has an output which is the resemble of a degree of a membership value driven by the

input of membership function. In particular, a Gaussian membership function (Eq. 3.24) can be a membership function.

$$\mu_{Ai}(x) = e^{[-\left(\frac{x-c_i}{2a_i}\right)^2]} \tag{3.24}$$

$$\mu_{Ai}(x) = \frac{1}{1+\left|x-\frac{c_i}{a_i}\right|^{2b}} \tag{3.25}$$

$$O_{1,i} = \mu_{Ai}(x), i = 1,\ 2 \tag{3.26}$$

$$O_{1,i} = \mu_{Bi-2}(y), i = 3,\ 4 \tag{3.27}$$

where μ_{Ai} and μ_{Bi-2} are the degree of membership functions for the fuzzy sets A_i and B_i, respectively, and $\{a_i, b_i, c_i\}$, are the leading parameters that can effect the shape of the membership function.

Layer 2: The circle node is labeled Π and each node in this layer is fixed or nonadaptive. The multiplication of the signal to the node and sending to next node leads to output node.

$$O_{2i} = w_i = \mu_{Ai}(x) * \mu_{Bi}(y), i = 1, 2 \tag{3.28}$$

where w_i is the output that represents the firing strength of each rule.

Layer 3: Each node in this layer is fixed or nonadaptive, and the circle node is labeled N. Each node is a calculation of the ratio between the *i-th* rules firing strength and the sum of all rules firing strengths.

$$O_{3i} = \overline{w}_i = \frac{w_i}{\sum_i w_i} \tag{3.29}$$

Layer 4: Each node in this layer is an adapted node with a node function defined as an output.

$$O_{4i} = \overline{w}_i f_i = \overline{w}_i (p_i x + q_i y + r_i) \tag{3.30}$$

where $\overline{w}_i$ is the firing power normalized from the previous layer (third layer) and $((p_i x + q_i y + r_i)$ is a parameter in the node.

Layer 5: The single node in this layer is a fixed or nonadaptive node, which calculates its overall output as the sum of all incoming signals from the previous node.

$$O_{5i} = \sum_i \overline{w}_i f_i = \frac{\sum_i w_i f_i}{\sum_i w_i} \tag{3.31}$$

3.2.2.4. ANFIS's Learning Algorithm

Neuro-adaptive learning techniques have a strategy for learning about a data set for the fuzzy modelling procedure. These learning techniques calculate the membership function parameters that allow it to monitor input/output data given to the associated ambiguous inference system. In the learning process, membership function parameters alter through the process. To overcome real world problems in a more efficient way, the task of the learning algorithm is that all the modifiers and parameters can be adjusted to match the ANFIS output with the training data. In order to increase the convergence rate, the hybrid network can be trained with a hybrid learning algorithm that combines the least square root method, and back

propagation learning method can be used. The least squares method can be used to define the optimal values of the result parameter in layer 4 with the fixed parameter. The decrease vector enables a measure of the fuzzy inference system modeling the input/output data for a given set of parameters. Once the uplift vector is obtained, any of several optimization routines can be implemented to adjust parameters to reduce some error measures. When the preliminary parameters are not constant, the search area grows and the convergence of education slows down. The hybrid algorithm consists of a forward transition and a reverse transition. When the optimal result parameters are found, backtracking begins. In the backward transition, errors propagate backwards and the preliminary parameters corresponding to the fuzzy clusters in the input area are updated by the gradient descend method. ANFIS uses least squares estimation and back propagation for membership function parameter estimation.

To minimize the mean square error function, the output error is used to adapt the preliminary parameters through the standard back propagation algorithm. This hybrid algorithm is known to be highly effective in ANFIS training.

3.2.3. Studies on the Thesis

In the part of the thesis, adaptive network based fuzzy logic inference method was used for PV cell unknown parameters estimation. This method has the features of learning of artificial neural networks and decision making of fuzzy logic method. In addition, it also subjectively enables numerical expressions to be added to verbal values.

Generally, PV modules operate in different weather conditions, so the parameters required depend on environmental conditions including solar radiation and temperature. Thus, the outdoor conditions suggest to correlate all paramaters.

I_{ph} values depend on cell temperature and irradiance. I_{ph} can be calculated by the following equation (Bai, et al., 2014; Jordehi, 2016; Kumar et al., 2017):

$$I_{ph} = \frac{G}{G_{ref}}[I_{ph,ref} + \alpha_{sc}(T_C - T_{C,ref})] \quad (3.32)$$

Here;

G_{ref} , $I_{ph,ref}$, $T_{C,ref}$ are solar irradiance, photocurrent and cell temperature at STC conditions, respectively. G, I_{ph} and T_C are the relevant parameters in real outdoor conditions, α_{sc} is the current temperature coefficient of the PV module.

Reverse saturation current (Io) changes with PV cell temperature and It can be calculated using the following equation (Bai, et al., 2014; Kumar et al., 2017):

$$I_0 = I_{o,ref}\left[\frac{T_C}{T_{ref}}\right]^3 \exp\left(\frac{q}{Kn}\left[\frac{E_{g,ref}}{T_{ref}} - \frac{E_g}{T_C}\right]\right) \quad (3.33)$$

Here;

$I_{o,ref}$ and T_{ref} are the reverse saturation current and PV cell temperature under STC conditions. I_0 and T_C are depends on parameters in actual outdoor conditions. $E_{g,ref}$ is the material band gap energy and is equal to 1.121 eV for silicon PV cell at STC.

The band gap energy (Eg) depends slightly on PV cell temperature in outdoor conditions and can be expressed as follows (Tossa, et al., 2014; Bai, et al., 2014):

$$E_g = E_{g,ref}(1 - 0.0002677(T_C - T_{ref})) \quad (3.34)$$

The ideality factor (n) can be estimated using the following equation:

$$n = n_{ref}\left(\frac{T_C}{T_{ref}}\right) \quad (3.35)$$

The effect of the R_S parameter cannot be neglected, since it is responsible for the shape of the I-V curve at maximum power and depends on the temperature of the photovoltaic cells and the radiation of the sun (Bai, et al., 2014). Therefore, it is rational to determine the R_S and R_P values corresponding to the thermal parameters of the material. The R_S formula can be defined as follows (Tossa, et al.,2012; Siddiqui et al., 2013; Ma et al., 2014; Jordehi, 2016; Kumar et al., 2017):

$$R_S = R_{S,ref} \frac{T_C}{T_{ref}} \left[1 - \beta_{oc} \ln\left(\frac{G}{G_{ref}}\right)\right] \quad (3.36)$$

Here;

$R_{S,ref}$ is the series resistance at STC conditions and R_S is the resistance value in real outdoor weather conditions. The value of β_{oc} approaches 0.217.

Regarding parallel resistance, high R_P values cause a flat slope of the short circuit point (Bai, et al.,2016). It is reported that the R_P value is inversely proportional to solar radiation in De Soto et al.,2006; Siddiqui et al.,2013; Ma et al.,2014; Tossa, et al., 2014 as follows:

$$R_P = R_{P,ref} \frac{G_{ref}}{G} \quad (3.37)$$

Here;

$R_{P,ref}$ is the parallel resistance under STC conditions. R_P is the parameter values under the actual outdoor weather condition.

3.2.3.1. Recommended ANFIS and PV Model

In this section, ANFIS based PV model is used to estimate PV cell unknown parameters of the PV cell with given external outdoor data.

The architecture of the proposed ANFIS-based model is shown in Figure 3.37. The input data consists of solar radiation (G) and cell temperature (T_{cell}), while the output is the photocurrent (I_{ph}), diode saturation current (I_0), parallel resistance (R_P), diode ideality factor (n) and series resistance (R_S) of the PV module. The algorithm uses a combination of the least-squares and back-propagation gradient descent methods to train the dataset.

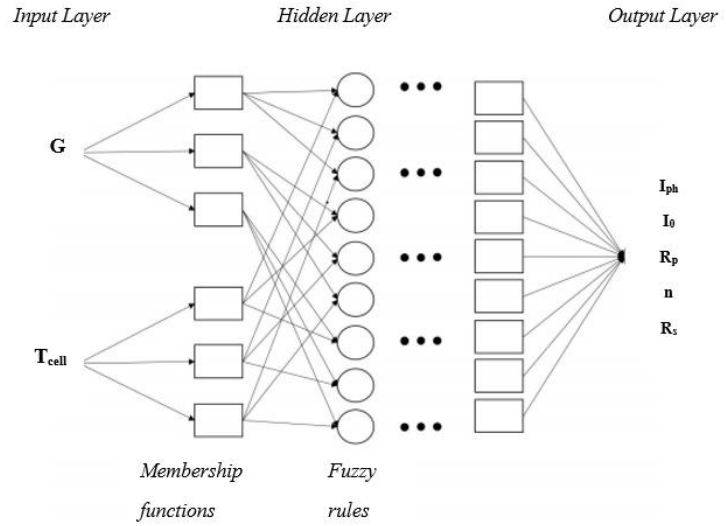


Figure 3.37. ANFIS architecture for the recommended photovoltaic model (Díaz et.al, 2019).

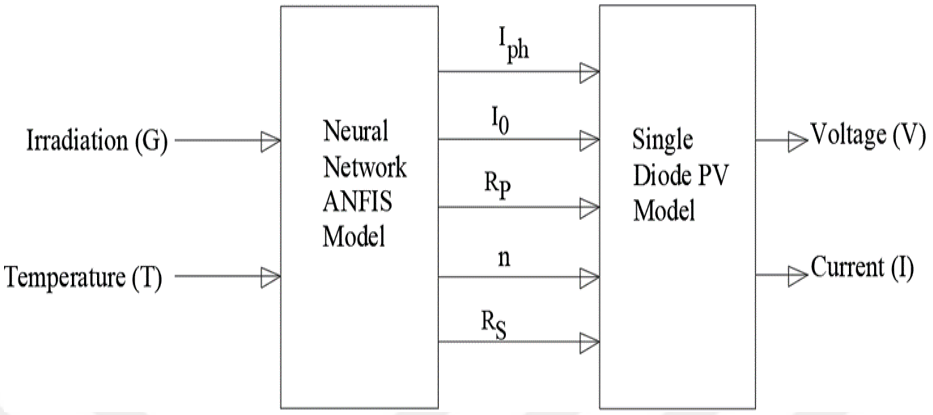


Figure 3.38. Recommended photovoltaic model

In this thesis, an adaptive network based fuzzy inference system (ANFIS) based prediction model is proposed to estimate the unknown parameters of the PV cell.

The unknown parameters can be determined by the proposed method based on the measurement data. The results of the simulations revealed that there is good relation between the measured and the predicted data. A higher R^2 value is the representation of the better prediction of the proposed PV model. That is, it can be understand the accuracy of the model and the prediction success of the values calculated in this type of algorithms by looking at the best R^2 values. These values are between 0 and 1, and R^2 value must be close to 1 to obtain a good result. If R^2 value is close to 1, it means that the link between the estimate and the actual output is strong, that is, the predicted value is very close to the actual output.

The manufacturer information of the photovoltaic module used for simulation is shown in Figures 3.39 and 3.40.

MITSUBISHI ELECTRIC PHOTOVOLTAIC MODULE

SPECIFICATION SHEET				
Manufacturer	MITSUBISHI ELECTRIC			
Model name	PV-UE130MF5N	PV-UE125MF5N	PV-UE120MF5N	PV-UE115MF5N
Cell type	Polycrystalline Silicon, 156mm x 156mm			
Number of cells	36 cells in a series			
Maximum power rating (Pmax)	130W	125W	120W	115W
Warranted minimum Pmax	123.5W	118.8W	114.0W	109.3W
Tolerance of maximum power rating	+10/-5%			
Open circuit voltage (Voc)	21.9V	21.8V	21.6V	21.5V
Short circuit current (Isc)	8.05A	7.90A	7.75A	7.60A
Maximum power voltage (Vmp)	17.4V	17.3V	17.2V	17.1V
Maximum power current (Imp)	7.47A	7.23A	6.99A	6.75A
Normal operating cell temperature (NOCT)	47.5 degree C			
Maximum system voltage	DC 600V			
Fuse rating	15A			
Dimensions	1495x674x46mm (58.9x26.5x1.81inch)			
Weight	13.5kg (29.8lbs.)			
Output terminal	(+) 800mm/(-) 1250mm with MC connector (PV-KBT4/6 -UR, PV-KST4/6 -UR)			
Module efficiency	12.9%	12.4%	11.9%	11.4%
Packing condition	2 pcs - 1 carton			
Certificate	IEC 61215 edition 2 (static load test 2400Pa passed), EN 61730, TUV Safety Class Ⅱ			

Figure 3.39. Mitsubishi Electric Photovoltaic Module Datasheet Information

ELECTRICAL CHARACTERISTICS

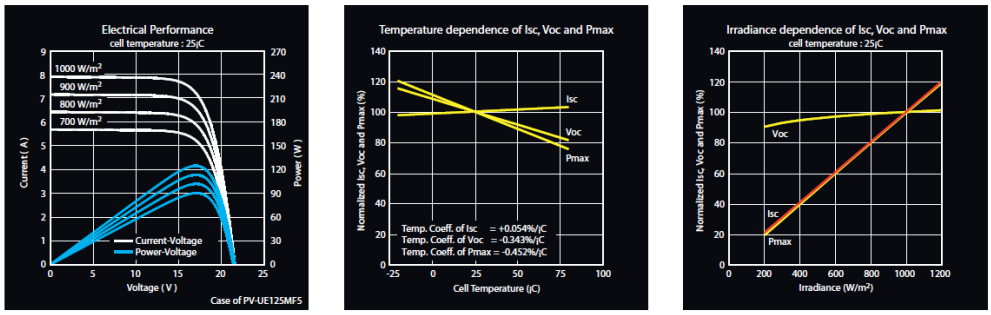


Figure 3.40. Mitsubishi Electric Photovoltaic Module Datasheet Electrical Characteristic

4. RESULT AND DISCUSSION

In this study, it was suggested that solar irradiance and cell temperature together are the good equivalent prediction parameters for I_{ph}, I_0 R_p, n and R_s. For the 2 inputs, 5 different ANFIS structures are constructed. Figure 4.1 shows the developed ANFIS model structure for PV modules.

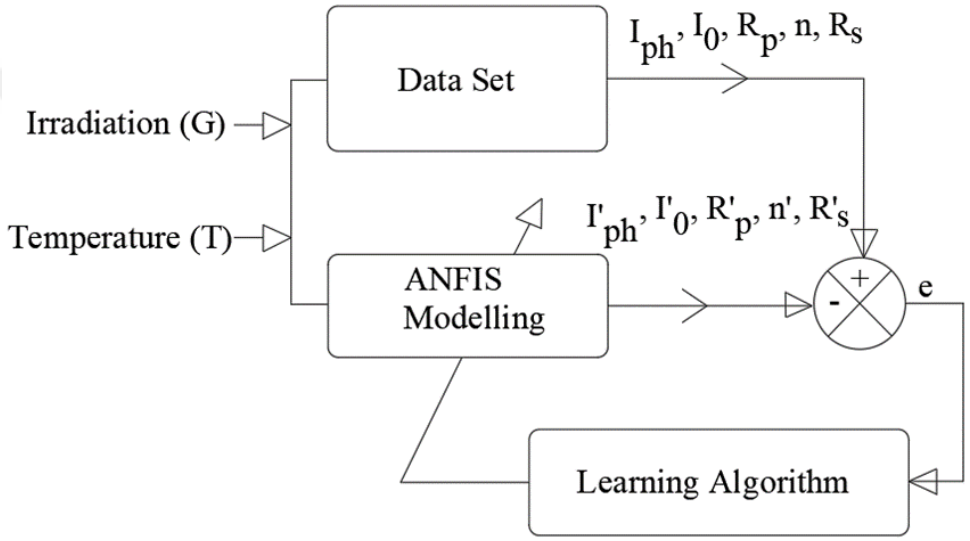


Figure 4.1. ANFIS models proposed for estimating equivalent electrical circuit parameters.

In this design, the Sugeno model in Fuzzy Inference System (FIS) was chosen. A model with two inputs and one output was designed (separately designed for each parameter). Input values are solar radiation and cell temperature. The outputs of the desired value are photo current, diode saturation current, parallel resistance, diode ideality burner and series resistance. Three membership functions are defined for each login. Thus, a total of 9 different rules were created. The figures below show ANFIS structures developed for photocurrent as an example.

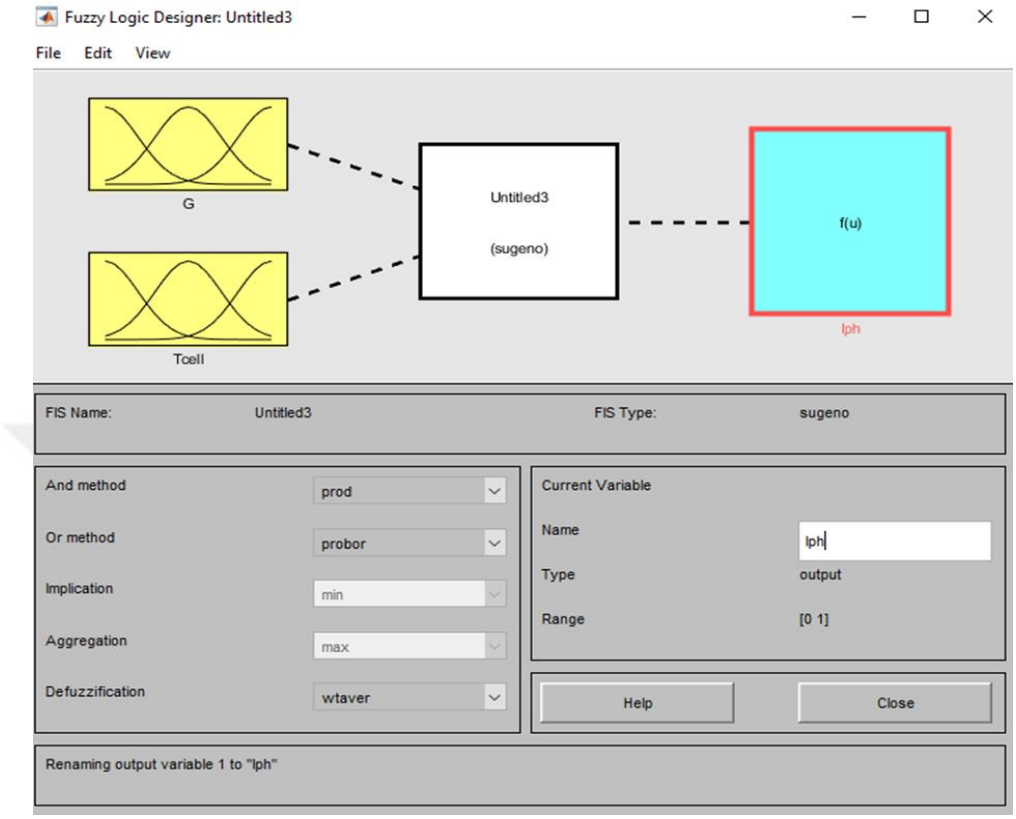


Figure 4.2. FLC Sugeno model interface

ANFIS GUI (Graphical User Interface) is used as a function of the Fuzzy Logic Toolbox included in the Matlab program. The 'anfisedit' command is typed in the command window, or can switch to ANFIS from an Edit menu while the fuzzy inference window is open.

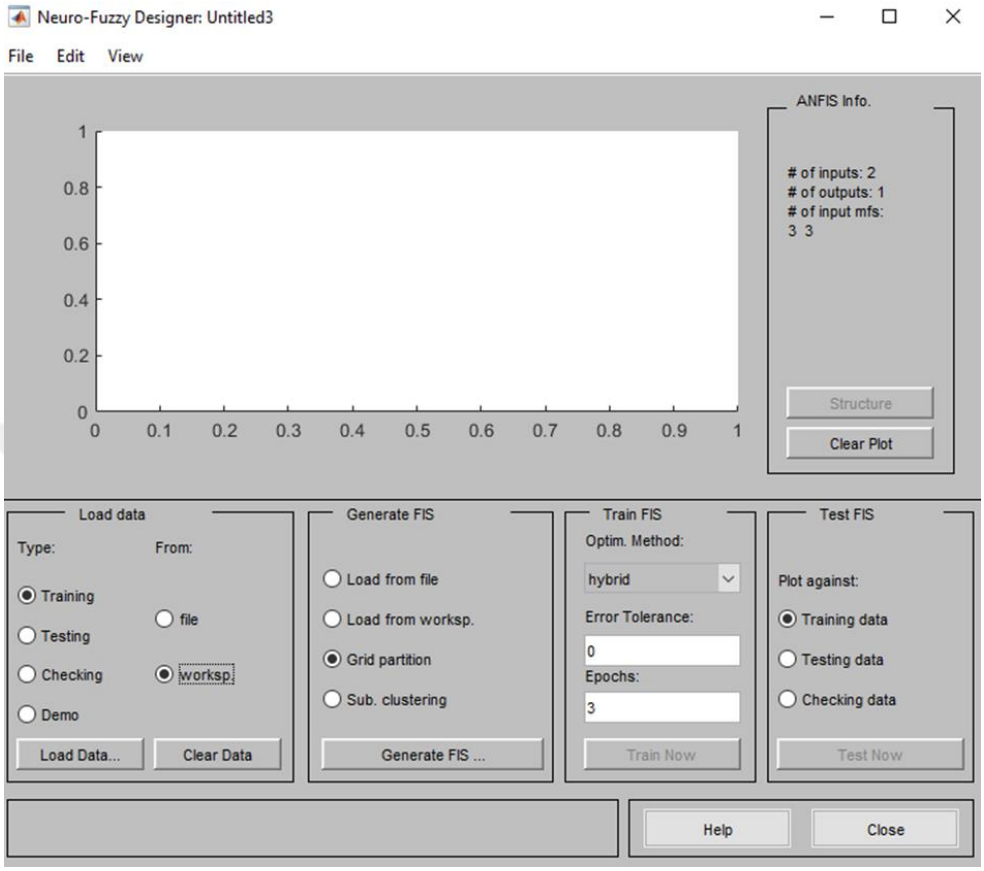


Figure 4.3. ANFIS graphical user interface

The data edited in Excel was transferred to the MATLAB / Workspace environment and saved. The data was retrieved using the Import Data button. When the model was created, the data was divided into two data sets:

- Training data set
- Test data set

Training data learns the relationship between network input-output data and edits membership function parameters until the specified number of loops or the

desired error level is reached. With the test data set, the capability of the model that has been trained and the parameters are edited is measured with data that it has never encountered before.

Training and test data sets were created using the Sandia National Laboratory characteristic model. In this study, a total of 1160 training data sets randomly selected from the external measurement data were used for training the network. 500 data sets were used for were used for testing (Hansen, 2015).

Once the datasets are loaded, one of two alternative methods is chosen to create a fuzzy inference system under 'FIS generation'. These methods;

- Grid partition
- Sub-clustering

In this work, a Grid partition is created for the model. The sub-clustering option is not used because there are many parameters.

ANFIS model structure is seen in Figure 4.4. The two black nodes (circles) on the far left of the figure reflect the criteria associated with the problem. In the second layer, three membership functions associated with each variable are assigned. In the third stage, $3^2 = 9$ rules are formed. Each output from the relevant rules is included in the 4th layer, and the outputs associated with all the rules are collected and the output value estimated by the system is reached in the 5th layer.

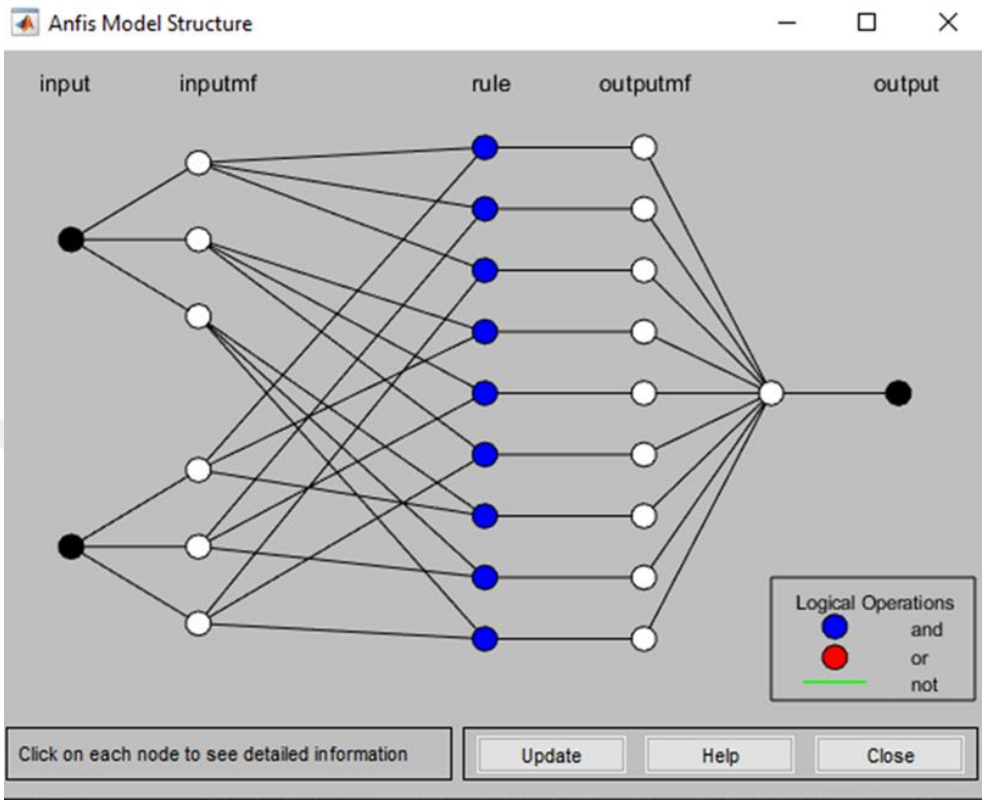


Figure 4.4. ANFIS model structure

There are 2 inputs as solar irradiance and cell temperature. Three different membership functions are defined for each entry. Solar irradiance data (G), cell temperature data (T_{cell}) and membership functions for output are exhibited in Figure 4.5, Figure 4.6, Figure 4.7 respectively.

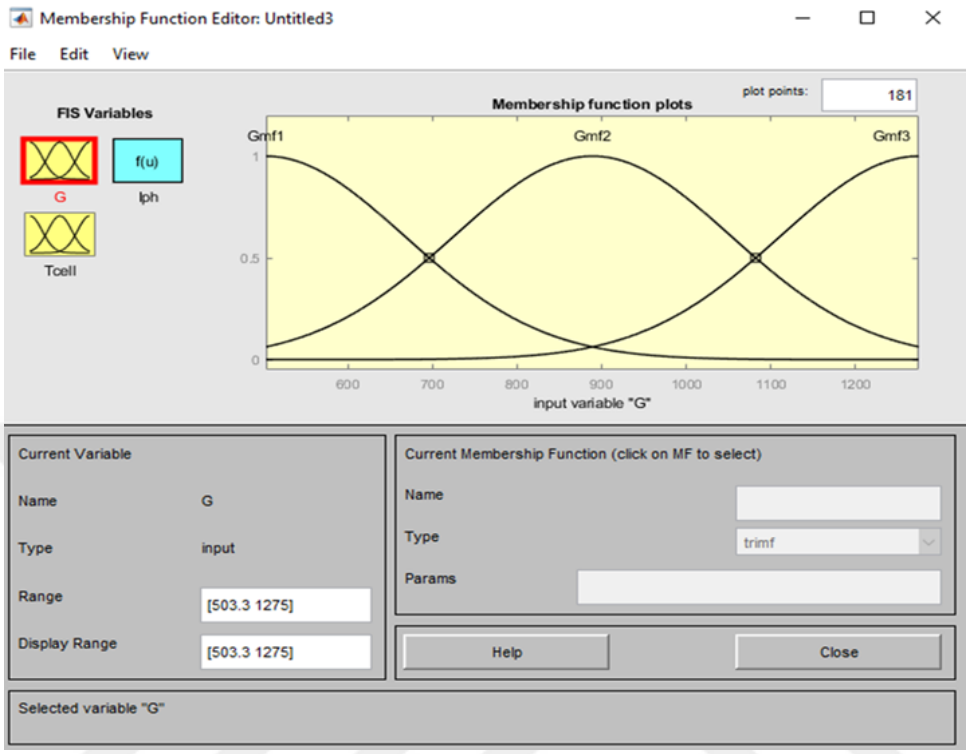


Figure 4.5. Membership functions for Solar irradiance data

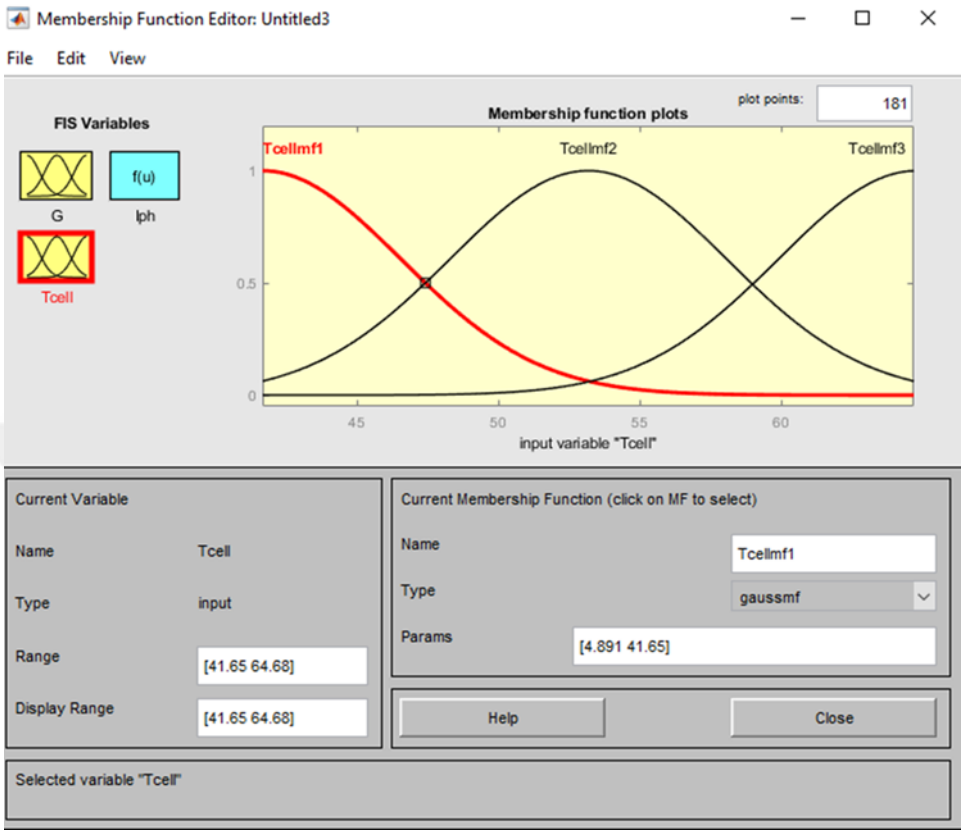


Figure 4.6. Membership functions for cell temperature data

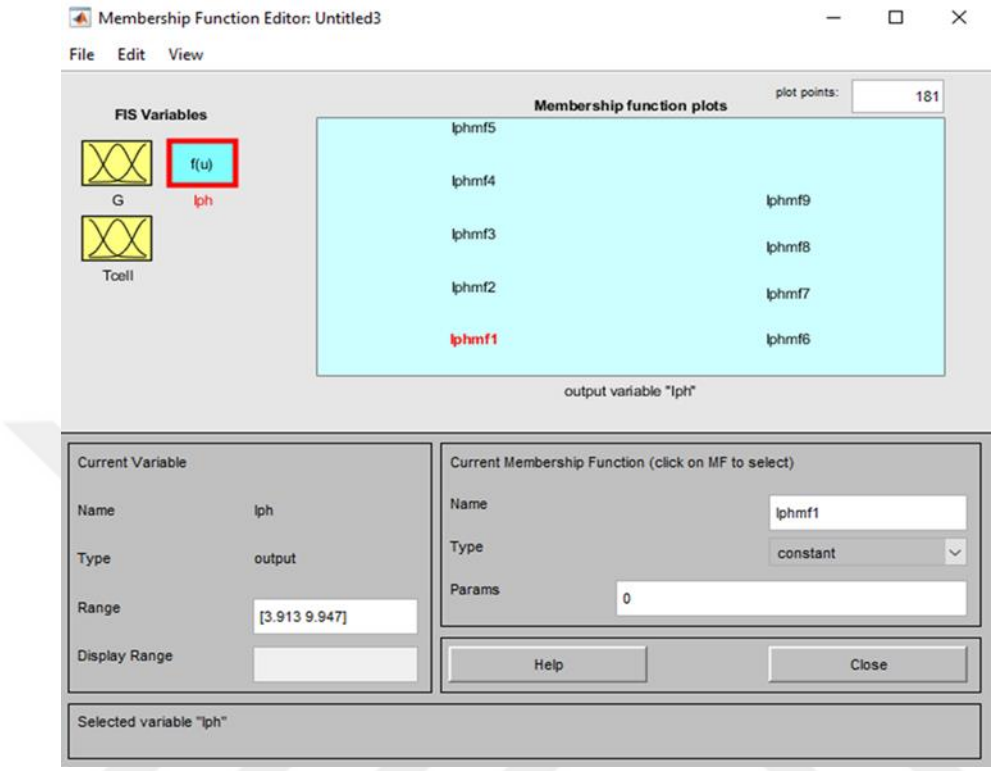


Figure 4.7. Output membership functions of the model created by Grid partitioning method

After the membership functions were defined, 9 different rules were created. Also, a value is obtained from each rule. The resulting output function values are converted into a single output value. The rules created in the rule editor are shown in Figure 4.8.

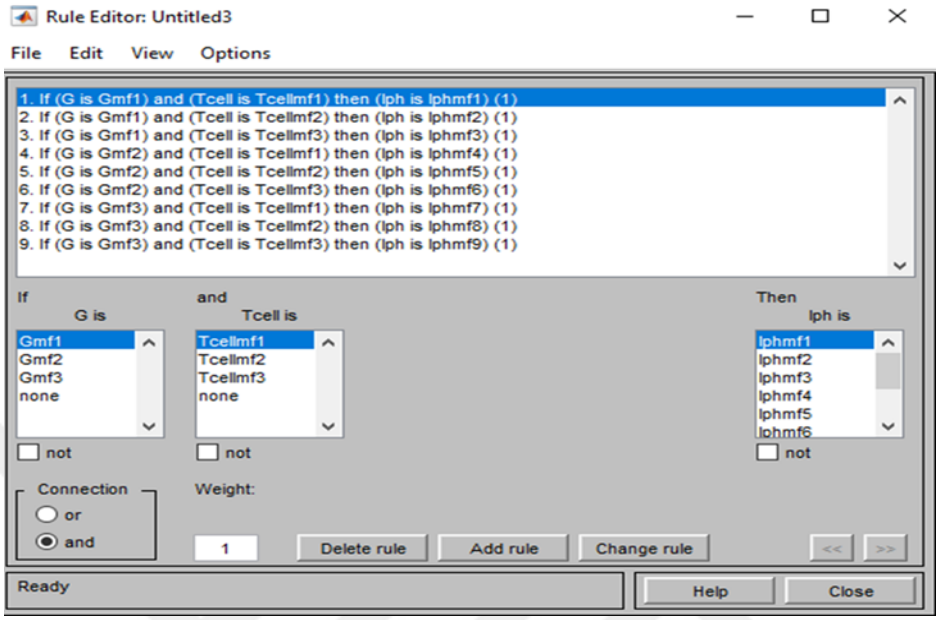


Figure 4.8. Rule editor designed for ANFIS

Figure 4.9 shows the graphical representation of the relationship between input and output values. Represents the output value with values entered according to the 9 rules created. In addition, it enables us to approach the expected value in the output with the training data previously loaded into the ANFIS interface.

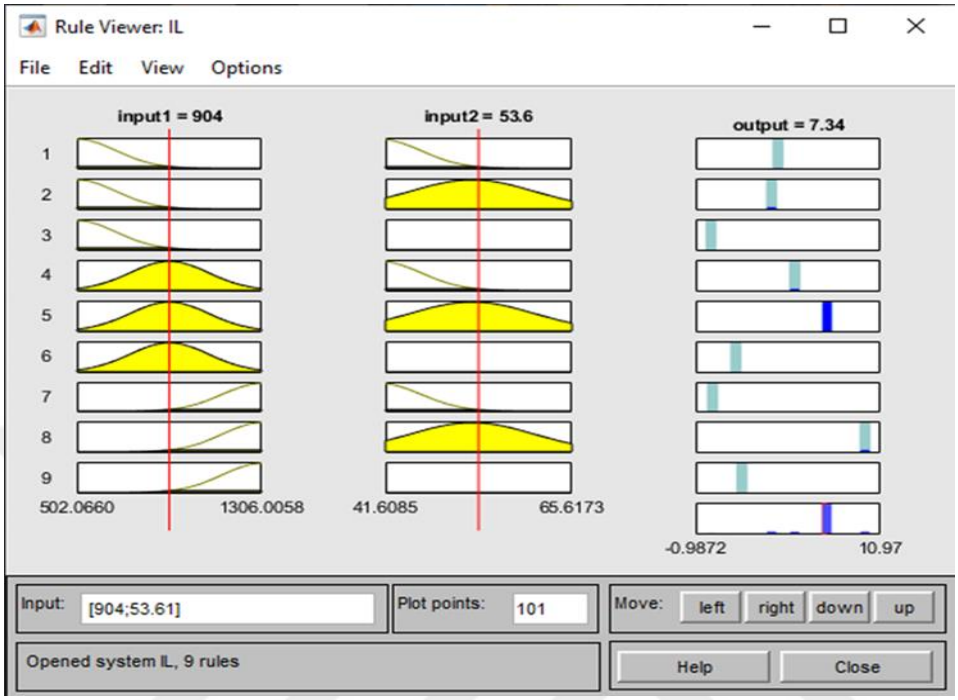


Figure 4.9. Rule editor designed for ANFIS

A total of 1160 different data sets were uploaded from the outdoor measurement data to the ANFIS interface. Training data sets are loaded as shown in Figure 4.10. Finally, after clicking the 'train now' tab in Figure 4.11, the approximate error in the system is shown.

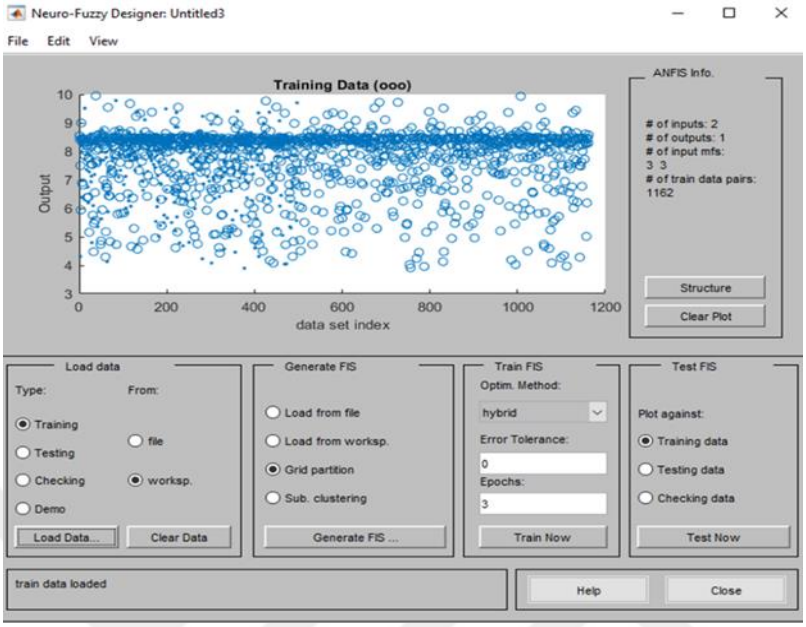


Figure 4.10. Loading the training data set

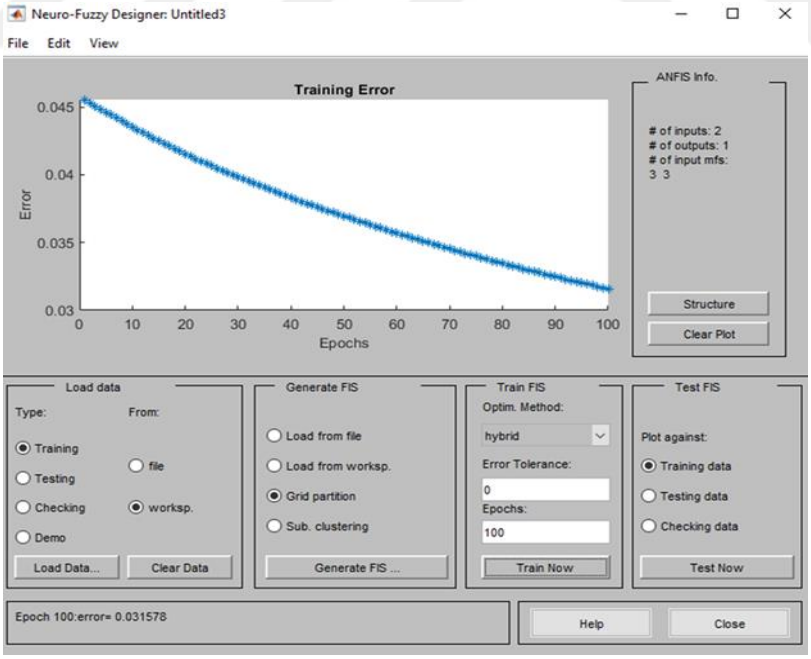


Figure 4.11. Training error of the ANFIS mode

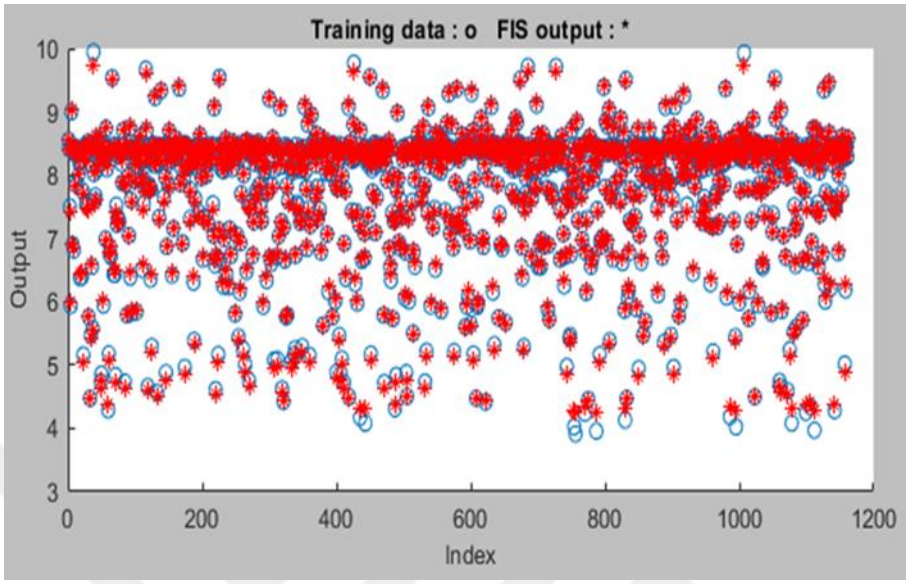


Figure 4.12. For the training data set Comparison of actual data and ANFIS extracted data for equivalent parameters of PV modules namely I_{ph}

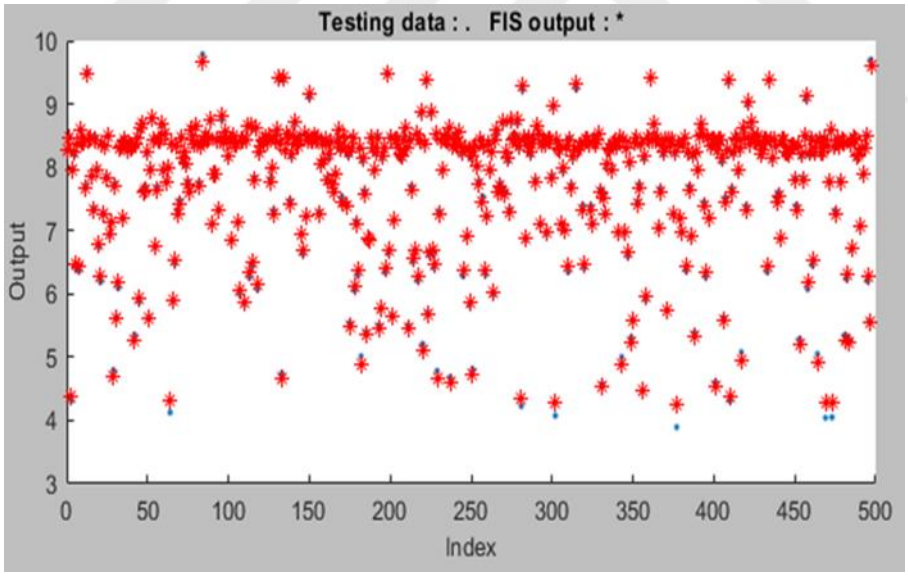


Figure 4.13. For the testing data set Comparison of actual data and ANFIS extracted data for equivalent parameters of PV modules namely I_{ph}

Figure 3.38 summarizes the basic configuration of the proposed PV model. It consists of a two-step process. First, a neural network is used to estimate five parameters simply by reading samples of temperature and irradiation. Second, these parameters are placed in the single diode electrical equivalent circuit model.

In order to test the learning ability of the network, it was tested by creating randomly selected test data sets that were not included in the training data set. It was seen that the obtained R^2 values were close to 1. it means that the bond between the prediction and the observed value is strong, that is, the predicted value is very close to the true value.

Table 4.1. Training and Test data sets best R^2 values

R^2	I_{ph}	I_0	R_P	n	R_S
Training data	0.9992	0,9999	0.9766	0.9994	0.9266
Test data	0.9991	0,9993	0.9726	0.9993	0.9159

The figures below show the best R^2 values found for the real data and estimated data of the training data set.

Table 4.2. Real and Estimated datas for training data set

G	T_{cell}	I_{ph}	I_0	R_p	n	R_s	V_{oc}	V_{mp}	I_{mp}	I_{sc}
539.5317	41.9636	4.1863	1.32E-07	235.4792	1.1231	0.2474	18.9418	15.0944	3.8259	4.1818
G	T_{cell}	I_{ph_est}	I_{0_est}	R_{p_est}	$n_{_est}$	R_{s_est}	V_{oc_est}	V_{mp_est}	I_{mp_est}	I_{sc_est}
539.5317	41.9636	4.2356	1.21E-07	234.2769	1.1237	0.2472	19.0604	15.1944	3.8726	4.2311

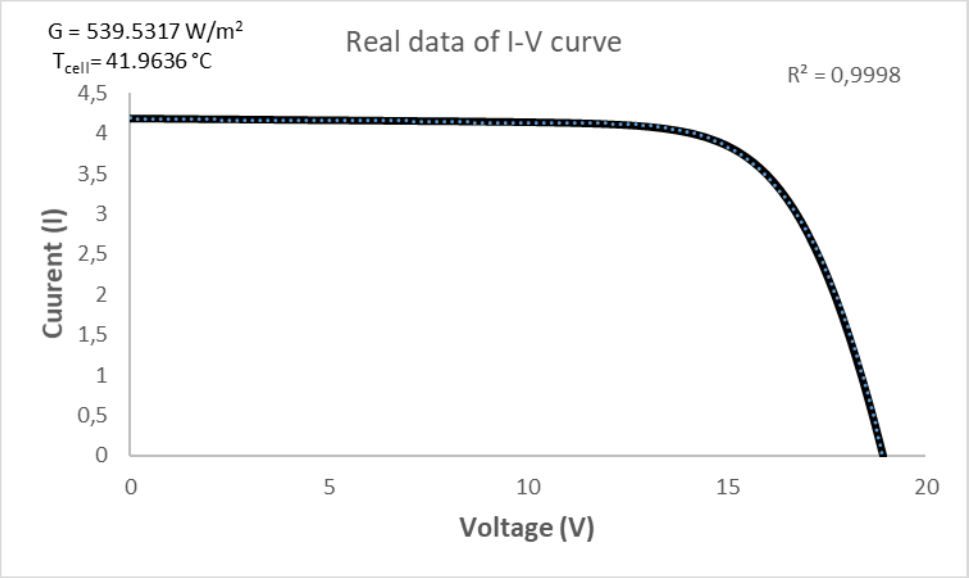


Figure 4.14. Real data of I-V curve

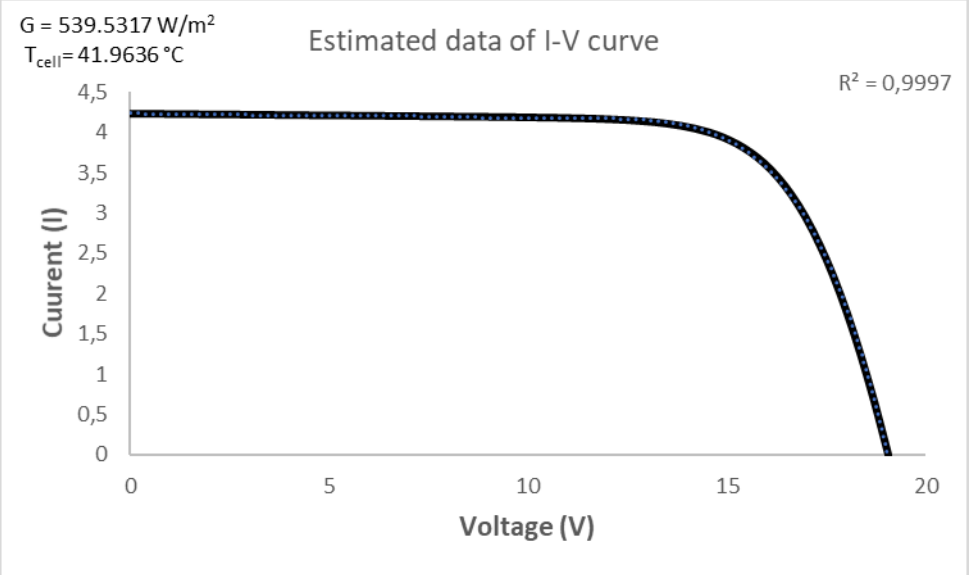


Figure 4.15. Estimated data of I-V curve

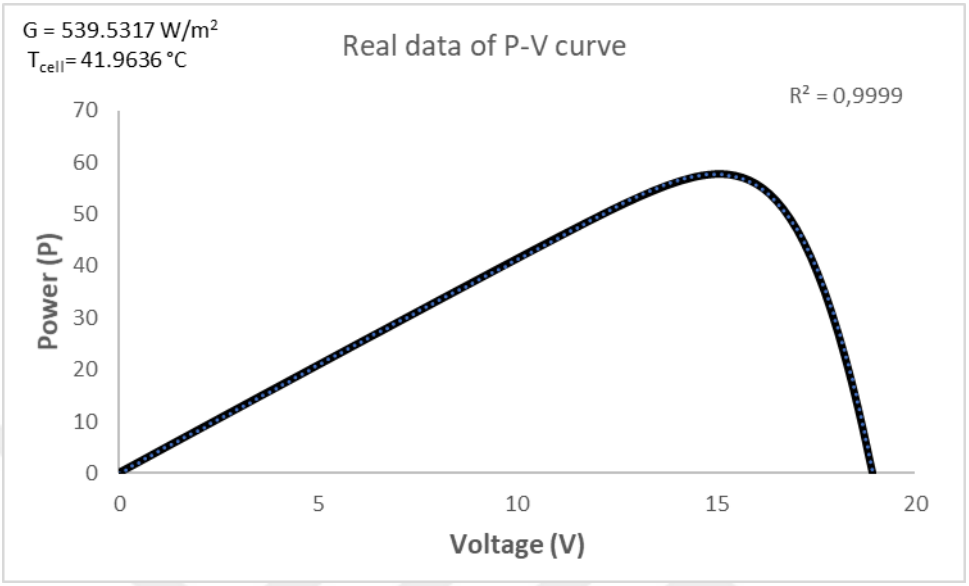


Figure 4.16. Real data of P-V Curve

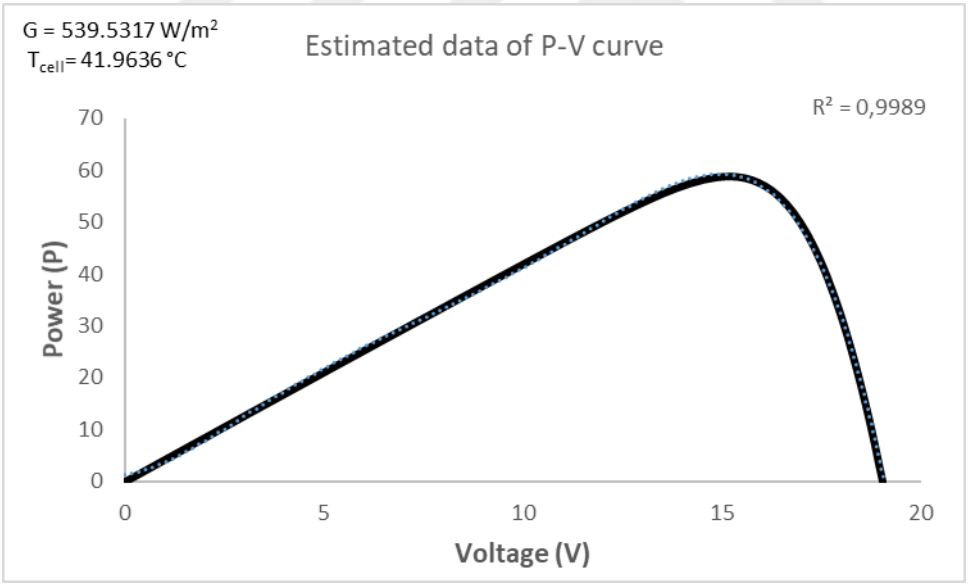


Figure 4.17. Estimated data of P-V curve

Table 4.3. Real and Estimated datas for training data set

G	T_{cell}	I_{ph}	I_0	R_p	n	R_s	V_{oc}	V_{mp}	I_{mp}	I_{sc}
830.5519	49.2877	6.4784	5.76E-07	235.6253	1.1885	0.25151	19.2846	14.8197	5.8892	6.4714
G	**T_{cell}**	**I_{ph_est}**	**I_{0_est}**	**R_{p_est}**	**$n_{_est}$**	**R_{s_est}**	**V_{oc_est}**	**V_{mp_est}**	**I_{mp_est}**	**I_{sc_est}**
830.5519	49.2877	6.5123	5.77E-07	234.0639	1.1889	0.25153	19.2937	14.821	5.9197	6.5053

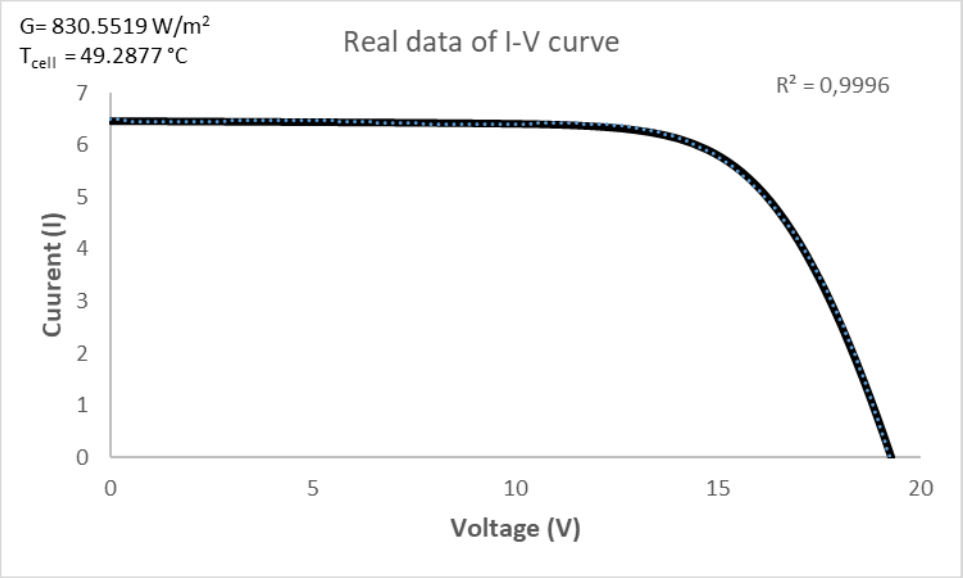


Figure 4.18. Real data of I-V curve

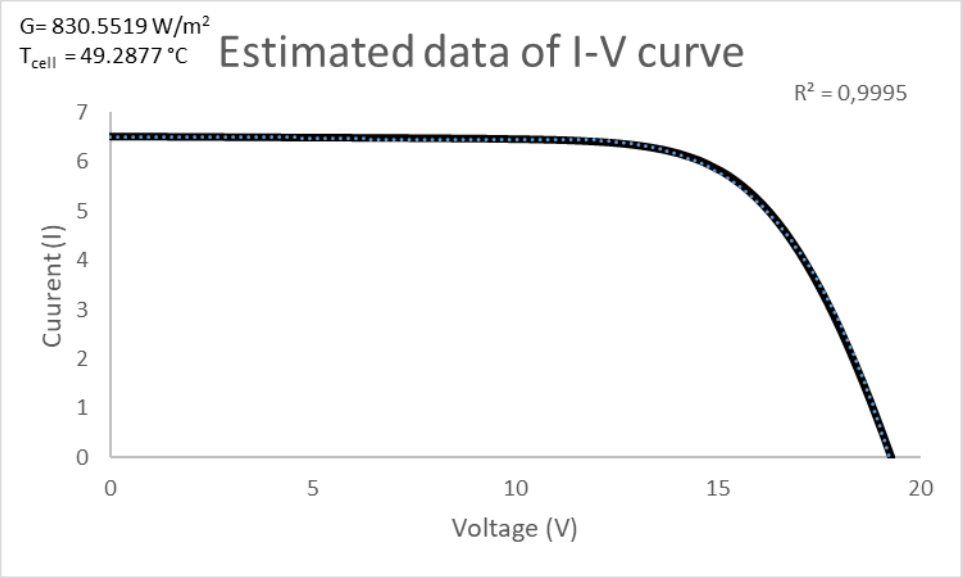


Figure 4.19. Estimated data of I-V curve

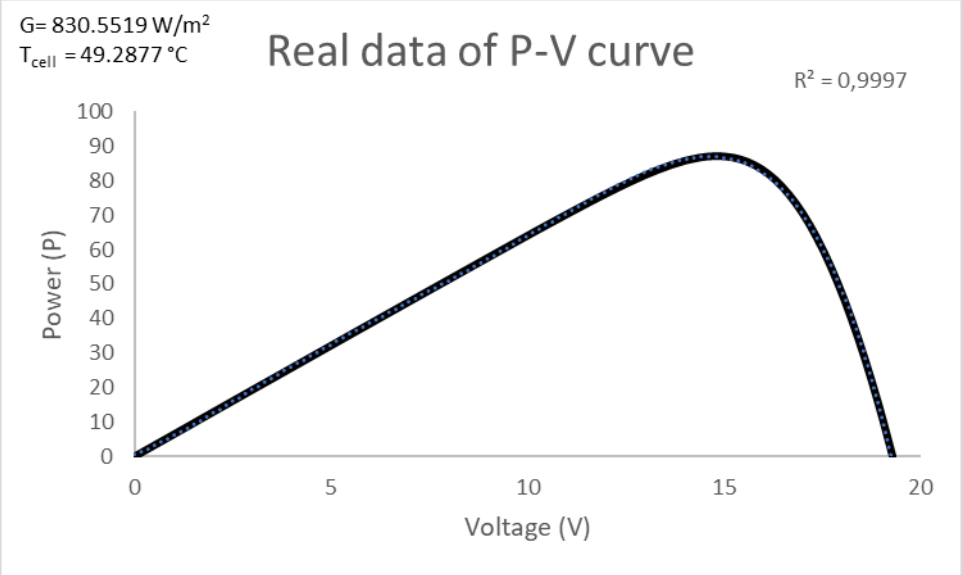


Figure 4.20. Real data of P-V curve

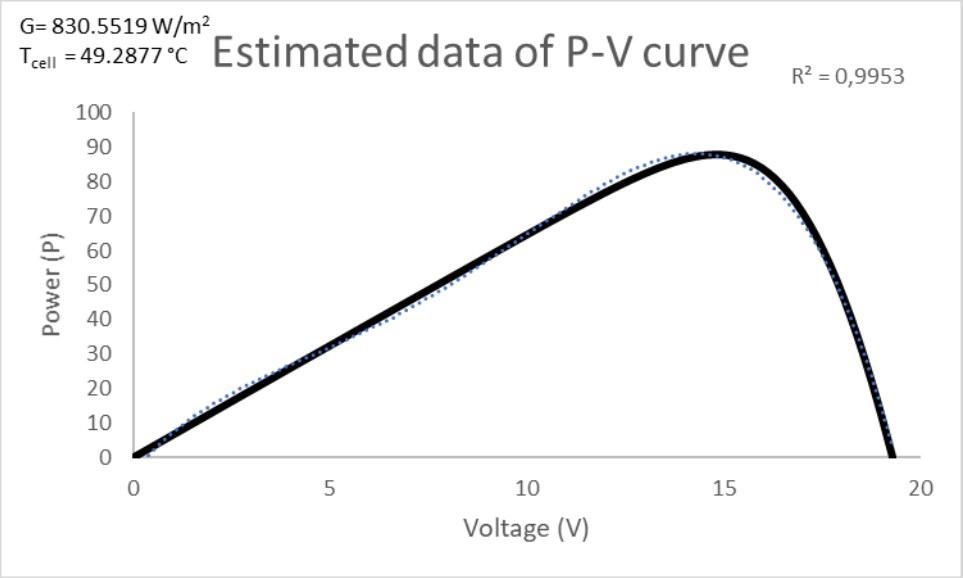


Figure 4.21. Estimated data of P-V curve

Table 4.4. Real and Estimated datas for training data set

G	**T_{cell}**	**I_{ph}**	**I_0**	**R_p**	**n**	**R_s**	**V_{oc}**	**V_{mp}**	**I_{mp}**	**I_{sc}**
1015.794	54.1486	7.9409	1.40E-06	235.8130	1.2328	0.2543	19.4527	14.5979	7.1736	7.9322
G	**T_{cell}**	**I_{ph_est}**	**I_{0_est}**	**R_{p_est}**	**n_{est}**	**R_{s_est}**	**V_{oc_est}**	**V_{mp_est}**	**I_{mp_est}**	**I_{sc_est}**
1015.794	54.1486	7.9569	1.41E-06	237.1611	1.2331	0.2535	19.4496	14.5959	7.1884	7.9484

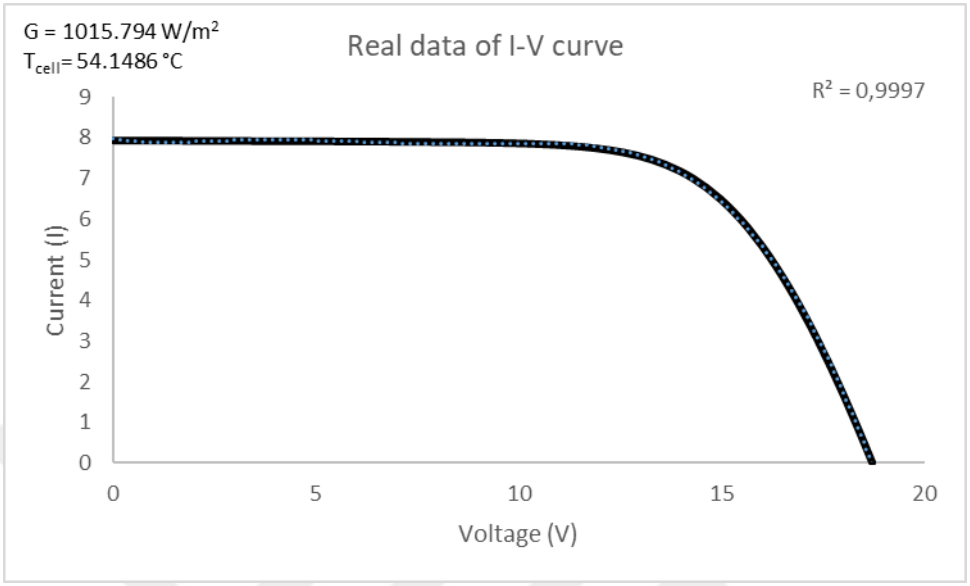


Figure 4.22. Real data of I-V curve

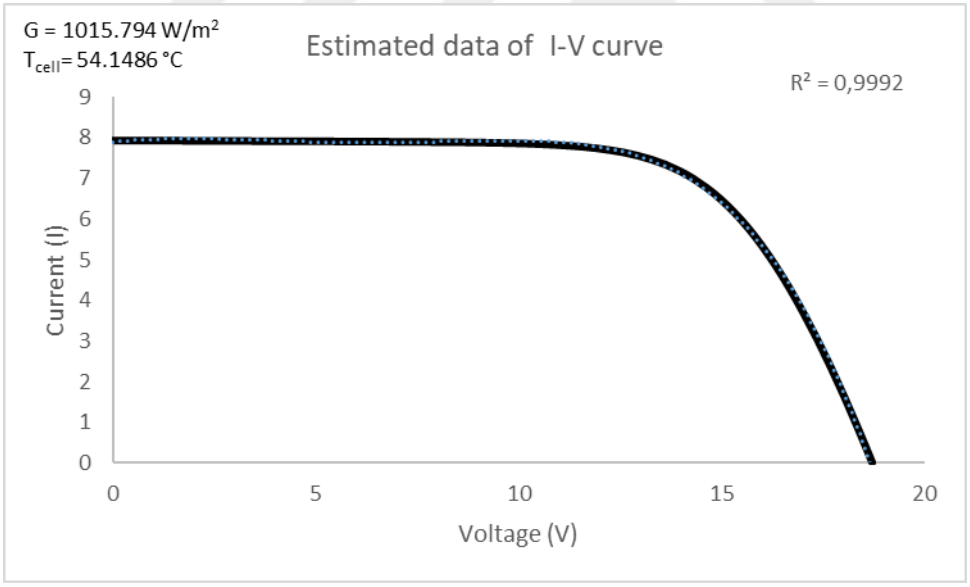


Figure 4.23. Estimated data of I-V curve

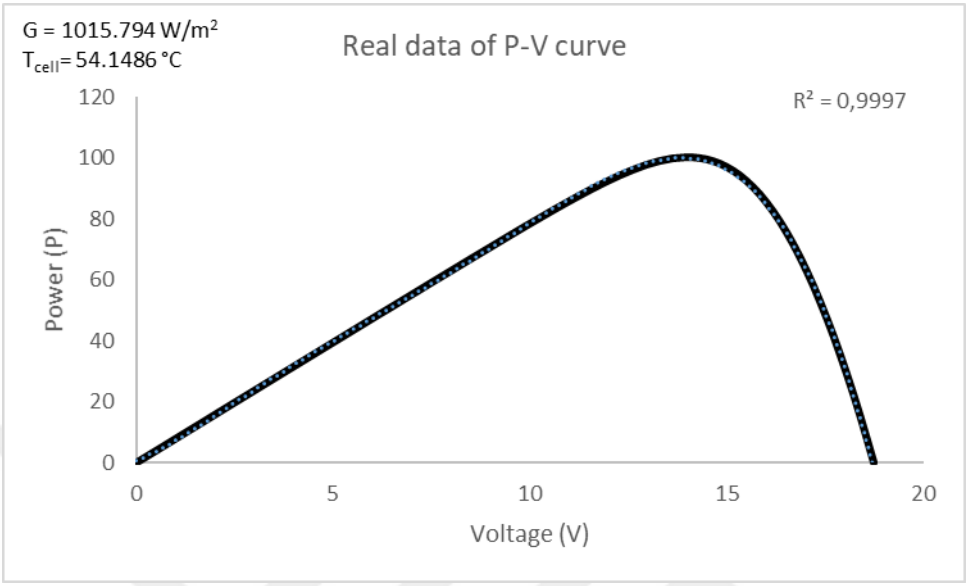


Figure 4.24. Real data of P-V curve

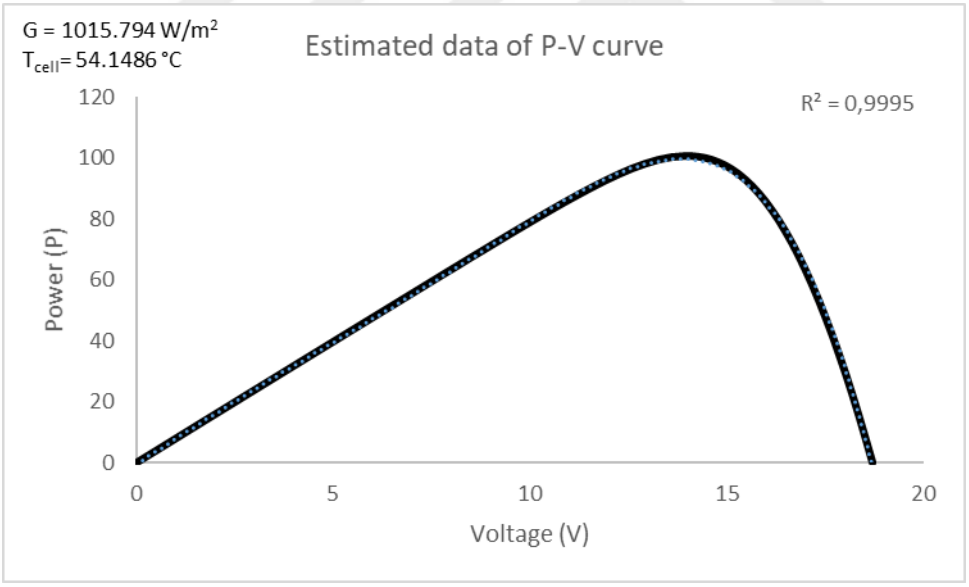


Figure 4.25. Estimated data of P-V curve

5. CONCLUSION

In this thesis, ANFIS method was proposed for the PV cell unknown parameter estimation. This method has the features of learning artificial neural networks and deciding on fuzzy logic method. Additionally, it allows for the subjective addition of numeric expressions and verbal values. In this thesis, the unknown five parameter values depending on the solar radiation and the temperature of the photovoltaic cell were estimated by ANFIS without requiring any equation solution.

The tables and graphs below show the best R^2 values found for PV cell five unknown parameters. It was seen that the obtained R2 values were close to 1. This result showed that the relationship between the real value of the parameters and their predicted value is strong, that is, the predicted value is very close to the true value. As a result, unknown parameters were calculated with ANFIS to an accuracy of about 1. I-V and P-V features drawn in the light of these results are given in chapter 4 and it is seen that the graphics are very close to each other.

Table 5.1 Best R^2 for PV cell five unknown parameters

	$\mathbf{I_{ph}}$	$\mathbf{I_0}$	$\mathbf{R_p}$	**n**	$\mathbf{R_s}$
$\boldsymbol{R^2}$	0.9992	0.9991	0.9915	0.9999	0.9736

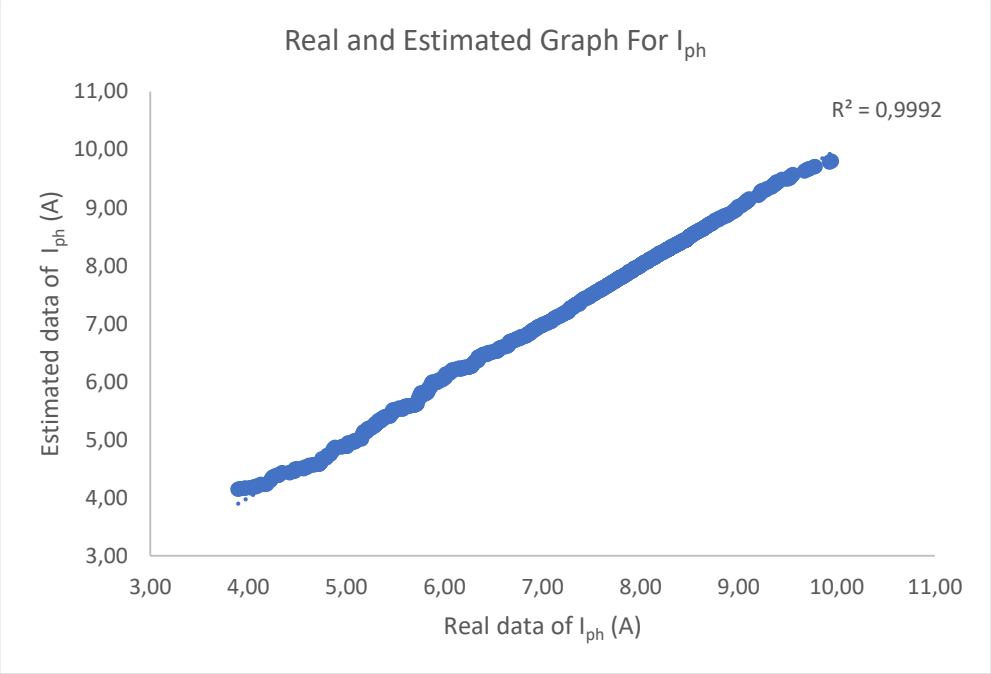


Figure 5.1. Real and Estimated values graph for I_{ph}

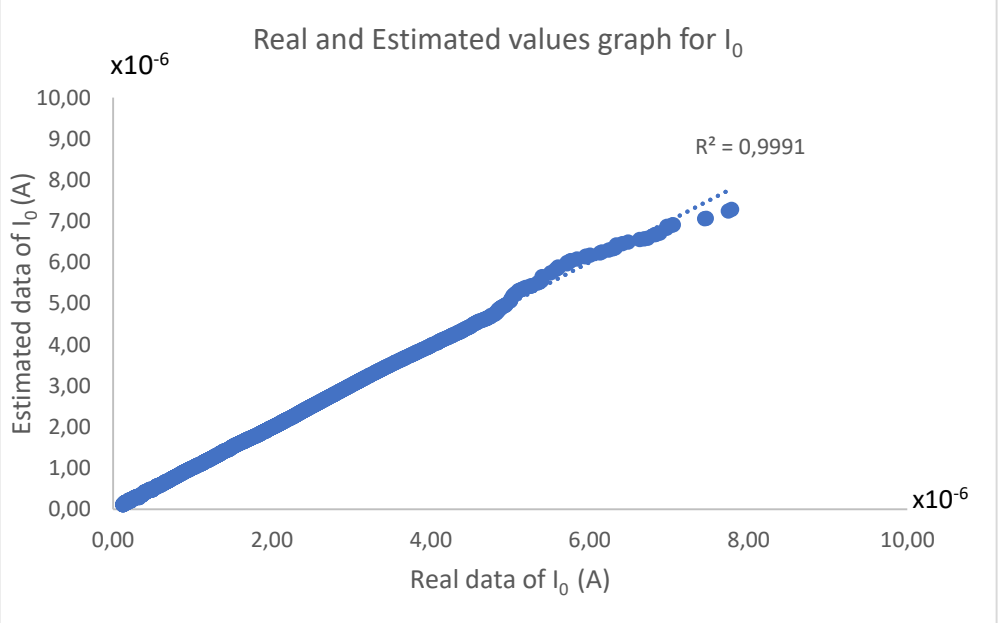


Figure 5.2. Real and Estimated values graph for I_0

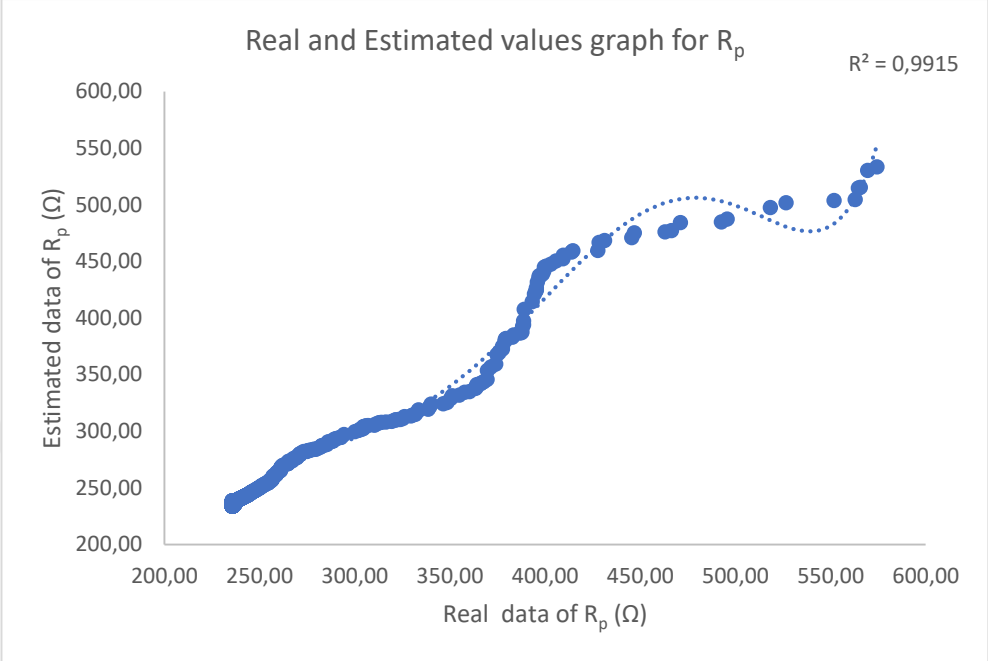


Figure 5.3. Real and Estimated values graph for R_p

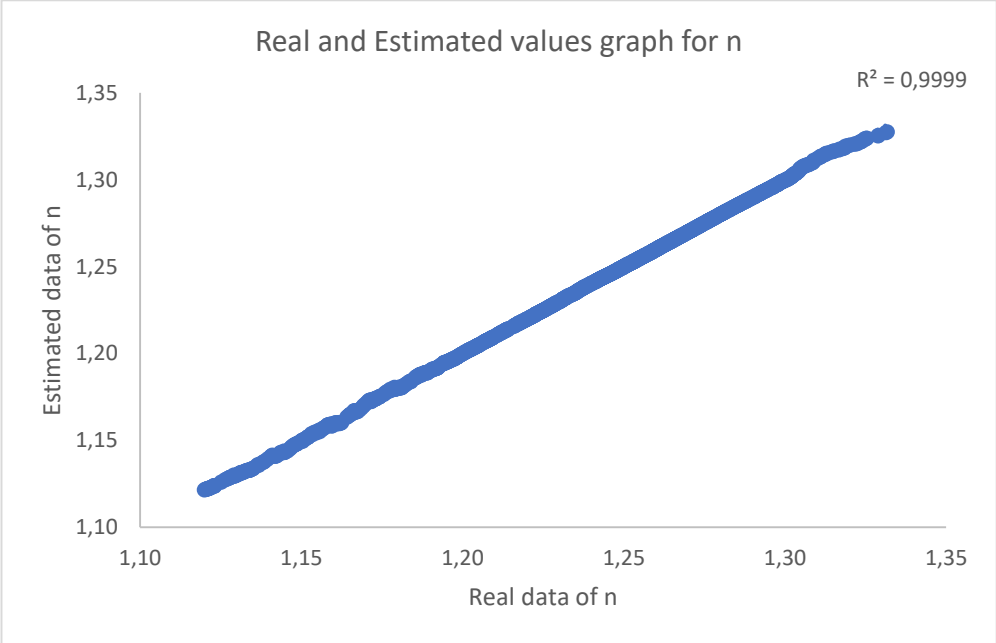


Figure 5.4. Real and Estimated values graph for n

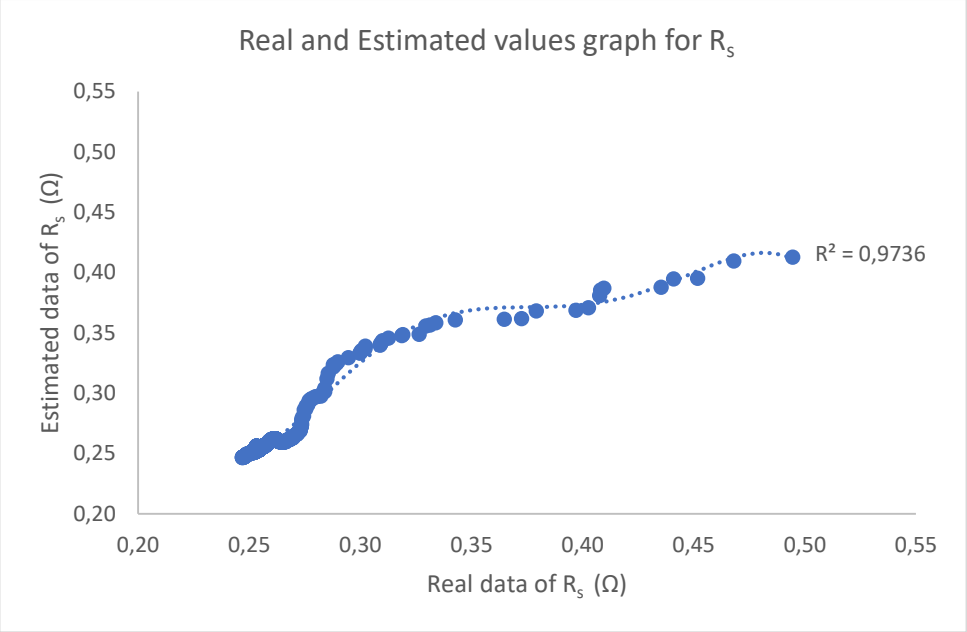


Figure 5.5. Real and Estimated values graph for R_s

The graphs below show the changes of five unknown parameter values of a photovoltaic cell depending on the radiation and cell temperature.

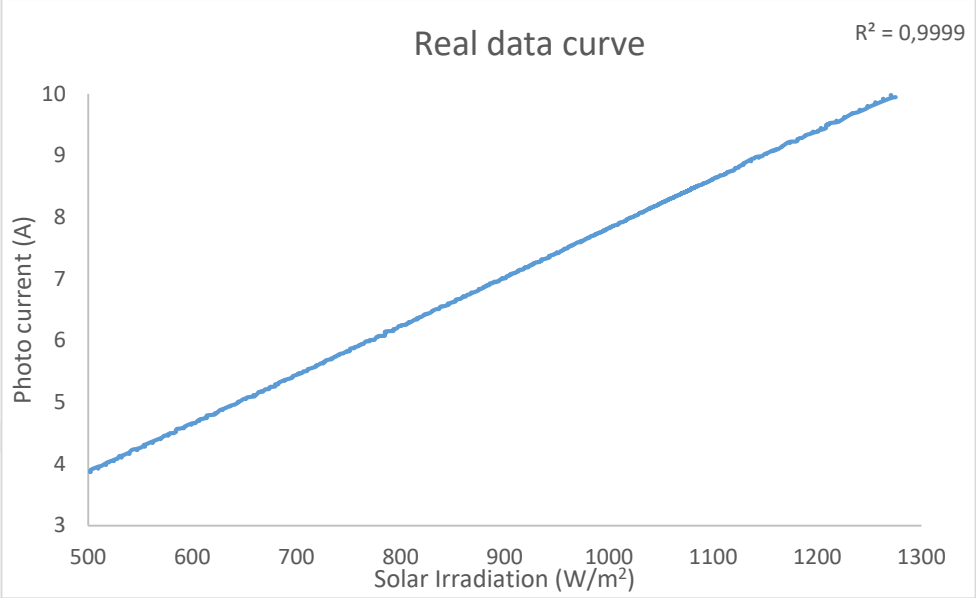


Figure 5.6. Change of photo current due to solar irradiation for real data

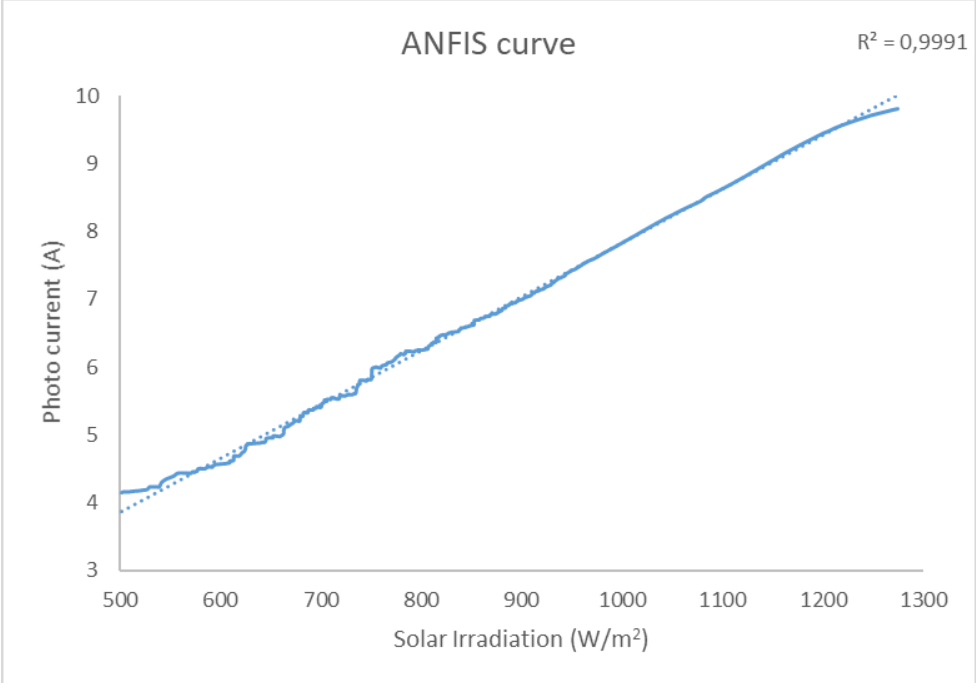


Figure 5.7. Change of photo current due to solar irradiation for ANFIS data

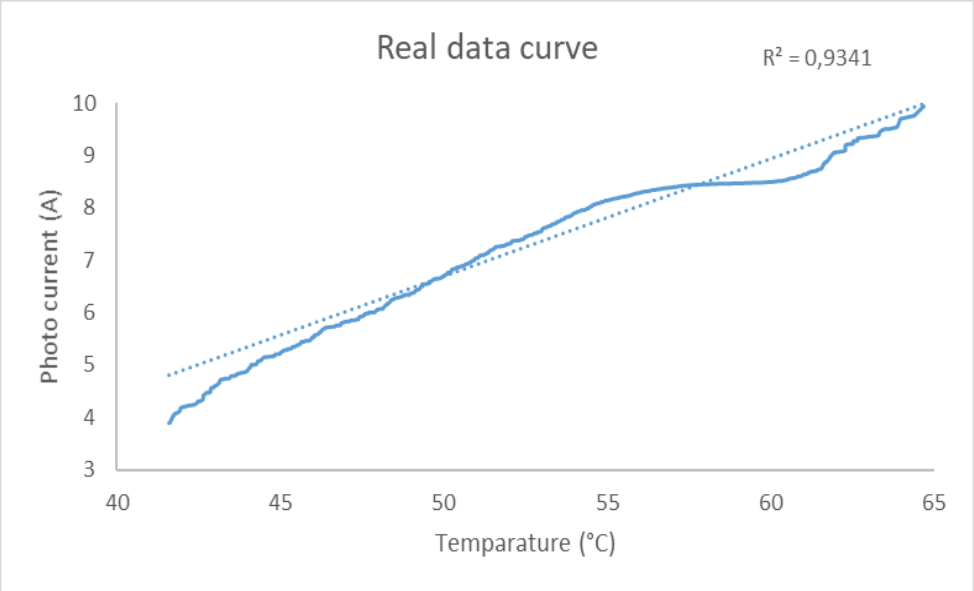


Figure 5.8. Change of photo current due to cell temperature for real data

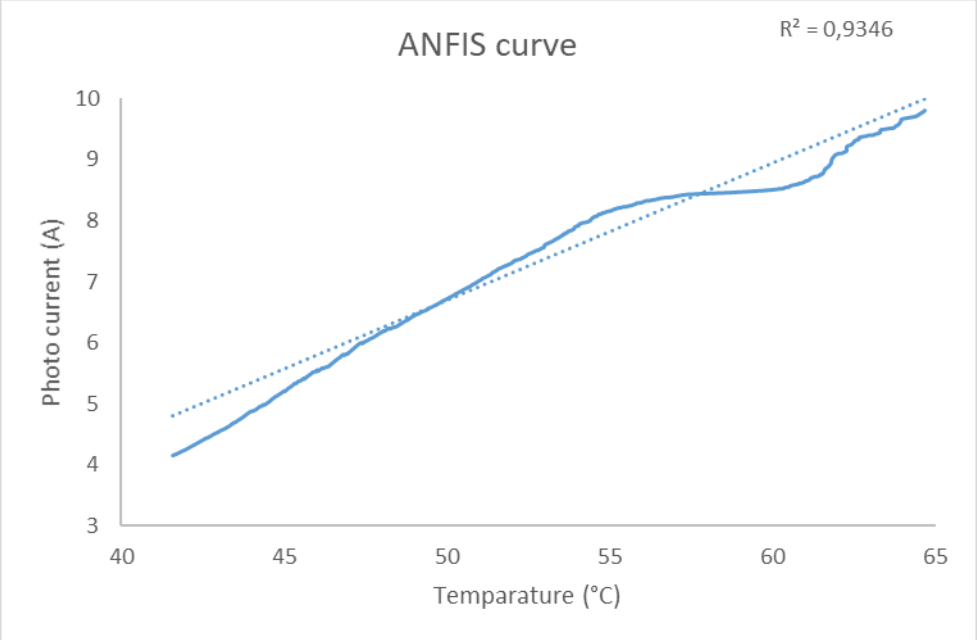


Figure 5.9. Change of photo current due to cell temperature for ANFIS data

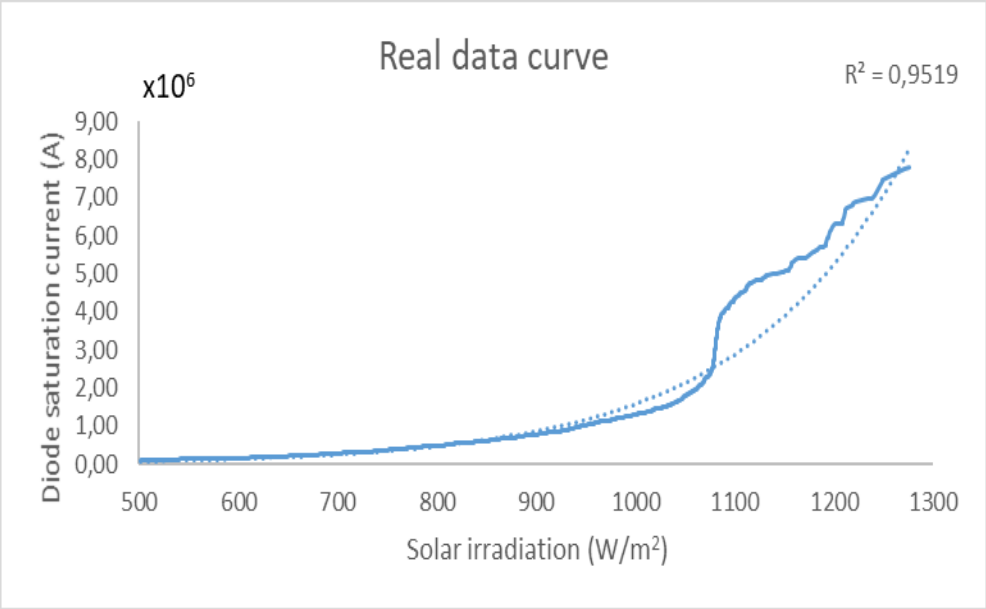


Figure 5.10. Change of diode saturation current due to solar irradiation for real data

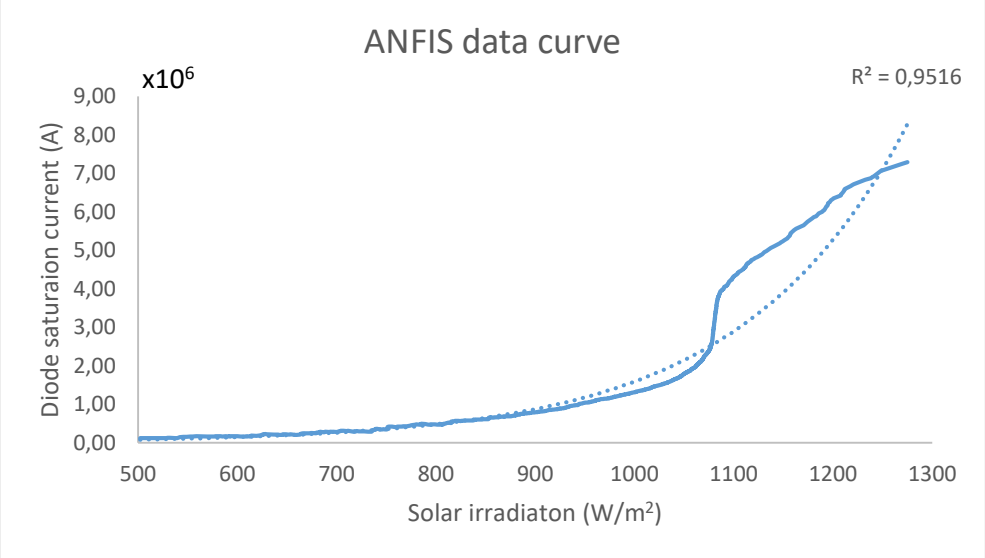


Figure 5.11. Change of diode saturation current due to solar irradiation for ANFIS data

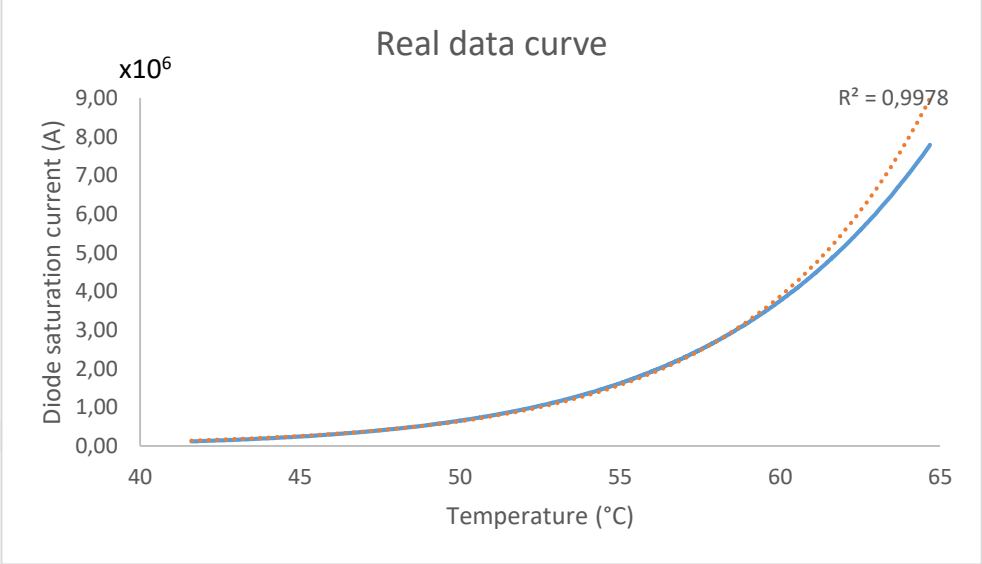


Figure 5.12. Change of diode saturation current due to cell temperature for real data

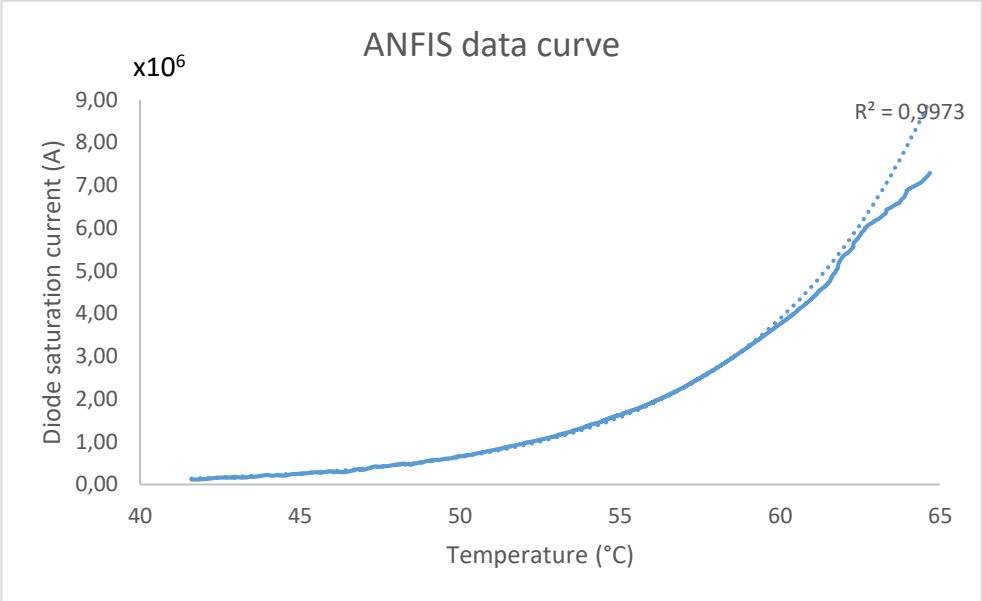


Figure 5.13. Change of diode saturation current due to cell temperature for ANFIS data

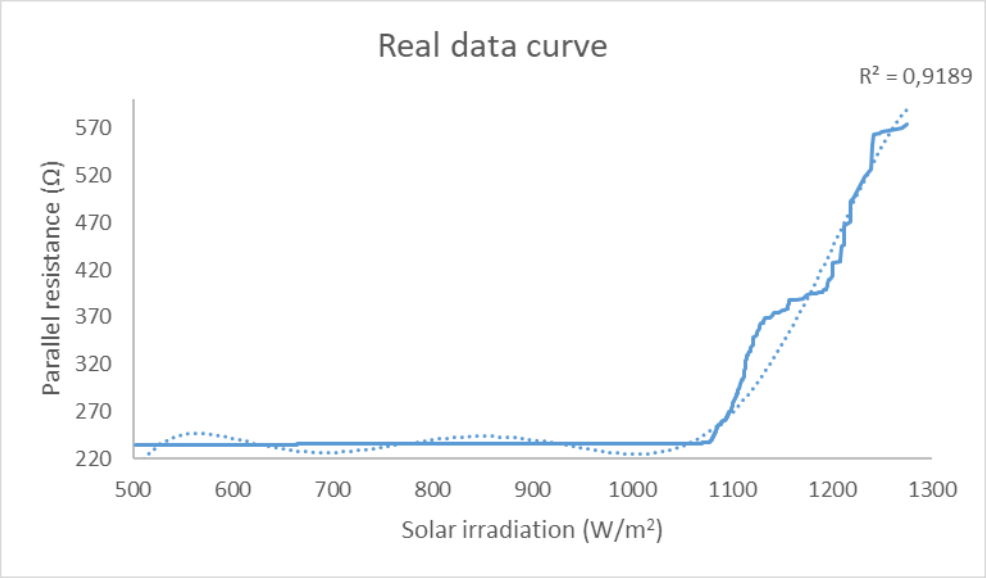


Figure 5.14. Change of parallel resistance due to solar irradiation for real data

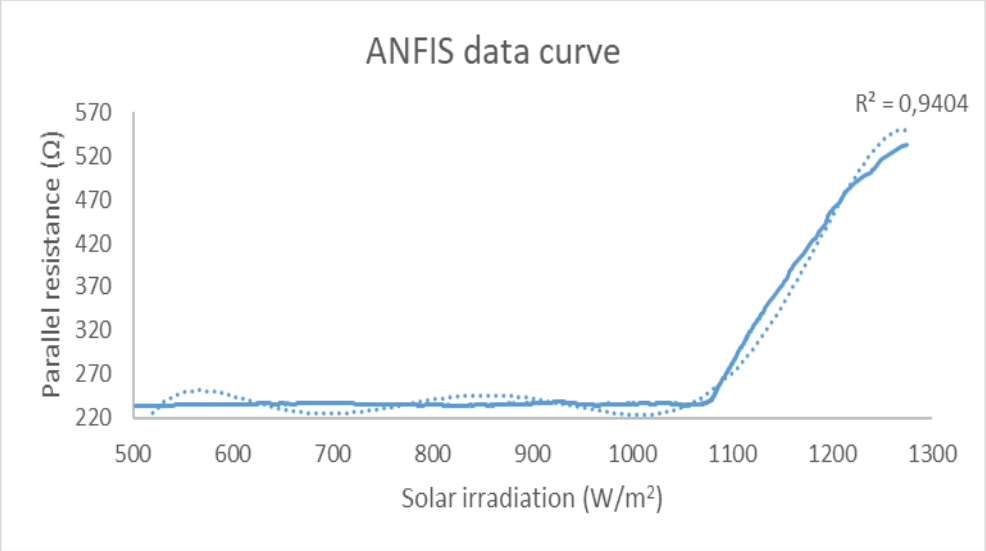


Figure 5.15. Change of parallel resistance due to solar irradiation for ANFIS data

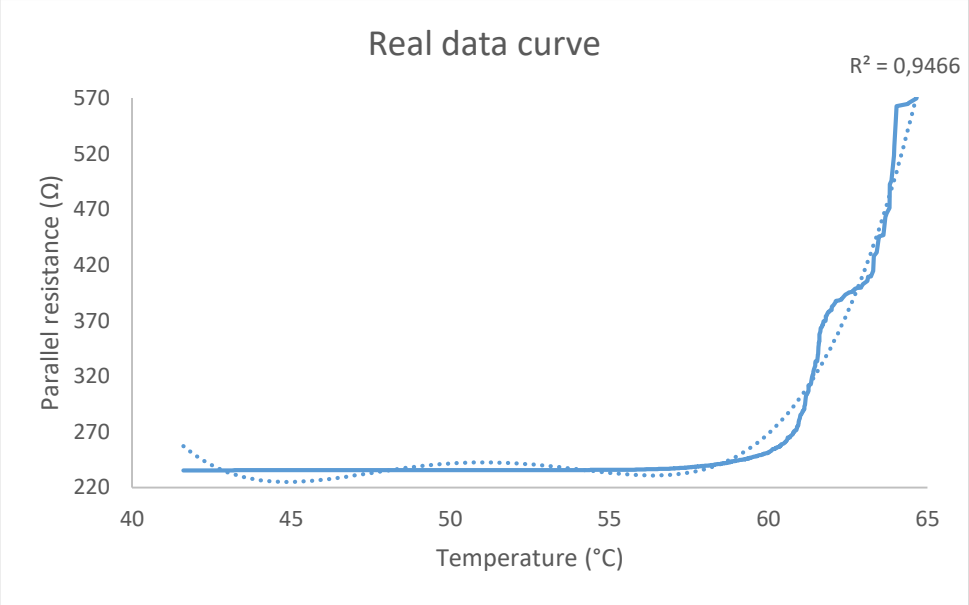


Figure 5.16. Change of parallel resistance due to cell temperature for real data

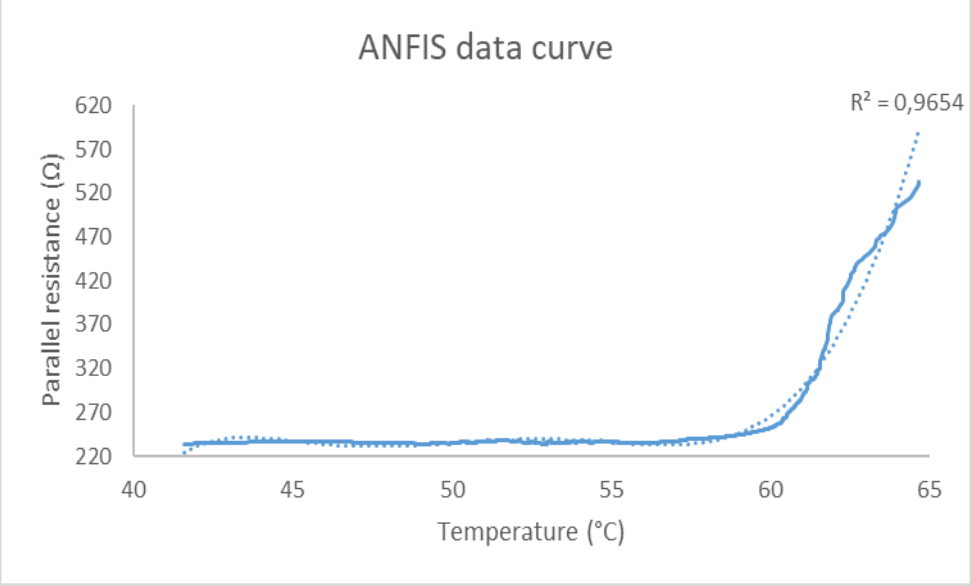


Figure 5.17. Change of parallel resistance due to cell temperature for ANFIs data

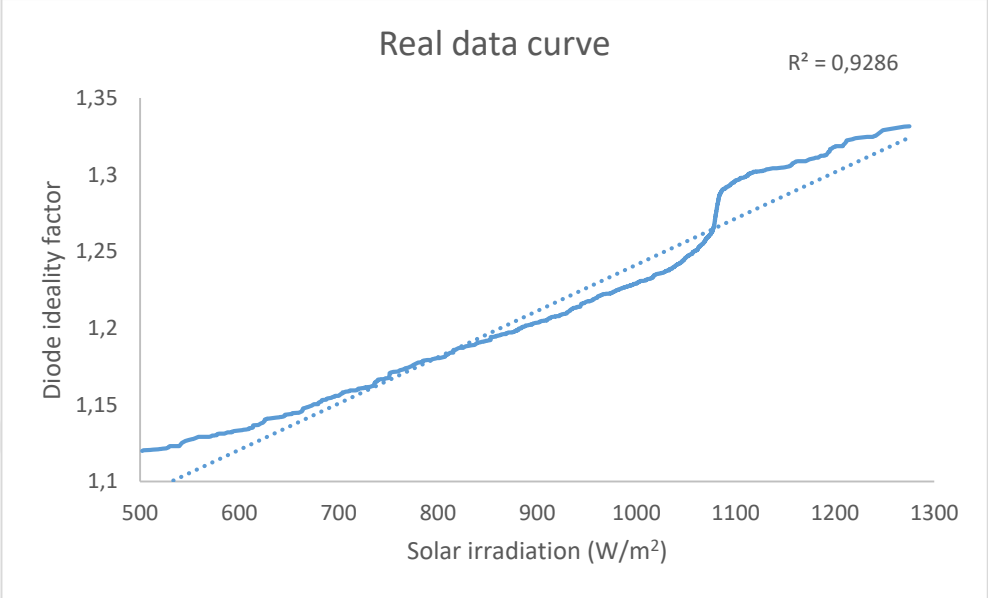


Figure 5.18. Change of diode ideality factor due to solar irradiation for real data

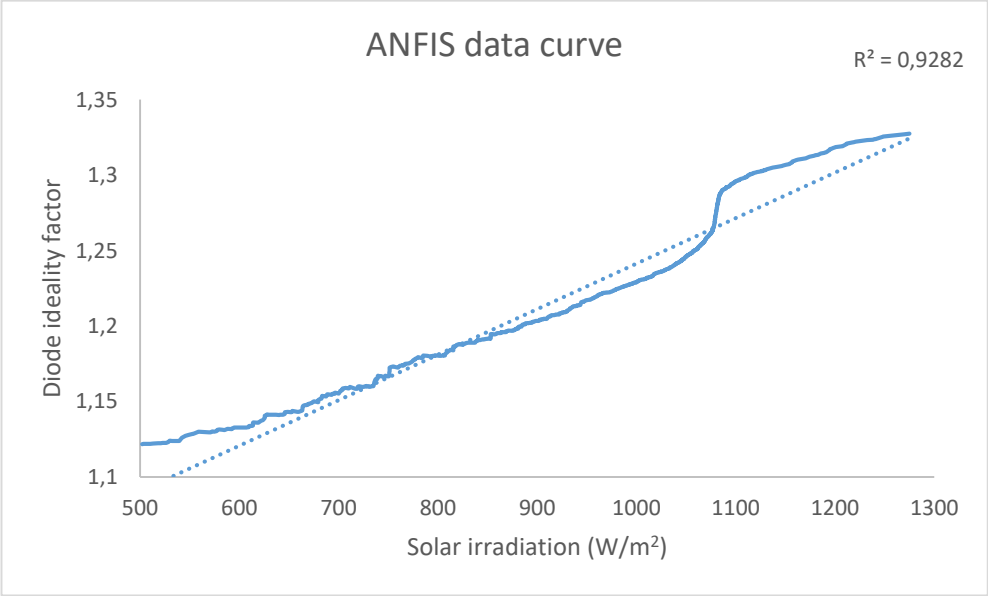


Figure 5.19. Change of diode ideality factor due to solar irradiation for ANFIS data

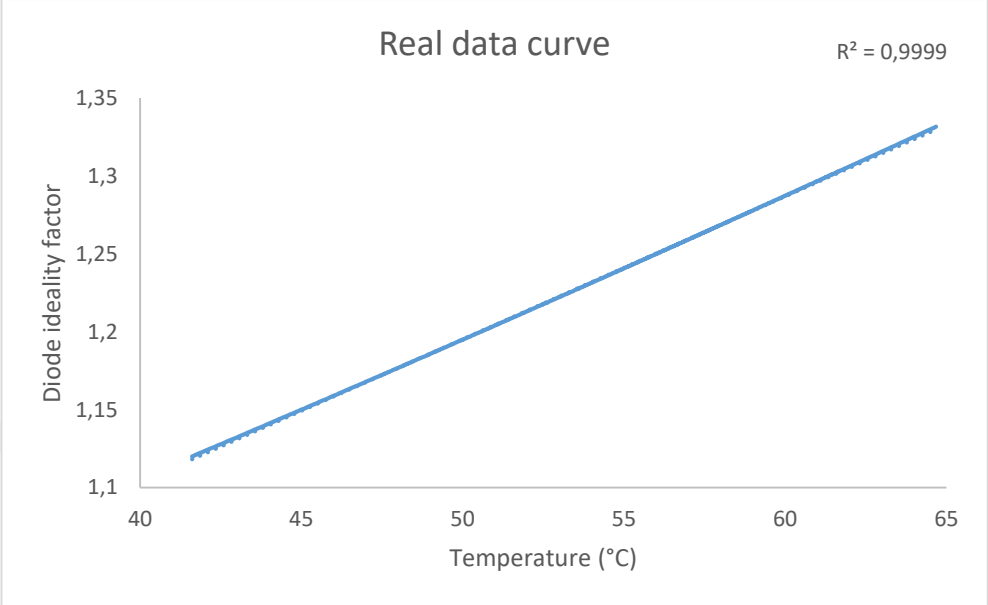


Figure 5.20. Change of diode ideality factor due to cell temperature for real data

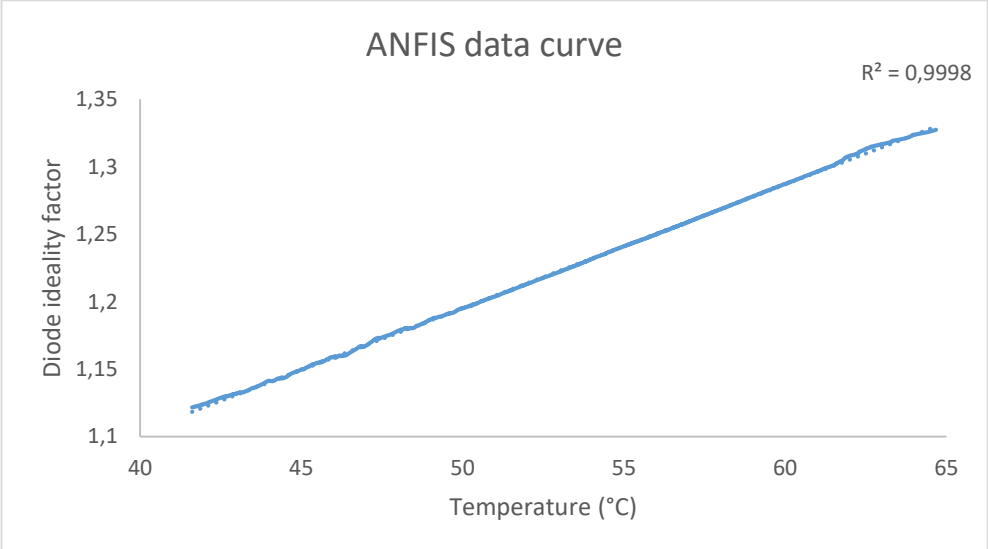


Figure 5.21. Change of diode ideality factor due to cell temperature for ANFIS data

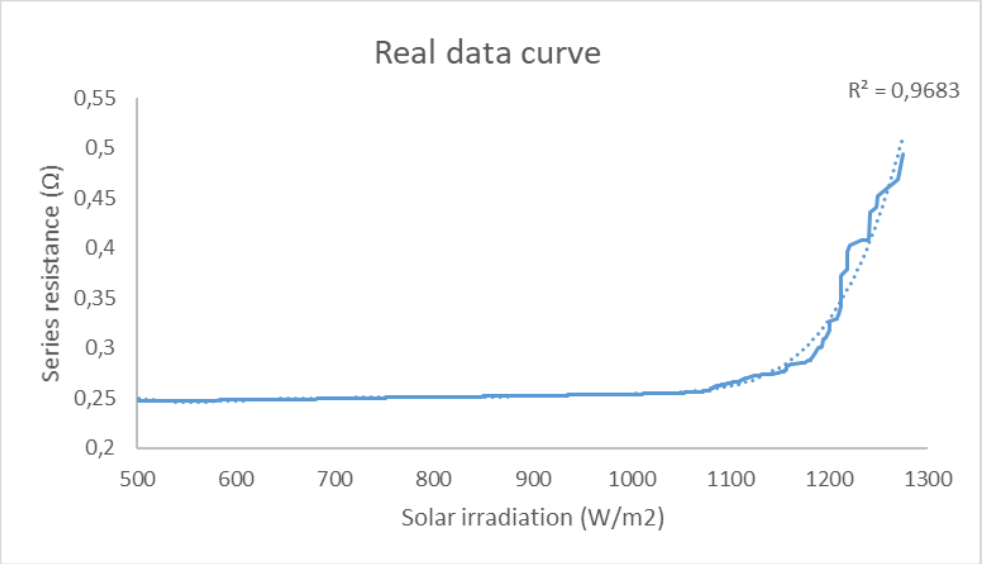


Figure 5.22. Change of series resistance due to solar irradiation for real data

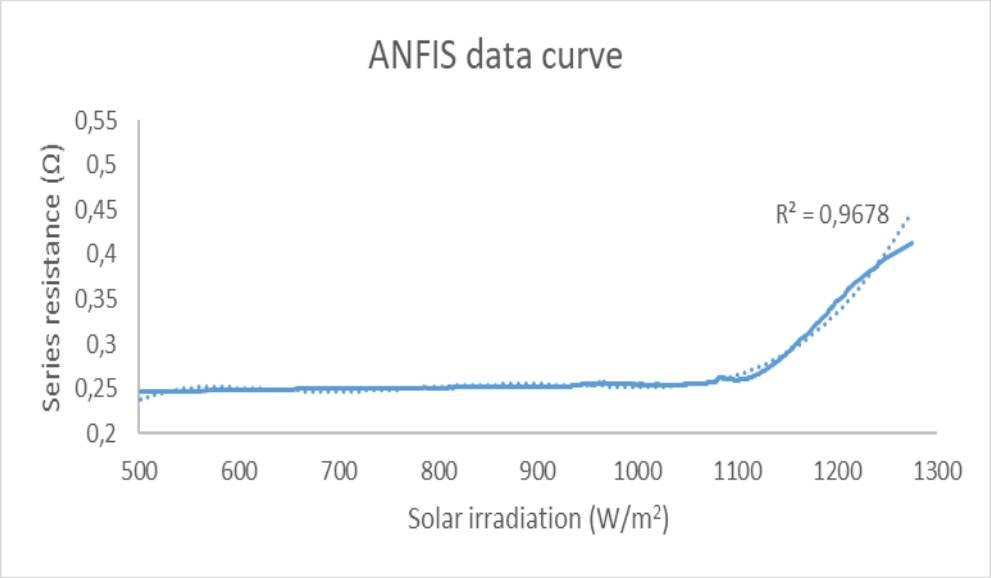


Figure 5.23. Change of series resistance due to solar irradiation for ANFIS data

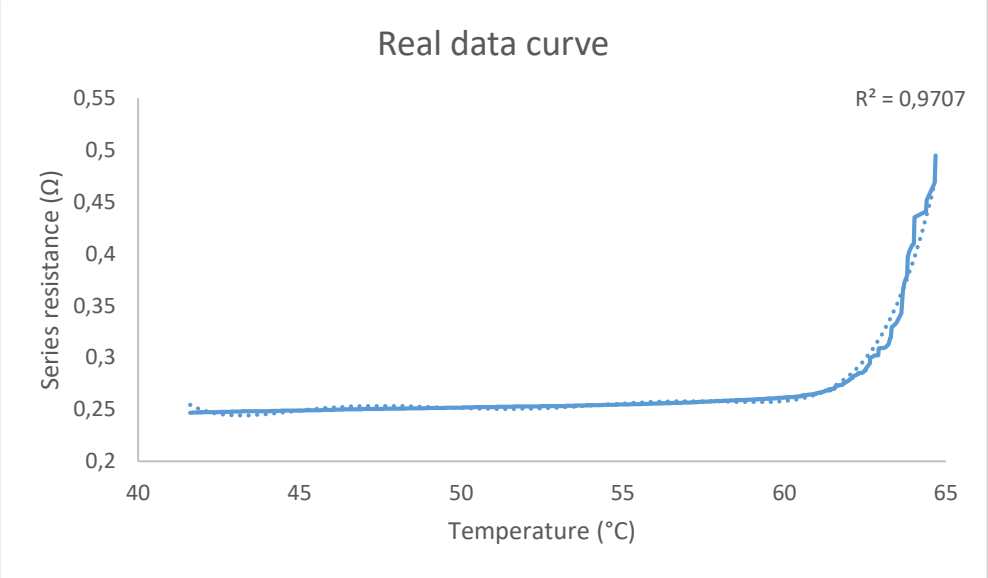


Figure 5.24. Change of series resistance due to cell temperature for real data

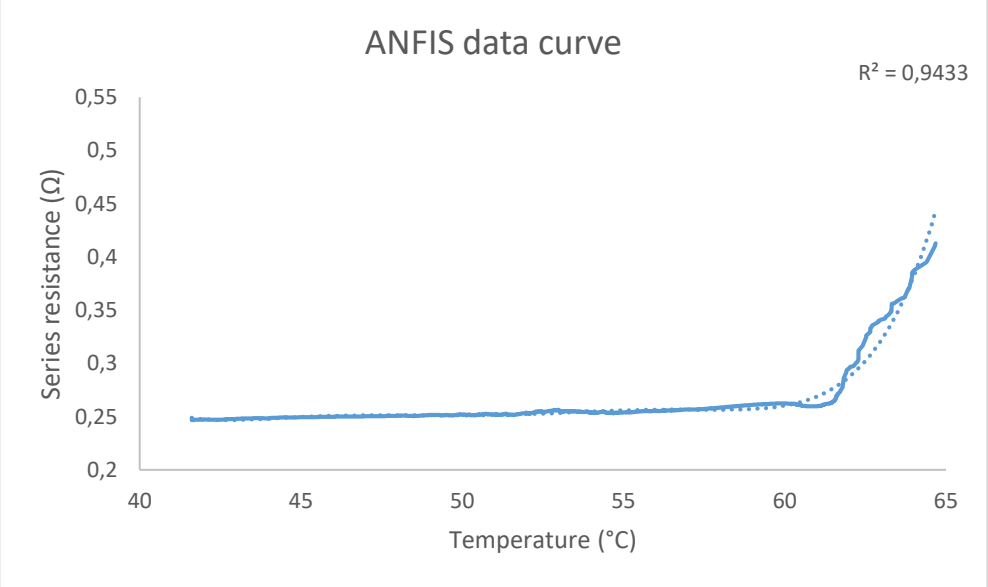


Figure 5.25. Change of series resistance due to cell temperature for ANFIS data

In the traditional PV model, the dependence of all model parameters on solar radiation and cell temperature is not included, so the accuracy and reliability of the performance estimate cannot be sufficient for all operating conditions. In this thesis, solar radiation and cell temperature have been accepted as variable parameters for all parameters of the PV module equivalent circuit model. Using ANFIS, it was estimated by simply reading solar irradiance and cell temperature samples. After that, these parameters were presented to the PV module's current-voltage equation to obtain electrical characteristics. The trained network was found to be sufficiently accurate in representing the change of parameters compared with other methods.

As a result, in this study, the unknown parameters of the single diode model, also known as the five parameters model of the photovoltaic cell; Photocurrent (I_{ph}), diode saturation current (I_0), diode ideality factor (n), series resistance (R_S) and parallel resistance (R_p) were tried to be estimated by ANFIS using experimental data. $I-V$ and $P-V$ characteristics were obtained by comparing the manufacturer's data sheet information and ANFIS output results in MATLAB / Simulink environment. Simulation results showed that using ANFIS to extract unknown parameters of PV module is a useful tool.

REFERENCES

A. Zadeh Lotfi, Fuzzy Logic, Neural Networks, and Soft Computing, Communications Of The Acm, Vol.37, No.3, March 1994.

Kropp, R., Solar Expected to Maintain its Status as the World's Fastest-Growing Energy Technology, Sustainability Investment News, 2009.

Kashif Ishaque, Zainal Salam, Hamed Taheri, and Amir Shamsudin. A critical evaluation of ea computational methods for photovoltaic cell parameter extraction based on two diode model. Solar Energy, 85(9):1768–1779, 2011.

Engin KARATEPE, Mutlu BOZTEPE, Metin ÇOLAK, Neural network based solar cell model, Energy Conversion and Management 47 (2006) 1159–1178

Bouzidi, K., Chegaar, M. ve Bouhemadou, A., Solar Cells Parameters Evaluation Considering the Series and Shunt Resistance, Solar Energy Materials and Solar Cells, 91 (2007) 1647-1651.

Chegaar, M., Azzouzi, G. ve Mialhe, P., Simple Parameter Extraction Method for Illuminated Solar Cells, Solid-State Electronics, 50 (2006) 1234-1237.

Chegaar, M., Ouennoughi, Z. ve Guechi, F., Extraction DC Parameters of Solar Cells Under Illumination, Vacuum, 75 (2004) 367-372.

Messenger, R.A. ve Ventre, J., Photovoltaic Systems Engineering, CRC Press LLC, 2004.

Villalva MG, Gazoli JR. Comprehensive approach to modeling and simulation of photovoltaic arrays. Power Electron IEEE Trans 2009; 24:1198–208.

Shivalkar R, JadhavH, DeoP. Feasibility study for the net metering implementation in rooftop solar PV installations across reliance energy consumers. In: proceedings of international conference on circuit, power and computing technologies (ICCPCT2015).IEEE;2015.p.1–6.

Sundareswaran K, Sankar P, Nayak P, Simon SP, Palani S.Enhancedenergy output from a PV system under partial shaded conditions through artificial bee colony.SustainEnergyIEEETrans2015;6:198–209.

Becquerel, E. (4 November 1839). Memoire sur les effets electriques produits sous l'influence des rayons solaires, Comptes Rendus, vol. 9, pp. 561–564.

Adams, W. G., and R. E. Day (15 June 1876). The Action of Light on Selenium, Proceedings of the Royal Society, vol. A25, pp. 113–117.

Masters, G.M., Renewable and Efficient Electric Power Systems, John Wiley & Sons, New Jersey, 2004.

K. Bouzidi, M. Chegaar_, A. Bouhemadou, Solar cells parameters evaluation considering the series and shunt resistance, Solar Energy Materials & Solar Cells 91 (2007) 1647–1651

M. Chegaar, G. Azzouzi, P. Mialhe, Simple parameter extraction method for illuminated solar cells, Solid-State Electronics 50 (2006) 1234–1237

Hasan Rıza ÖZÇALIK, Şaban YILMAZ, Erdal KILIÇ, Güneş Pilinin Bir Diyotlu Eşdeğer Devre Yardımıyla Matematiksel Modelinin Çıkartılması ve Parametrelerinin İncelenmesi, KSU Mühendislik Bilimleri Dergisi, 16(1),2013

Ayşegül TOPRAK, Hamdi Şükür KILIÇ, Ahmet TOPRAK, Abdullah KEPCEOĞLU, Güneş Pilinin Tek Diyot R_S Model Parametrelerinin Hesaplanması Ve I-V İle P-V Karakteristiklerinin İncelenmesi, Selçuk Üniversitesi Sosyal ve Teknik Araştırmalar Dergisi Sayı: 12, 2016, ss. 13-22

Vincenzo Stornelli, Mirco Muttillo, Tullio de Rubeis, and Iole Nardi, A New Simplified Five-Parameter Estimation Method for Single-Diode Model of Photovoltaic Panels (2019); DOI: 10.3390/en12224271

Wook Kim, Woojin Choi, A novel parameter extraction method for the one-diode solar cell model (2010); DOI: https://doi.org/10.1016/j.solener.2010.03.012

Ahmed HUSSEIN, A simple approach to extract the unknown parameters of PV modules, Turk J Elec Eng & Comp Sci (2017) 25: 4431-4444; doi:10.3906/elk-1703-14

A.A. Kulaksız, ANFIS-based parameter estimation of one-diode equivalent circuit model of PV modules, 2011 IEEE 12th International Symposium on Computational Intelligence and Informatics (CINTI), DOI: 10.1109/CINTI.2011.6108541

Huang Wei, Jiang Cong, Xue Lingyun, Song Deyun, Extracting Solar Cell Model Parameters Based on Chaos Particle Swarm Alogorithm, 2011 International Conference on Electric Information and Control Engineering, DOI: 10.1109/ICEICE.2011.5777246

Sanjaykumar J. Patel, Ashish K. Panchal, Vipul Kheraj, Extraction of solar cell parameters from a single current–voltage characteristic using teaching learning based optimization algorithm, Applied Energy Volume 119, 15 April 2014, Pages 384-393, DOI: 10.1016/j.apenergy.2014.01.027

T. Bendib, F. Djeffal, D. Arar and M. Meguellati, Fuzzy-Logic-based Approach for Organic Solar Cell Parameters Extraction, Proceedings of the World Congress on Engineering 2013 Vol II, WCE 2013, July 3 - 5, 2013, London, U.K.,

P. Wolf, V. Benda, Identification of PV solar cells and modules parameters by combining statistical and analytical methods, Solar Energy Volume 93, July 2013, Pages 151-157, DOI: 10.1016/j.solener.2013.03.018

M.F. AlHajri, K.M. El-Naggar, M.R. AlRashidi, A.K. Al-Othman, Optimal extraction of solar cell parameters using pattern search, Renewable Energy Volume 44, August 2012, Pages 238-245, DOI: 10.1016/j.renene.2012.01.082

Fawzan Salem, Mohamed A. Awadallah, Parameters estimation of photovoltaic modules: comparison of ANN and ANFIS, International Journal of Industrial Electronics and Drives 2014 Vol.1 No.2, DOI: 10.1504/IJIED.2014.059230

Ghias Farivar, Behzad Asaei, Photovoltaic Module Single Diode Model Parameters Extraction Based on Manufacturer Datasheet Parameters, 2010 IEEE International Conference on Power and Energy, DOI: 10.1109/PECON.2010.5697712

Ali M. Humada, Mojgan Hojabri, Saad Mekhilef, Hussein M. Hamada, Solar cell parameters extraction based on single and double-diode models: A review, Renewable and Sustainable Energy Reviews Volume 56, April 2016, Pages 494-509, DOI: 10.1016/j.rser.2015.11.051

Francesco Caracciolo, Enrico Dallago, *Member, IEEE*, Daniele Gianluigi Finarelli, Alessandro Liberale, and Patrick Merhej, IEEE Journal of Photovoltaics (Volume: 2 , Issue: 2 , April 2012), DOI: 10.1109/JPHOTOV.2011.2182181

F. Ghani , G. Rosengarten , M. Duke , J.K. Carson, The numerical calculation of single-diode solar-cell modelling parameters, Renewable Energy Volume 72, December 2014, Pages 105-112, DOI: 10.1016/j.renene.2014.06.035

Oana Mares , Marius Paulescu , Viorel Badescu, A simple but accurate procedure for solving the five-parameter model, Energy Conversion and Management Volume 105, 15 November 2015, Pages 139-148, DOI: 10.1016/j.enconman.2015.07.046

Ayedh H. ALQahtani, Simplified and Accurate Photovoltaic Module Parameters Extraction Approach using Matlab, 2012 IEEE International Symposium on Industrial Electronics, DOI: 10.1109/ISIE.2012.6237355

Jianbo Bai a, Sheng Liu, Yuzhe Hao, Zhen Zhang, Meng Jiang, Yu Zhang, Development of a new compound method to extract the five parameters of PV modules, Energy Conversion and Management 79:294–303 · March 2014, DOI: 10.1016/j.enconman.2013.12.041

Brown SH (2009) Multiple linear regression analysis: a matrix approach with Matlab. Ala J Math 34:1–3

Cheng CT, Lin, JY, Sun YG, Chau K (2005) Long-term prediction of discharges in Manwan Hydropower using adaptive-network-based fuzzy inference systems models. Adv Nat Comput 1152-1161

Dorofki M, Elshafie AH, Jaafar O, Karim OA, Mastura S (2012) Comparison of artificial neural network transfer functions abilities to simulate extreme runoff data. 2012 International conference on environment, energy and biotechnology, pp 39–44

Duch W, Jankowski N (1999) Survey of neural transfer functions. Neural comput Surv 2:163–212

W. Suparta and K.M. Alhasa, Modeling of Tropospheric Delays Using ANFIS, SpringerBriefs in Meteorology, DOI 10.1007/978-3-319-28437-8_2

Haykin S (ed) (2009) Neural network and machine learning. Pearson Prentice Hall, New York

Jain AK, Jianchang M, Mohiuddin KM (1996) Artificial neural networks: a tutorial. Computer 29 (3):1–44

Jang JSR (1993) ANFIS: adaptive network-based fuzzy inference systems. IEEE Trans Sys Man Cybern 23:665–685

Jang JS, Sun CT (1995) Neuro-fuzzy modeling and control. Proc IEEE 83(3):378–406

McCulloch WS, Pitts WH (1943) A logical calculus of the ideas immanent in nervous activity. Bull Math Biophys 5:115–133

Nayak PC, Sudheer KP, Rangan DM, Ramasastri KS (2004) A neuro-fuzzy computing technique for modeling hydrological time series. J Hydrol 291(1):52–66

Shafiullah GM, Ali AS, Thompson A, Wolfs PJ (2010) Predicting vertical acceleration of railway wagons using regression algorithms. IEEE Trans Intel Syst 11(2):290–299

Suparta W, Alhasa KM (2013) A comparison of ANFIS and MLP models for the prediction of precipitable water vapor. 2013 IEEE international conference on space science and communication (IconSpace), pp 243–248

Tang H, Tan CK, Yi Z (2007) Neural networks: computational models and applications. Stud Com Intell, vol 53. Springer, Berlin

Nun Pitalúa-Díaz, Fernando Arellano-Valmaña, Jose A. Ruz-Hernandez, Yasuhiro Matsumoto, Hussain Alazki, Enrique J. Herrera-López, Jesús Fernando Hinojosa-Palafox, A. García-Juárez, Ricardo Arturo Pérez-Enciso 1 and Enrique Fernando Velázquez-Contreras, An ANFIS-Based Modeling Comparison Study for Photovoltaic Power at Different Geographical Places in Mexico, Energies 2019, 12, 2662; doi:10.3390/en12142662

Di Piazza Maria Carmela, Vitale Gianpaolo, Photovoltaic Sources Modeling and Emulation, Springer-Verlag London 2013, DOI 10.1007/978-1-4471-4378-9

Hansen Clifford, Estimating Parameters for the Pvsyst Version 6 Photovoltaic Module Performance Model, Sandia National Laboratories,2015

Mitsubishi Electric Photovoltaic Module Datasheet (https://www.mitsubishielectricsolar.com/images/uploads/documents/specs/UE5_Specification_Sheet_115-130W.pdf)

CIRRICULUM VITAE

She studied primary, high school and university in Şanlıurfa. She continues his graduate education at Çukurova University.